Femtosecond laser processing on hard-to-process materials and its application to CMP process

王, 成武

https://doi.org/10.15017/1654868

出版情報：九州大学, 2015, 博士（工学）, 課程博士
バージョン：
権利関係：全文ファイル公表済

FEMTOSECOND LASER PROCESSING ON HARD-TO-PROCESS MATERIALS AND ITS APPLICATION TO CMP PROCESS

Doctoral Dissertation
March 2016

CHENGWU WANG

Supervisor
Professor Syuhei Kurokawa

Department of Mechanical Engineering
Graduated School of Engineering

Kyushu University

ABSTRACT

Owing to extremely short pulse duration, high pulse repetition rate and high fluence, femtosecond (fs) laser has attracted considerable interest of large amount of researchers from the fields of aerospace, microelectronics, biomedical engineering. Femtosecond laser ablation has been used for material functionalization especially surface micromachining of semiconductor materials recently. Femtosecond laser processing is considered as an invaluable optimization tool for achieving a particular surface morphology. However, the effects of laser-induced surface morphology on hard-to-process materials such as SiC and Diamond have not been adequately investigated yet. In this study, the authors firstly utilized femtosecond laser as a pre-process to induce surface morphology changes on the next generation power device materials such as Diamond and SiC called hard-to-polish materials in CMP process due to their extremely high chemical stability and high Mohs hardness.

Then the author carried out varies of experiments for SiC substrate. Firstly, to investigate the changes of SiC surface morphology, the author elaborated the evolution of surface morphologies on SiC substrate irradiated by femtosecond laser at different conditions such as different scanning pitches, different scanning velocities, different repetition rates and different fluence. It was found that different laser processing parameters formed different surface morphologies on SiC substrate. The formation mechanism of laser-induced periodic surface structures (LIPSS) on SiC surface was also discussed. Secondly, we carried out CMP process to investigate

the polishing behaviors of the areas irradiated at different laser power on Si-face of SiC. We found that the oxidized areas could be faster removed in CMP process than the non-irradiated areas and the areas irradiated at relatively low laser power which could not induce laser ablation. Finally, we utilized this result to polish laser-irradiated C-face of SiC substrates. We compared the Material Remove Rate of Transverse mode irradiation and Cross-scan mode irradiation. It was found that better surface and higher material removal rate (MRR) of laser-irradiated substrate than that of non-irradiated substrate were realized in the experiments. The mechanism was investigated by XRD and XPS analysis.

After femtosecond laser irradiation for diamond, quasi-radical site with a thickness of about 10nm as well as laser-induced ripples were observed. Simultaneously, Raman spectral analysis indicates that the surface of diamond substrate was formed to be a structure mixed with amorphous and regularly-structured diamond.

Finally, we implemented internal processing of femtosecond laser for power device materials Si, sapphire, and SiC substrate. Different phenomena of internal absorption type processing as well as the corresponding reasons were discussed.

TABLE OF CONTENTS

CHAPTER 1

1.1 Construction Guidelines

This dissertation was mainly focused on the researches of femtosecond laser surface processing on hard-to-process materials and its applications to CMP process. In this study, we firstly introduced the developments and applications of hard-to-process materials as well as femtosecond laser, and then proposed the present problems of CMP technique. As solutions to these problems, we firstly implemented femtosecond laser irradiation for surface micromachining on SiC and Diamond substrates. In this part, the effect of processing factors on surface morphologies was investigated; the polishing properties of laser-irradiated SiC were also studied and discussed after CMP process. Finally, internal processing of femtosecond laser for substrates such as Si, Sapphire, and SiC were preliminarily carried out to investigate the internal absorption processing phenomena for dicing process. The schematic diagram of construction Guidelines of this study was shown in **Fig.1.1**.

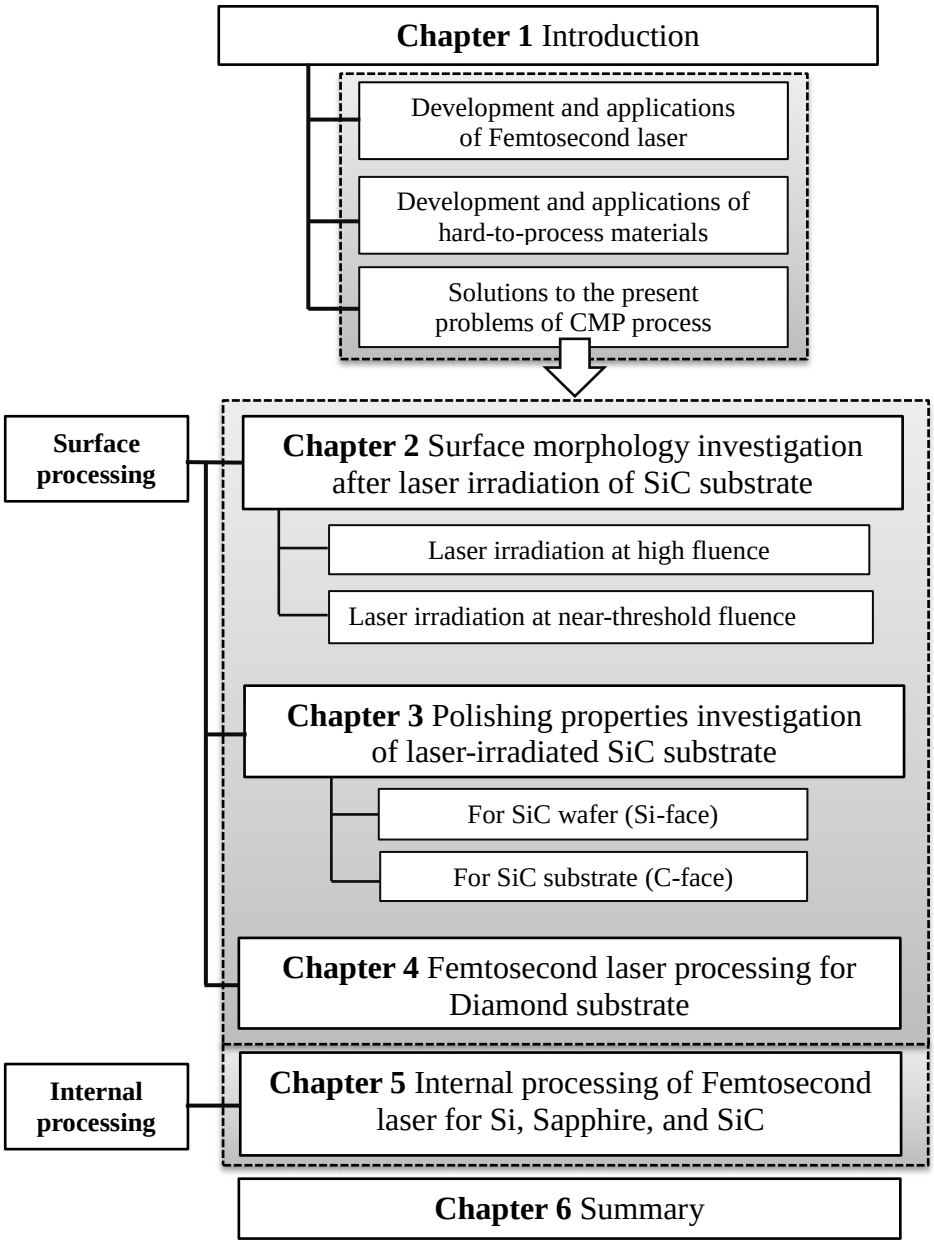

Fig.1.1 Schematic diagram of construction Guidelines

1.2 Development of semiconductor materials and the present problems in its CMP process

Since been successfully made in the middle of 19th century, silicon (Si) has been studied and applied in lots of fields as an outstanding semiconductor material. In 1947, physicists John Bardeen, William Shockley and Walter Brattain successfully invented the first transistor by using semiconductor material germanium at Bell Labs, which was considered as an important invention of 20th century, because transistor can be used for demodulation, rectification, amplify, signal modulation, etc. It further accelerated the realization of IC (integrated circuits), triggering the Second Industrial Revolution. In 1970s, the invention of quartz light guide fiber and GaAs laser (either was made from semiconductor material quartz or GaAs) promoted the development of fiber communication technique, and finally lead to the Information Revolution. Semiconductor Si has been used in several fields, such as economy and defense. It is being used in more than 95% of communication semiconductor devices. According to the predictions [1] of Semiconductor Industry Association in Japan, the semiconductor market of the world will run up to 370,000 million dollars in 2017. It was also indicated that the biggest proportion ratio was in Asia pacific market, which will achieve approximately 230,000 million dollars. Integrated circuits (IC) were stated as the main semiconductor product, which takes over the most market share among semiconductor devices of Total Discrete, Optoelectronics, Sensor and Total IC.

Owing to the performance limitations of semiconductor Si, it was gradually found

that the behaviors of power devices made of Si were difficult to be further improved, especially in atmospheres such as intensive radiation and high frequency electric field, high-intensity magnetic field, high voltage, and high temperature atmosphere. Consequently, new substrate material with better properties should be developed. Silicon carbide (SiC) are considered as the next generation semiconductor materials due to its outstanding properties such as excellent thermal conductivity, high resistance to radiation, high energy-saving efficiency, high breakdown voltage of insulation destruction, and larger band gap than other substrate materials. **Table 1.1** shows some main properties of semiconductors materials Si, SiC, GaN and dielectric material Diamond. Due to higher manufacturing efficiency and superior properties, SiC was considered as the next generation semiconductor material with great potential. It has superior properties and vast market potential applications and development prospect, as shown in **Fig.1.2**. In the manufacturing process of integrated circuits (IC), high surface planarization and extremely high surface roughness of substrates are required. CMP (Chemical Mechanical Polishing) is an indispensable and important technique which meets these demands. Nevertheless, it is still extremely difficult to polish the hard-to-polish materials such as SiC and diamond due to their high chemical stability and high Mohs hardness, as shown in **Table 1.2.** According to its vast potential market share and development prospect of these semiconductor materials, new technique regarding how to realize high polishing efficiency and high surface precision for these materials in CMP process should be developed.

Table 1.1 Main properties of Si, SiC, GaN and Diamond[2]

	Si	4H-SiC	GaN	Diamond
Band gap[eV]	1.12	3.26	3.42	5.47
Breakdown field of insulation [MV/cm]	0.3	2.8	3	8
Thermal conductivity [W/cmK]	1.5	4.9	1.3	20

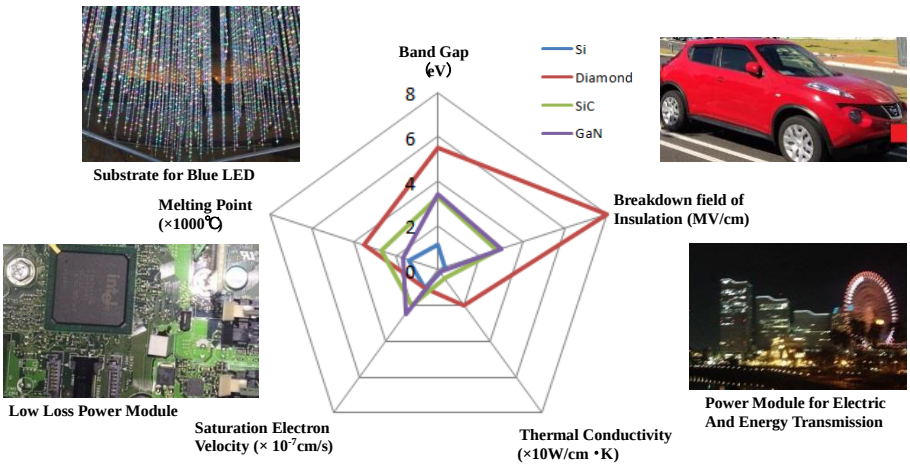

Fig.1.2 Main property comparisons and applications of Si, Diamond, SiC, GaN

Table 1.2 Mohs Hardness of Diamond, SiC, GaN and Sapphire

Material	Mohs Hardness
Diamond	10
SiC	9.15
GaN	9
Sapphire	9

1.3 Developments of laser technology and the applications of femtosecond laser

The reaction of material and laser has been studied for more than 50 years since ruby laser was firstly applied from 1960 [3]. Owing to its four characteristics such as high coherence, high luminance, high monochromaticity and high directionality, laser was widely applied in many fields, pushing forward human civilization afterwards. Laser can be distinguished into three types according their polarizations: circular polarization, elliptical polarization and linear polarization, as shown in **Fig.1.3**, where, X, Y and X indicate the electric field vector, magnetic field vector and propagation direction electromagnetic wave respectively.

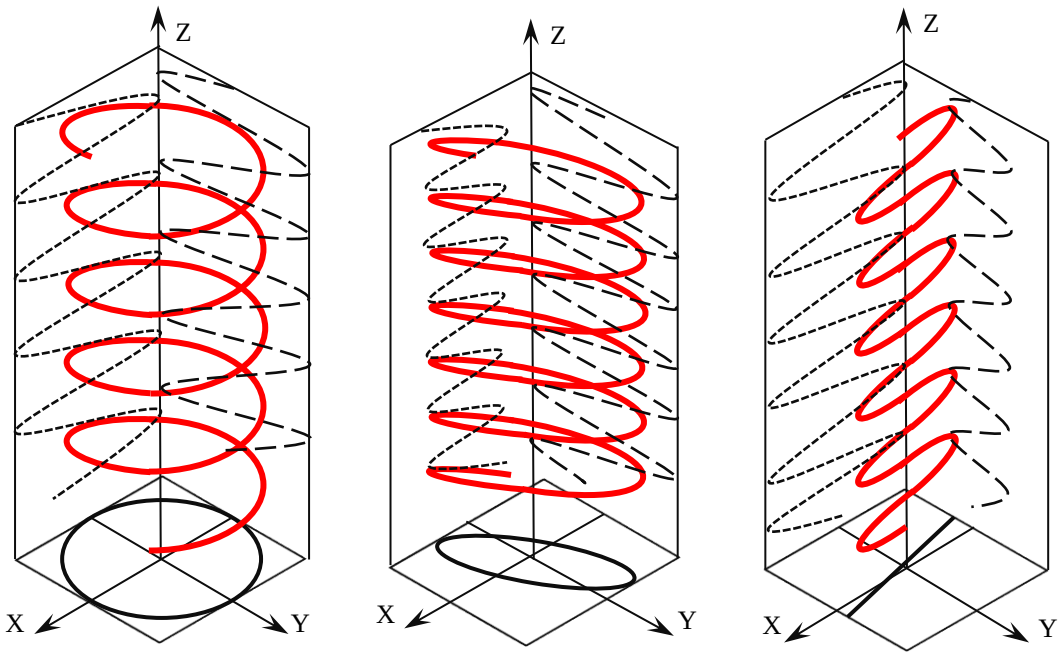

(a) Circular polarization (b) Elliptical polarization (c) Linear polarization

Fig.1.3 Three types of laser polarization

Even through it was quite effectively and popular in industry than traditional contacting machining or other machining using expensive vacuum equipment, the large heat-affected area of successive laser and long pulse laser restricted its applications in machining precision. Excimer laser with short pulse duration can be used for microscale precision machining, however its applications was also limited because it will be absorbed by many transparent materials. After the development of mode-locking technique, extremely short pulse duration of 6 fs was realized [4], which contributed to the emergence of short pulse femtosecond laser. Femtosecond laser firstly come into being in the United States and have large amount of applications for ultrafast science, metrology, ophthalmology, medical devices, optoelectronics, and chemistry in recent years, owing to its extremely high fluence and overwhelmingly short pulse duration.

Higher precision attributed to considerably smaller heat-affected area can be realized by using femtosecond laser in precision machining process, comparing to the traditional carbon dioxide laser, neodymium-doped yttrium aluminum garnet (Nd: YAG) laser. Femtosecond laser can be used for surface machining as well as internal machining for transparent materials. Waveguides and three-dimensional optical storage inside transparent materials was successfully realized in 1996 [5, 6]. Special application demands such as high accuracy and high performance during different environments have attractive more attentions in recent years on complicated three-dimensional microstructures, which have potential applications for medical apparatus, microelectronics, aerospace, biomedical engineering and

microelectromechanical system. In recent years, several typical three-dimensional femtosecond laser processing have been realized. Micro-fabrications with high precision were successfully realized by using a titanium sapphire laser laser (λ = 780 nm, τ = 150 fs, 76 MHz) on resins [7]. Two-photon absorption (TPA) played an important role in fabricating those three dimension micro structures, a rotatable gearwheel, a micro chain and micro bull structures. Fabrication for microfluidic device with free movable microplate has been successfully carried out inside photosensitive glass by femtosecond laser (λ = 775 nm, τ = 150 fs, 1 kHz) [8].

Many researchers have studied the reactions of femtosecond laser with different materials at different experimental conditions. Non-linear affect is triggered owing to its extremely short pulse duration and high peak power during extremely short time, further leading to Multi-photon absorption [9] or Coulomb explosion [10-12], which have been assumed as the main mechanisms in femtosecond laser machining of dielectric materials, accompanying with irradiation patterns of colour center [13, 14], micro-explosion [15], ablation, refractive index modulation [16-19], self-organization structure [20, 21].

As shown in **Fig.1.4,** Linear polarization femtosecond laser contains two perpendicular vectors, an electric field and a magnetic field, which play important roles in laser-material reaction during its propagation. Several studies have been considerably carried out for nano/micro structuring formation in vacuum, liquid and gaseous environments [22]. Laser induced periodic surface structures (LIPSS) have been observed on a multitude of femtosecond laser-ablated material surfaces. Low

spatial frequency (LSFL) with a periodicity of 350~600 nm and high spatial frequency (HSFL) with a periodicity of 50~200 nm were induced on different metallic films surface at different ambient environment [22]. Formation of nano/micro patterns induced by femtosecond laser on semiconductors (ZnO [23, 24], AlGaInP [25], Si [26-29], InP, etc.) have also been carried out by several means. Nanoscale patterns with periodicity of 780nm in the direction perpendicular to laser polarization and periodic patterns of 390nm in the direction parallel to laser polarization were induced on crystalline silicon by low pulse number femtosecond laser (λ =800 nm, τ = 50 fs, 1kHz). According to large amount of literatures, it has been revealed that the surface morphology of LIPSS depends on irradiation condition [30], laser fluence [31], pulse duration [32], wavelength, incidence angle, polarization of incident laser beam [33-35] and material thermal properties [32]. Researchers have proposed several different explanations to investigate the mechanism of laser ablation. Viewpoints such as self-organization [36, 37], interference, melting, second harmonics [38, 39], resolidification, coulomb explosion and surface plasma waves [10, 40, 41], have been put forwarded for the explanations of LIPSS formation mechanism according to theoretical analysis.

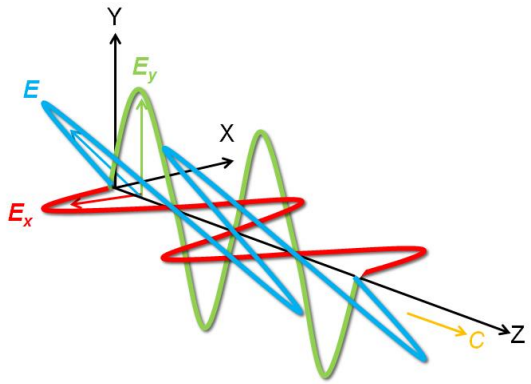

Fig.1.4 Linear polarization laser with vector diagram

The typical femtosecond laser-irradiated surface with uniform periodic structures was reported in [42]. In order to control the surface morphology of fs laser-induced surface, alternate linearly polarized fs laser ablation with orthogonal polarization directions were implemented for fabricating microstructures. It has been reported that parallel LIPSS structures of about 270 nm were induced on ZnO surface by fs laser beam (λ = 800 nm, τ= 125 fs, 1 kHz, 3 J/cm^2) with a vertical polarization direction. On the contrast, the ripples were fabricated into submicron periodic square structures with a spatial periodicity of 290 nm by another incident laser beam with a horizontal polarization direction [42]. It was presumed that the latter laser fluence was not strong enough to ablate the previously induced ripples structures thoroughly.

In recent years, femtosecond laser induced surface morphologies on crystal SiC surface and the corresponding formation mechanism have also been investigated and proposed, respectively. Nanoparticles with average period of 80 nm were fabricated on the surface of 6H-SiC crystal by circularly polarized 400nm fs laser with pulse

energy of 1.1μJ/pulse. Nano scale ripples with periods of 80, 100 and 150 nm were induced by linearly polarized laser beams with different wavelength / pulse energy combination of 400nm (0.9 μJ/pulse), 510nm (1.0 μJ/pulse), and 800nm (4.0 μJ/pulse), respectively [43]. High special frequency periodic ripples (HSFL) with average width of 200nm perpendicular to laser polarization were fabricated by femtosecond laser (λ = 800 nm, τ = 150 fs, 100 Hz) with constant fluence of 0.3 J/cm^2 on 4H-SiC crystal surfaces in a vacuum chamber [44]. Incubation effect and redistributed electric field were reported responsible for these cross-patterned periodic surface structures [28]. However, the surface morphologies formed by fs laser on single crystal diamond and 4H-SiC substrate under normal pressure and temperature at different process parameters have not yet been reported adequately. The physical mechanisms of formation of uniform ripples on single crystal diamond and 4H-SiC are still poorly understood. Accordingly, we implemented femtosecond laser to irradiated SiC and diamond for the investigation of surface morphology change and tried to explain the mechanism.

1.4 Solutions to solve the present problems and Research objectives

According to the present research status and the development trend as well as the present problems in CMP process of the outstanding power device materials SiC and diamond, we exploited femtosecond laser as a pre-process technique for surface treatment for electric power material SiC and diamond substrates. The effect of laser processing parameters on the substrate surface morphologies of SiC and diamond were investigated. After fs laser irradiation, as a finish process, we polished the irradiated substrates in CMP process, to investigate the application of laser irradiation on CMP process. The general manufacturing procedure for semiconductor materials and the main research project are shown in **Fig.1.5**. The contents shown in the red frame were mainly paid attentions in this study.

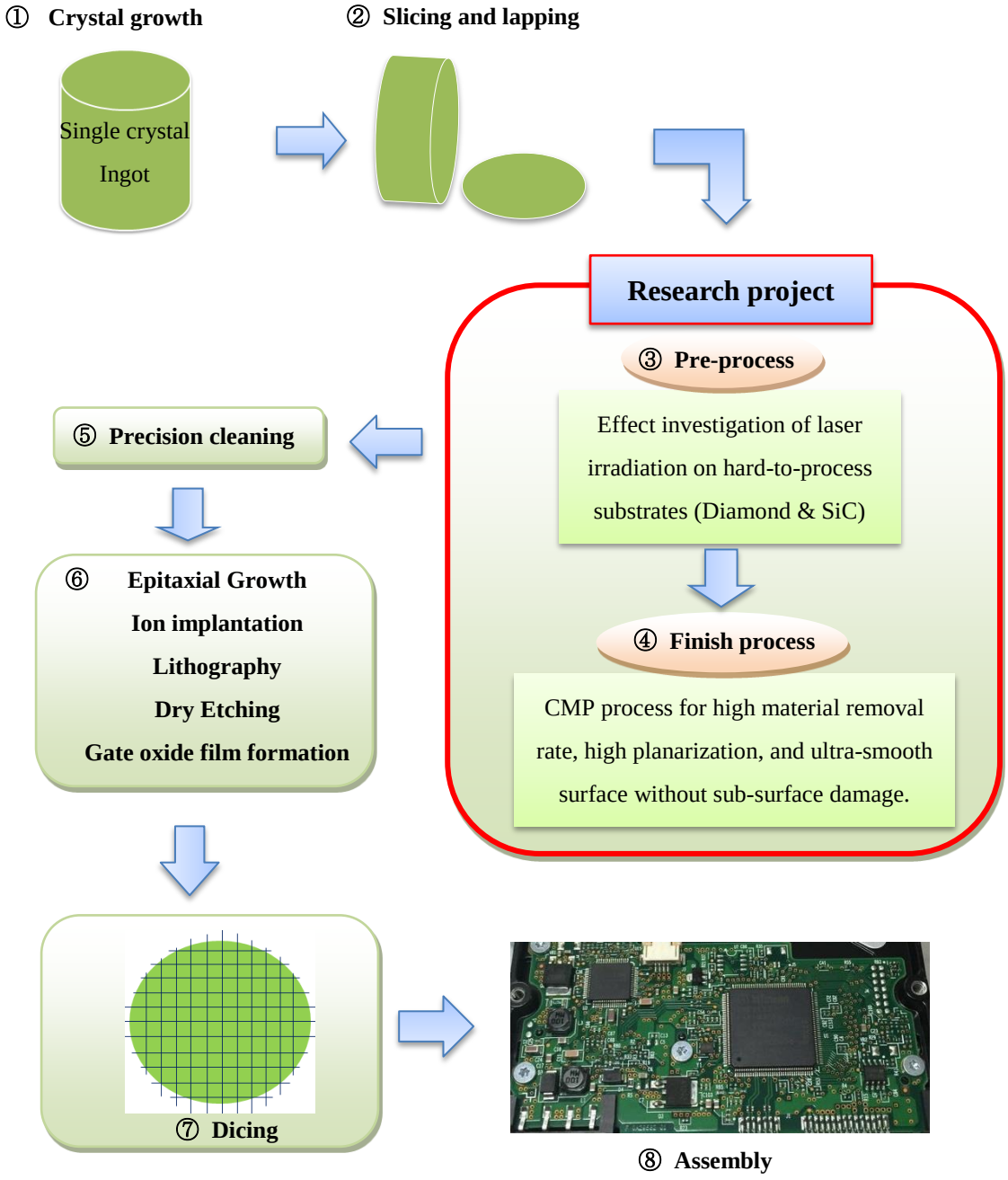

Fig.1.5 Manufacturing procedure of electric power substrate and research project

1.4.1 Femtosecond laser apparatus for this study

The femtosecond laser equipment t-pulse 200 and its schematic diagram were shown in **Fig.1.6** and **Fig.1.7** respectively. It was produced by Amplitude Systems Co. Ltd. **Table 1.3** shows the main parameters of this femtosecond laser system. The femtosecond laser oscillator consists of new laser materials, including high quality doped materials Ytterbium. Ytterbium doped laser materials can be directly diode-pumped, thus eliminating the need for an intermediate pump laser used in traditional Titanium: Sapphire lasers [45]. High thermal efficiency and femtosecond pulses with high average power are the outstanding characters of this laser system. This Ytterbium laser system generates extremely short femtosecond pulses with a width of 373fs, wavelength of 1030nm and maximum repetition rate of 10 MHz.

Fig.1.6. Over view of femtosecond laser processing system

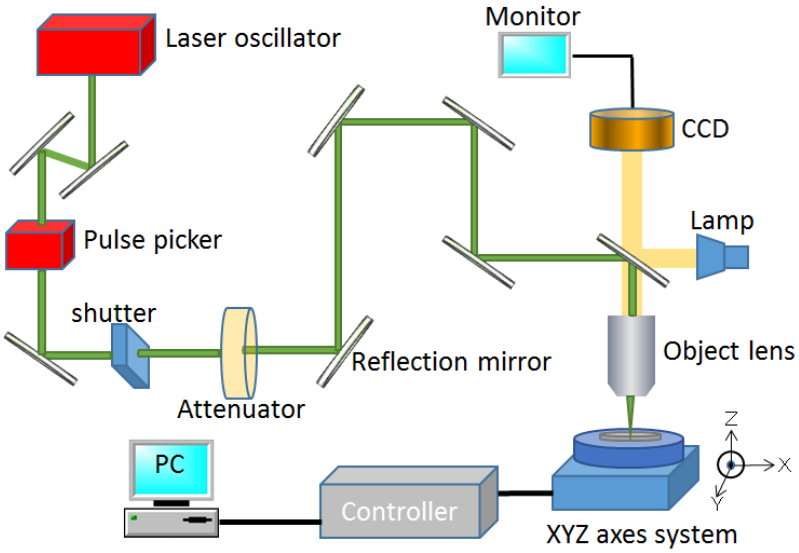

Fig.1.7. Schematic diagram of femtosecond laser experimental equipment

Table 1.3 Main parameters of femtosecond laser process system

t-pulse 200 Made by Amplitude Systems Co. Ltd.	
Average power	≧2W max.
Peak power	≧500 kW
Pulse duration	< 400 fs
Pulse energy	≧200 nJ/pulse
Beam quality	M^2 ≦1.2
Spatial mode	TEM_{00}
Warm up time	≦30min
Repetition rate	1 Hz to 10 MHz
Wavelength	1030 nm

The main optical system and XYZ axes system were shown in **Fig.1.8.** Main parameters of femtosecond laser spot and specifications of electric XYZ stage were respectively shown in **Table 1.4** and **Table 1.5**. A special scanning control program was designed for femtosecond laser machining system. The interface of controlling software is shown in **Fig.1.9**. With the help of this controlling program, sample substrates were irradiated by femtosecond laser on the three-dimensional XYZ stage with a resolution of 0.1μm. The scanning trajectory of femtosecond laser's spot was designed as a zigzag pattern, and the interval between adjacent trajectories was set at suitable pitch to ensure that the whole surface was wholly irradiated by femtosecond laser, with high average power, exceptional energy per pulse and excellent pulse-to-pulse stability [46]. The substrates were irradiated at a scanning speed of 100 mm/s by linearly polarized femtosecond laser beam focused with a focal spot of 3μm in diameter. All the experiments were done in normal air atmosphere.

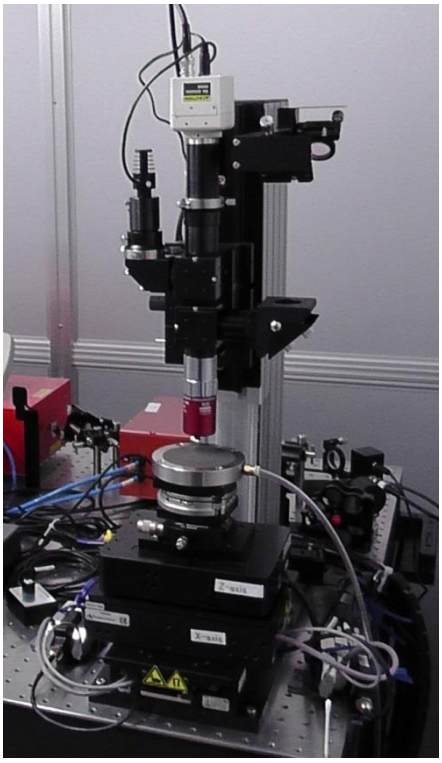

Fig.1.8. Detailed image of the main optical system and XYZ axes system

Table 1.4 Parameters of femtosecond laser spot

Pulse energy	≧75 nJ/pulse *1
Pulse width	≦400 fs *2
Peak power	≧180 kW *3
Spot diameter	≦φ3 μm *3,*4
Fluence	≧1.5 J/cm^2 *3,*4

*1) In the case that the pulse energy from oscillator beyond 200 nJ/pulse.

*2) According to shipment data of the femtosecond laser manufacturer.

*3) Calculated value.

*4) Measured in atmosphere.

Table 1.5 Specifications of electric XYZ stage

Specifications	XY stage	Z stage
Maximum displacement	100 mm	4.8 mm
Minimum displacement	10 nm	60 nm
Bidirectional reproducibility	80 nm	0.5μm
Epaxial precision	1.5 μm	3 μm
Maximum speed	300 mm/s	5 mm/s
Resolution combinated with XPS controller	about 1 nm	about 0.1μm

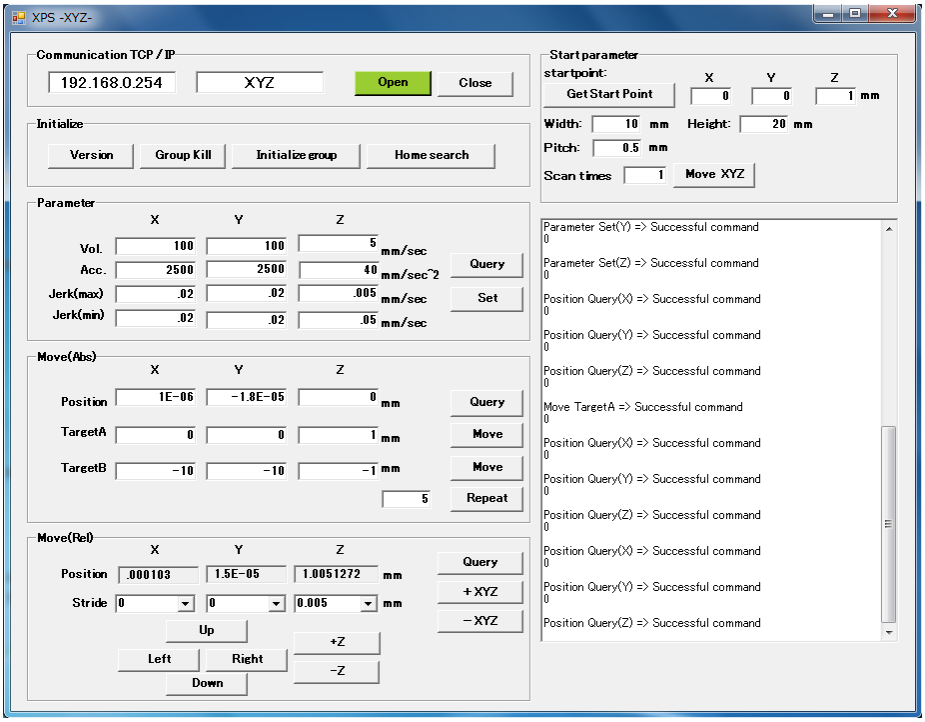

Fig.1.9 Interface overview of software used for controlling XYZ axes system

1.4.2 Basic elements of Chemical mechanical polishing (CMP) process

Chemical mechanical polishing (CMP) has been widely and effectively used for producing high-quality surface, especially for improving global surface planarization for ultra-LSI devices. It is considered as an effective technique for semiconductor devices to improve global surface planarization without surface defects, little or no substrate damage, and high material removal rate.

CMP Process model is shown in **Fig.1.10**. It contains some main elements of polishing pad, slurry, and diamond conditioner, as well as polishing ambient condition, mechanical condition, etc. The mechanism of CMP was shown in **Fig.1.11**. During CMP process, the wafer is oxidized by chemical reaction in slurry, leading to a chemical reaction layer, which is easier cut down by the mechanical action of abrasive grain than non-oxidized wafer. Atomic layer level planarity and high planarization can be achieved by CMP process for semiconductor substrates. The main polishing parameters of CMP process were listed in **Fig.1.12**. Large quantities of studies have been done for understanding the effect of these parameters on how to improve the material remove rate (MRR) and surface accuracy of SiC wafer efficiently in CMP process. The research group of Professor Doi has been studied CMP for many years, pouring his efforts on this technique with other researchers.

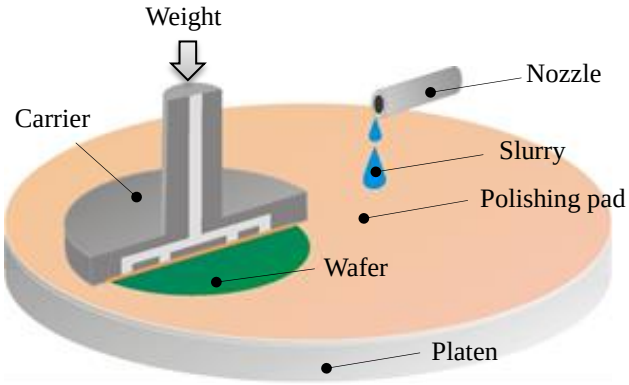

Fig.1.10 Schematic diagram of CMP Process

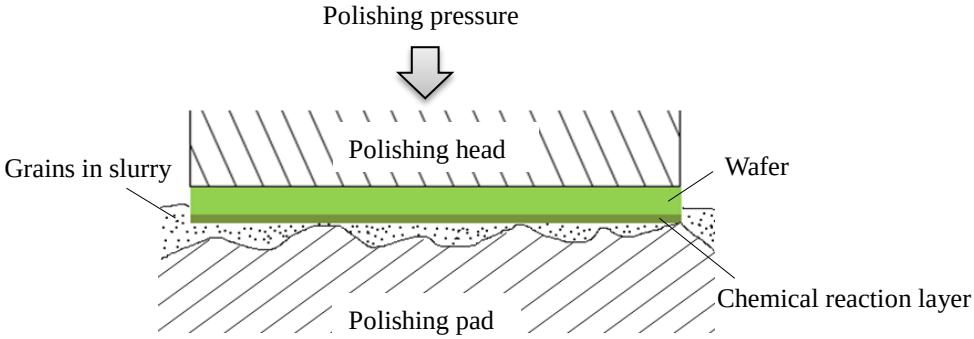

Fig.1.11 Principle of CMP Process

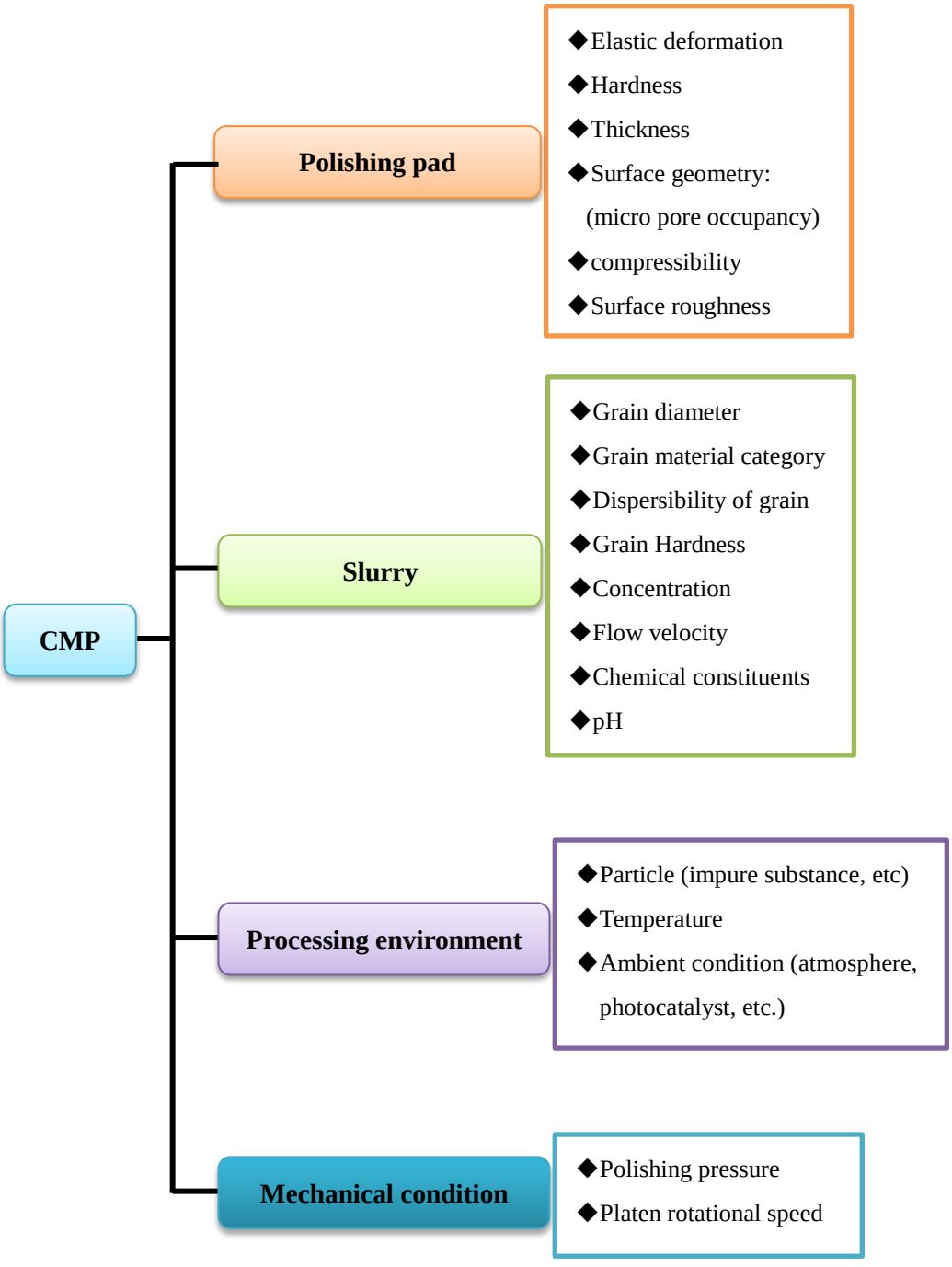

Fig.1.12 Main parameters of CMP process

1.4.3 Experimental condition settings of CMP process

In our study, the experimental conditions of CMP process shown in **Table 1.6** were employed. The apparatus LAPMASTER-15 utilized in polishing experiments is shown in **Fig.1.13.**

Table 1.6 Experimental conditions in polishing process

Work piece		**Single crystal 4H-SiC chip / Si**
Polishing machine		LAPMASTER-15
Rotational speed [min^{-1}]		50
Polishing pad		Polyurethane foamed pad (IC1000)
Polishing pressure [kPa]		120
Slurry		Colloidal silica (COMPOL-80)
	Concentration of slurry [%]	7.5
	Abrasive size [nm]	80
	pH	11
	Flow rate [mL/min]	5
Processing atmosphere		Air

Fig.1.13. Exterior of polishing equipment LAPMASTER-15

The weight difference before and after CMP process was checked for MRR evaluation. The product type of the balance used in our experiments is SHIMADZU AUW220D shown in **Fig.1.14**, which has a weight measurement range of 1mg~220g, as well as a resolution of 0.01mg. The MRR was calculated by formula (1).

$$\text{Removal rate (nm/min)} = \frac{Weight\ difference\ before\ and\ after\ polishing\ (g)}{Density\ (g/cm^3) \times Wafer\ area\ (cm^2) \times Polishing\ time\ (min) \div 10^{-7}}$$

Where, the density of SiC is 3.21g/cm^3. (1)

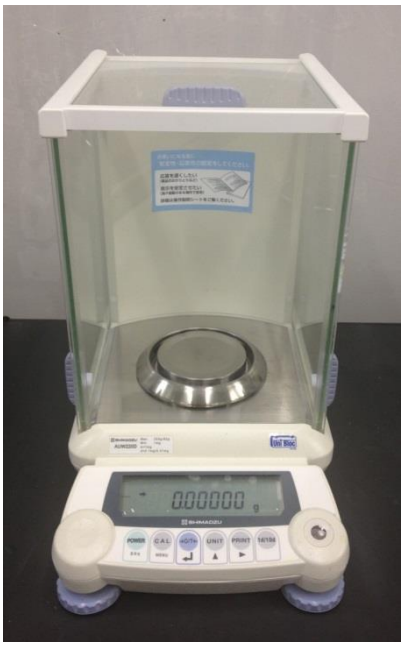

Fig.1.14. Exterior of weight measurement equipment SHIMADZU AUW220D

Reference

[1] http://semicon.jeita.or.jp/statistics/docs/20150602WSTS.pdf

[2]Hiroyuki Matsunami, Technology of semiconductor SiC and Its application, Nikkan Kogyo Shimbun

[3]T. Maiman. Stimulated optical radiation in ruby [J]. Nature 1960, 187 (4736):493～494

[4] R. Fork , C. Cruz , P. C. Becker et al. Compression of optical pulses to six femtoseconds by using cubic phase compensation [J]. Opt. Lett., 1987, 12 (7):483～485

[5] K. M. Davis, K. Miura, N. Sugimoto, and K. Hirao, Writing waveguides in glass with a femtosecond laser, Optics Letters Vol. 21, Issue 21, pp. 1729-1731 (1996)

[6] E. N. Glezer, M. Milosavljevic, L. Huang, R. J. Finlay, T.-H. Her, J. P. Callan, and E. Mazur, Three-dimensional optical storage inside transparent materials, Optics Letters Vol. 21, Issue 24, pp. 2023-2025 (1996)

[7]Hong-Bo Sun, and Satoshi Kawata, Two-Photon Laser Precision Microfabrication and Its Applications to Micro–Nano Devices and Systems, JOURNAL OF LIGHTWAVE TECHNOLOGY, VOL. 21, NO. 3, MARCH 2003

[8] M. Masuda, K. Sugioka , Y. Cheng, T. Hongo, K. Shihoyama, H. Takai, I. Miyamoto, K. Midorikawa, Direct fabrication of freely movable microplate inside photosensitive glass by femtosecond laser for lab-on-chip application, Appl. Phys. A 78, 1029–1032 (2004)

[9] G Mainfray and G Manus, Multiphoton ionization of atoms, Rep. Prog. Phys. 1991, 54(10)1333~1372.

[10] Y.Y. Dong, P. Molian, Coulomb explosion-induced formation of highly oriented nanoparticles on thin films of 3C–SiC by the femtosecond pulsed laser, Appl. Phys. Lett., 84 (2004), p.10

[11] W. G. Roeterdink, L. B. F. Juurlink, O. P. H. Vaughan, J. Dura Diez, M. Bonn, and A. W. Kleyn, Coulomb explosion in femtosecond laser ablation of Si (111), Appl. Phys. Lett. 82, 4190 (2003)

[12] E.M. Snyder, S. Wei, J. Purnell, S.A. Buzza, A.W. Castleman Jr, Femtosecond laser-induced Coulomb explosion of ammonia clusters, Chemical Physics Letters 248 (1996) 1-7

[13] Lilia C. Courrol, Everson B. dos Santos, Ricardo E. Samad, Izilda M. Ranieri, Laércio Gomes, Anderson Z. de Freitas, Sônia L. Baldochi, Nilson D. Vieira Júnior, Stabilized color centers created by high-intensity ultra-short pulse laser in pure YLF crystals,Journal of Luminescence 122–123 (2007) 318–321

[14] J. Dickinson, S. Orlando, S. Avanesyan et al. Color center formation in soda lime glass and NaCl single crystal s with femtosecond laser pulses [J]. Appl. Phys. A , 2004 , 79 (426) :859～864

[15] E. N. Glezer and E. Mazur, Ultrafast-laser driven micro-explosions in transparent materials, Applied Physics Letters, Vol. 71, p. 882, 1997

[16] Hengchang Guo, Hongbing Jiang, Ying Fang, Chao Peng, Hong Yang, Yan Li and Qihuang Gong, The pulse duration dependence of femtosecond laser induced refractive index modulation in fused silica, Journal of Optics A: Pure Appl. Opt.2004, 6 787

[17]C. Schaffer, A. Brodeur, J. Garcia et al. Micromachining bulk glass by use of femtosecond laser pulses with nanojoule energy [J]. Opt. Lett., 2001, 26 (2):93～95

[18]K. Miura, J. Qiu , H. Inouye et al . . Photowritten optical waveguides in various glasses with ult rashort pulse laser [J] .Appl. Phys. Lett., 1997, 71 (23):3329～3331

[19]A. St relt sov, F. Borrelli. Study of femtosecond laser written waveguides in glasses [J].J. Opt. Soc. Am. B, 2002, 19(10):2496～2504

[20] Yves Bellouard, and Max-Olivier Hongler,Femtosecond-laser generation of

self-organized bubble patterns in fused silica, 28 March 2011 / Vol. 19, No. 7 / OPTICS EXPRESS 6807

[21] E. Toratani, M. Kamata, M. Obara. Self-fabrication of void array in fused silica by femtosecond laser processing [J]. Appl. Phys. Lett., 2005, 87 (17):171103

[22] Catalina Albua, Adrian Dinescu, Mihaela Filipescu, Magdalena Ulmeanu, Marian Zamfirescu, Periodical structures induced by femtosecond laser on metals in air and liquid environments, Applied Surface Science 278 (2013) 347–351

[23] Xin Jia, Lingling Dong, Fabrication of complex micro/nanopatterns on semiconductors by the multi-beam interference of femtosecond laser, Physics Procedia 56 (2014) 1059 – 1065

[24] X.D. Guo, R.X. Li, Y. Hang, Z.Z. Xu, B.K. Yu, H.L. Ma, X.W. Sun, Raman spectroscopy and luminescent properties of ZnO nanostructures fabricated by femtosecond laser pulses, Materials Letters 61 (2007) 4583–4586

[25] Vladimir Lebedev, Yauhen Katsiashou, Viktoryia Makarevich, Generation of regular femtosecond pulses in AlGaInP semiconductor laser, Optics Communications,Volume 284, Issue 12, 1 June 2011, Pages 3008–3010

[26] Chengyun Zhang, JianwuYao, ShengLan, VyacheslavA. Trofimov, TatianaM.Lysak, Effects of plasma confinement on the femtosecond laser ablation of silicon, Optics Communications 308(2013)54–63

[27] Yuncan Ma, Jinhai Sib, Xuehui Sun, Tao Chen, Xun Hou, Progressive evolution of silicon surface microstructures via femtosecond laser irradiation in ambient air, Applied Surface Science 313 (2014) 905–910

[28] Xu Ji, Lan Jiang, Xiaowei Li, Weina Han, Yang Liu, Andong Wang, Yongfeng Lu, Femtosecond laser-induced cross-periodic structures on a crystalline silicon surface under low pulse number irradiation, Applied Surface Science 326 (2015) 216–221

[29] J. Bonse, S. Baudach, J. Krüger, W. Kautek, M. Lenzner, Femtosecond laser

ablation of silicon–modification thresholds and morphology, Appl. Phys. A 74, 19–25 (2002)

[30] G.R.B.E. Römer, A.J. Huis in't Veld, J. Meijer, M.N.W. Groenendijk, On the formation of laser induced self-organizing nanostructures, CIRP Annals – Manufacturing Technology 58 (2009) 201–204.

[31] H.X. Qian, W.Zhou, H.Y.Zheng, X.R.Zeng, H.C.Sheng, Evolution of periodic structures on InP(100) surface irradiated with femtosecond laser, Materials Letters 124 (2014) 235–238

[32] P. Simon, J. Ihlemann, Ablation of submicron structures on metals and semiconductors by femtosecond UV-laser pulses, Applied Surface Science 109r110 1997. 25–29

[33] A.Y. Vorobyev, C. Guo, Femtosecond laser structuring of titanium implants, Applied Surface Science 253 (2007) 7272–7280.

[34] R. Serra, V. Oliveira, J.C. Oliveira, T. Kubart, R. Vilar, A. Cavaleiro, Large-area homogeneous periodic surface structures generated on thesurface of sputtered boron carbide thin films by femtosecond laserprocessing, Applied Surface Science 331 (2015) 161–169

[35] M. Huang, F. Zhao, Y. Cheng, N. Xu, Z. Xu, Origin of laser-induced near-subwavelength ripples: interference between surface plasmons and incident laser, ACS Nano 3 (2009) 4062–4070.

[36] J. M. Li, J. T. Xu, Self-organized nanostructure by a femtosecond laser on silicon, Laser Phys. 19 (2009) 121–124.

[37] Olga Varlamova, Florenta Costache, Jürgen Reif, Michael Bestehorn, Self-organized pattern formation upon femtosecond laser ablation by circularly polarized light, Applied Surface Science, Volume 252, Issue 13, 30 April 2006, Pages 4702–4706

[38] X.D. Guo, R.X. Li, Y. Hang, Z.Z. Xu, B.K. Yu, H.L. Ma, B. Lu, X.W. Sun, Femtosecond laser-induced periodic surface structure on ZnO, Materials Letters

62 (2008) 1769–1771

[39] Haugen, Subwavelength ripple formation on the surfaces of compound semiconductors irradiated with femtosecond laser pulses, Appl. Phys. Lett. 82 (2003) 4462–4464.

[40] J. Reif, F. Costache, M. Henyk, S.V. Pandelov, Ripples revisited: non-classical morphology at the bottom of femtosecond laser ablation craters in transparent dielectrics, Applied Surface Science 197 (2002) 891–895.

[41] T.Q. Jia, F.L. Zhao, M. Huang, H.X. Chen, J.R. Qiu, R.X. Li, Alignment of nanoparticles formed on the surface of 6H-SiC crystals irradiated by two collinear femtosecond laser beams, Appl. Phys. Lett., 88 (2006), p. 111117

[42] M Huang, F L Zhao, T Q Jia, Y Cheng, N S Xu and Z Z Xu, A uniform 290 nm periodic square structure on ZnO fabricated by two-beam femtosecond laser ablation, Nanotechnology 18 (2007) 505301 (6pp)

[43] X.J. Wu, T.Q. Jia, F.L. Zhao, M. Huang, N.S. Xu, H. Kuroda, Z.Z. Xu, Formation mechanisms of uniform arrays of periodic nanoparticles and nanoripples on 6H-SiC crystal surface induced by femtosecond laser ablation, Appl. Phys. A86, 491–495 (2007)

[44] Go Obara, Hisashi Shimizu, Taira Enami, Eric Mazur, Mitsuhiro Terakawa, and Minoru Obara, Growth of high spatial frequency periodic ripple structures on SiC crystal surfaces irradiated with successive femtosecond laser pulses, Optics Express Vol. 21, Issue 22, pp. 26323-26334 (2013)

[45] http://www.amplitude-systemes.com/t-pulse-oscillators.html

CHAPTER 2

FEMTOSECOND LASER PROCESSING FOR SIC SUBSTRATE (SI-FACE)

-Surface morphology evolution after laser irradiation at different conditions-

2.1 Introduction

We firstly elaborated the evolution of surface morphologies of semiconductor material SiC substrate by fs laser irradiation patterns of single point irradiation, single line scanning and plane scanning. We further demonstrated that the ripples distribution was irrelevant to laser scanning direction and SiC crystal direction. Furthermore, we carried out experiments at series of femtosecond laser processing parameters such as different scanning pitches, different scanning velocities, different repetition rates, and different fluences to investigate the surface morphology changes of SiC substrate. The dependences of Laser Induced Periodic Surface Structures (LIPSS) on energy deposition at the overlapped areas of interval laser pulses corresponding to different laser processing parameters were investigated. The uniformity of the large-area LIPSS structures was also discussed. The horizontal LIPSS structures induced in Transverse irradiation mode processing were further fabricated during Cross-scan irradiation mode process into new LIPSS structures which were still in accordance with laser scanning orientation. It should be noted that laser-induced debris after Transverse irradiation mode processing played an important role in surface formation of Cross-scan irradiation mode. Femtosecond laser irradiation on 4H-SiC substrate at near-threshold fluence was also investigated.

We proposed different combinations of scanning speeds and scanning times of femtosecond laser irradiation for SiC substrate, and investigated the irradiation effects.

These experimental results will play a paramount role on further research of micro/nano patterns fabrication of semiconductor materials 4H-SiC. From referential point of view, it is inspiring to understand the formation mechanism of nanostructure morphology induced by femtosecond laser on 4H-SiC and has a potential for further application. These data were expected to provide important prospects for further study related to femtosecond laser processing for wide-bandgap semiconductor 4H-SiC substrate.

2.2 Experiment

2.2.1 Introduction for experiment

We carried out laser irradiation experiments on silicon carbide (SiC) surface with wavelength of 1030nm, pulse duration of 373fs and different pulse repletion rates. The schematic diagram of femtosecond laser experimental equipment is shown in **Fig.2.1**.The symmetric Gaussian distribution laser beam was controlled by a metallic shutter after it passed out from Pulse Picker used for adjusting laser parameters. This fast rotary solenoid drove metallic shutter was used to control the access of laser beam to attenuator consisted neutral density filters. The output power of the perpendicularly incident laser beam was controlled by adjusting the intensity of input electricity and the combination of variable neutral density filters. The laser beam was delivered through an optical mirror system and travelled through a

microscope objective (0.42 NA 50x) with a work distance of 17mm. Then the laser beam with a spot size of about 3μm was irradiated perpendicularly onto as-polished SiC substrate mounted on a computer-controlled XYZ axes system. This computer-controlled three-dimensional XYZ transfer stage consists of XY orthogonal stage and Z stage. The maximum and minimum displacements of XY stage are 100mm and 10nm respectively, with a maximum scan speed of 300mm/s and combined resolution of 1nm. The maximum and minimum displacements of Z stage are 4.8mm and 60nm respectively, with a maximum scan speed of 5mm/s and combined resolution of 0.1μm. A charge coupled device (CCD) camera was connected to optical observation system to monitor the real laser processing situation. During laser processing a specially designed program was prepared for controlling the scanning trajectory of the focused laser beam. As shown in **Fig.2.2**, after each laser processing of horizontal direction, the beam scanning trajectory was changed into vertical direction, and then it was controlled for another horizontal direction process.

The interval between adjacent beam scanning trajectories is called Pitch here, as shown in **Fig.2.2**. Single point, single line and plane irradiation experiments were carried out at laser fluence of 0.44 J/cm^2 and a repetition rate of 10MHz. Experiments for investigating the dependence of ripples distribution on scanning and crystal direction were carried out at a fluence of 1.75 J/cm^2, a pulse repetition rate of 500 kHz and scanning speed of 100mm/s.

SiC substrates (as-polished Si-face) were irradiated by femtosecond laser at different laser processing pitches (4, 3, 3.5, 2.5, 2, 1.5, 1, 0.5, 0.2, 0.1, 0.05, unit: μm), different scanning speed scanning velocities (300, 200, 100, 50, 25, 10, 5, 2, unit: mm/s), and different pulse repetition frequencies (100 kHz, 500 kHz, 1 MHz) for LIPSS structures investigation. After femtosecond laser irradiation, SiC substrates were cleaned in deionized water by ultrasonic for 1 hour to remove the laser-induced debris for further morphology observation by scanning electron microscope (SEM).

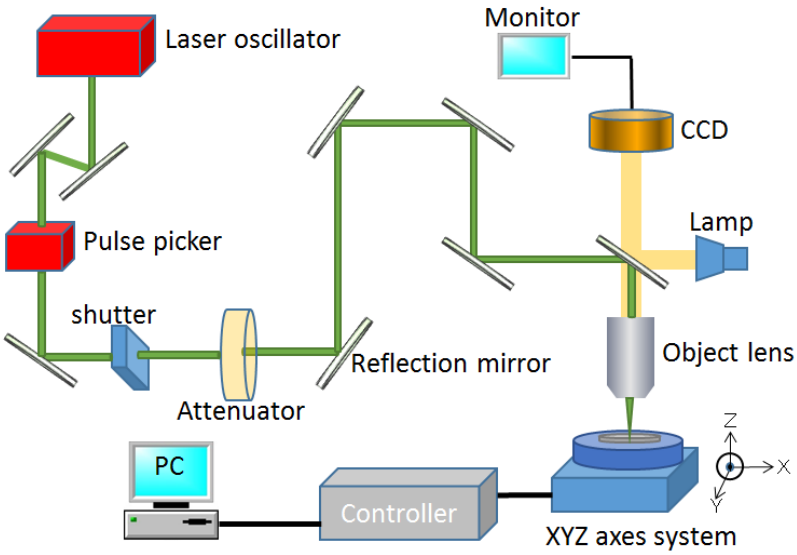

Fig.2.1. Schematic diagram of femtosecond laser experimental equipment

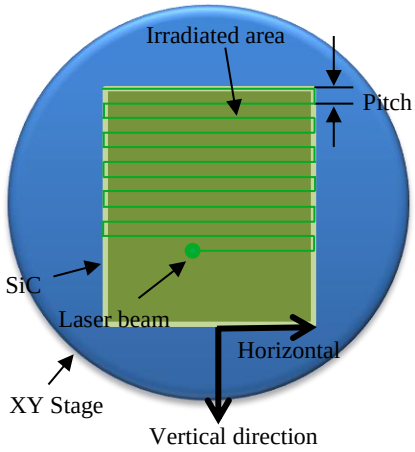

Fig.2.2. Vertical view of XYZ axes stage

2.2.2 Principle of SEM

The observation equipment of SEM adopted in our experiment is shown in **Fig.2.3**. Its main structure is shown in **Fig.2.4**. Electron beam from electronic gun is firstly converged by electronic lens. Then the direction of the focused electron beam is changed by the magnetic field yielded in the scanning coil. The focused beam is scanned on the surface of specimen. During this scanning process, secondary electrons will be emitted. The generation rate of secondary electrons mainly depends on the surface morphology of the specimen. A detector is adopted for collecting and signalizing the secondary electrons for final output by monitor.

Fig.2.3 Exterior of SEM

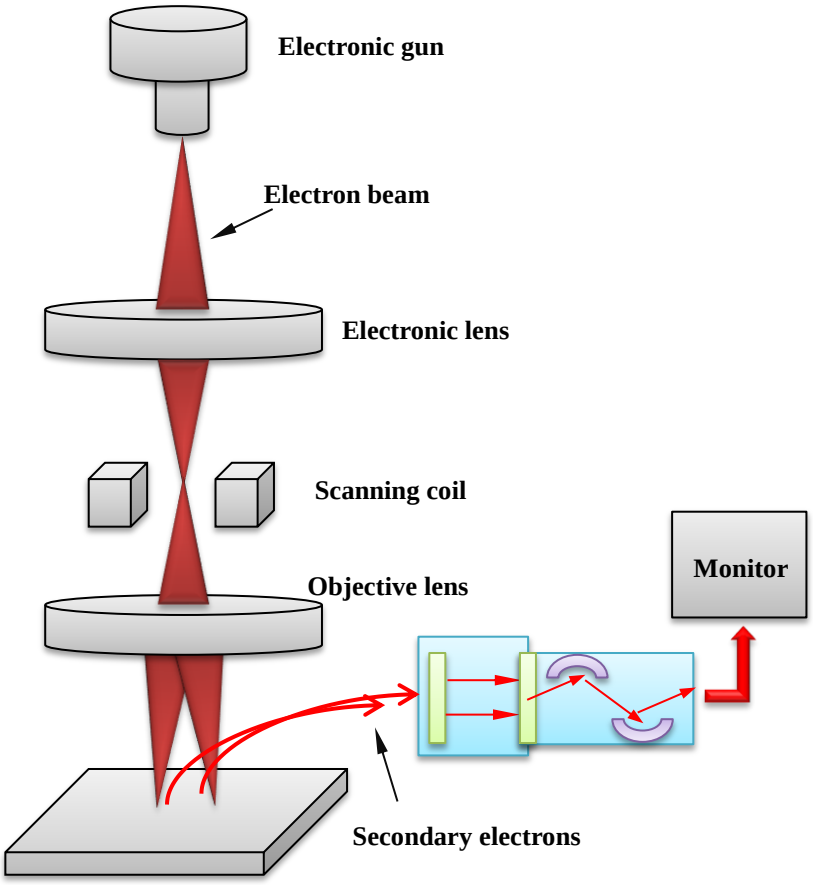

Fig.2.4 schematic diagram structure of SEM

2.3 Results and discussion

2.3.1 Femtosecond laser process for single point, single line and plane irradiation

As shown in **Fig.2.5**, fs laser ablations were carried out at laser fluence of 0.44 J/cm^2 and a repetition rate of 10MHz. After single point irradiation shown in **Fig.2.5** (a), a crater was induced by fs laser with ambient fine spattering debris. After ultrasonic cleaning in deionized water for 1 hour, the debris was removed, remaining large consolidation grains around the crater with a diameter of approximately 6μm. During laser irradiation, coulomb explosion, accompanied with ultrafast melting [1] and free electron heating took place in femtosecond laser machining [2]. Coulomb explosion induced by the absorption of surface defects [3] and multiphoton absorption intensely occurred during laser irradiation on SiC surface. Ejection of substantial debris accompanying with phase change was attributed to the interaction between laser beam and laser-excited intense plasma [2]. The material on SiC surface was removed according to ultrafast laser melting, vaporization, photomechanical fragmentation and coulomb explosion [3]. As shown in **Fig.2.5** (d), the ambient SiC crystal lattice was transferred to thermal motion by excited electrons during extremely short time expected as many picoseconds [4]. During multiphoton ionization and free electron heating, emission of free electron and laser energy deposition with no equilibrium resulting from ultrafast energy irradiation yielded intense plasma [2]. Agglomerative grains could not be thoroughly removed even though it was cleaned by using ultrasonic for 1 hour, indicating that the debris

firstly triggered during coulomb explosion resulting in phase explosion and collateral thermal damage [3] was further recast and consolidated. Solid-gas-solid transformation and re-solidification were assumed to be responsible for this phenomenon. Meanwhile, debris was also observed after 100 mm/s laser irradiation of one line scanning and surface scanning, as shown in **Fig.2.5** (b) and **Fig.2.5** (c). A groove of about 4μm and LIPSS structures less than 200nm were respectively observed after ultrasonic cleaning. As shown in **Fig.2.5** (e), LIPSS structures [5, 6] induced by high energy density region of Gauss distribution laser beam was also observed at the bottom of the groove; meanwhile, irregular coarse side wall of the groove was induced due to ambient low energy density region of Gauss distribution fs laser beam.

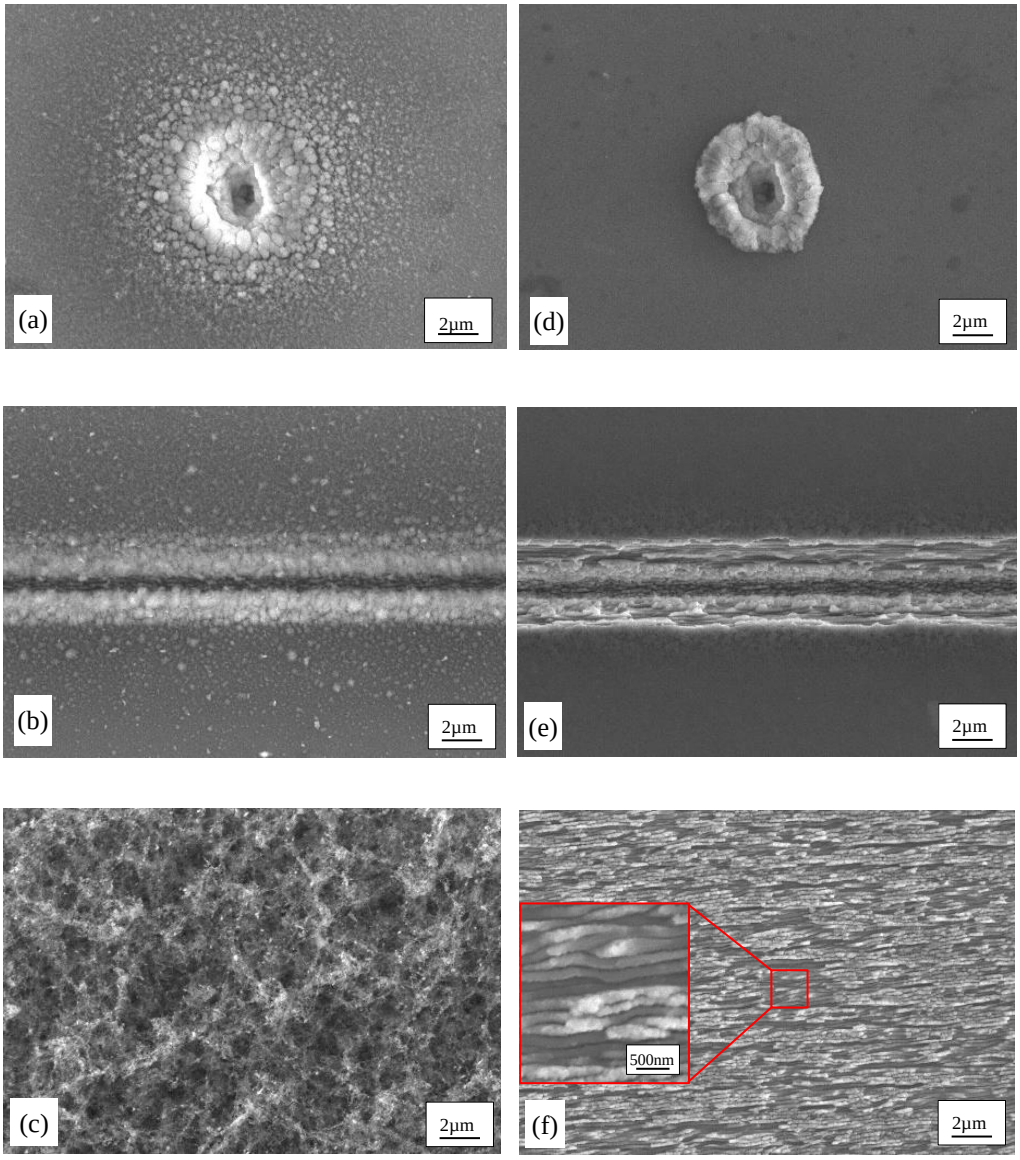

Fig.2.5 SEM images of Si-face ablated at fs laser fluence of 0.44 J/cm^2.
(a) Single point irradiation, (b) one line scanning, and (c) plane scanning indicates uncleaned surfaces.(d), (e) and (f) respectively indicate images corresponding to (a), (b) and (c) after 1 hour ultrasonic cleaning

2.3.2 Investigation for the effects of laser's scanning direction and crystal orientation on ripples structure.

Fig.2.6 shows the distribution of laser-irradiated marks at different direction in surface of single crystal SiC substrate. All of these kinds of marks were irradiated by femtosecond laser at a fluence of 1.75 J/cm^2, a pulse repetition rate of 500 kHz, a wave length of 1030nm, a pulse duration of 373 fs and scanning speed of 100mm/s. After femtosecond laser irradiation, periodic ripple structures emerged in the substrate surface. The width of the laser-induced mark was about 2.5μm, while the width of periodic ripples less than 200nm. Even though the same surface was irradiated by femtosecond laser at different scanning directions, the arrangement direction of ripples are all horizontal. The arrangement direction of ripples is independent on scanning direction and crystal direction.

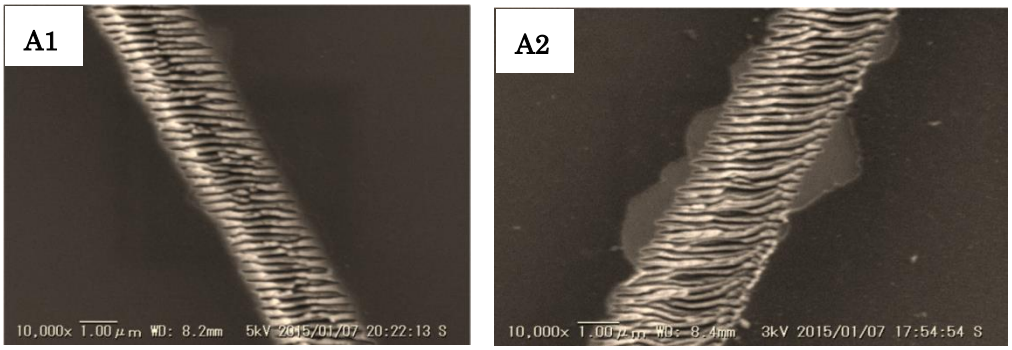

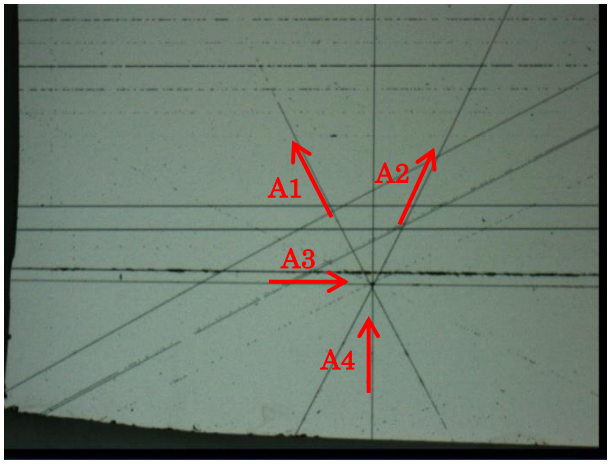

Fig.2.6
Distribution of laser-induced ripples after different direction laser scanning.

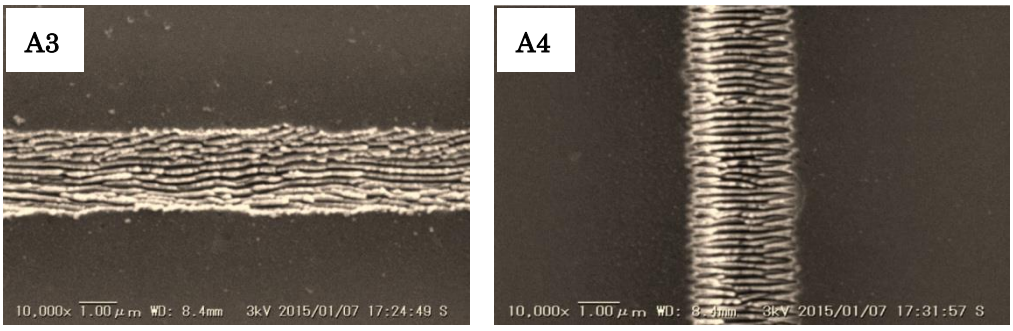

2.3.3 Evaluation of surface morphology at different laser process parameters.

2.3.3.1 The effect of different scanning pitches on surface morphology

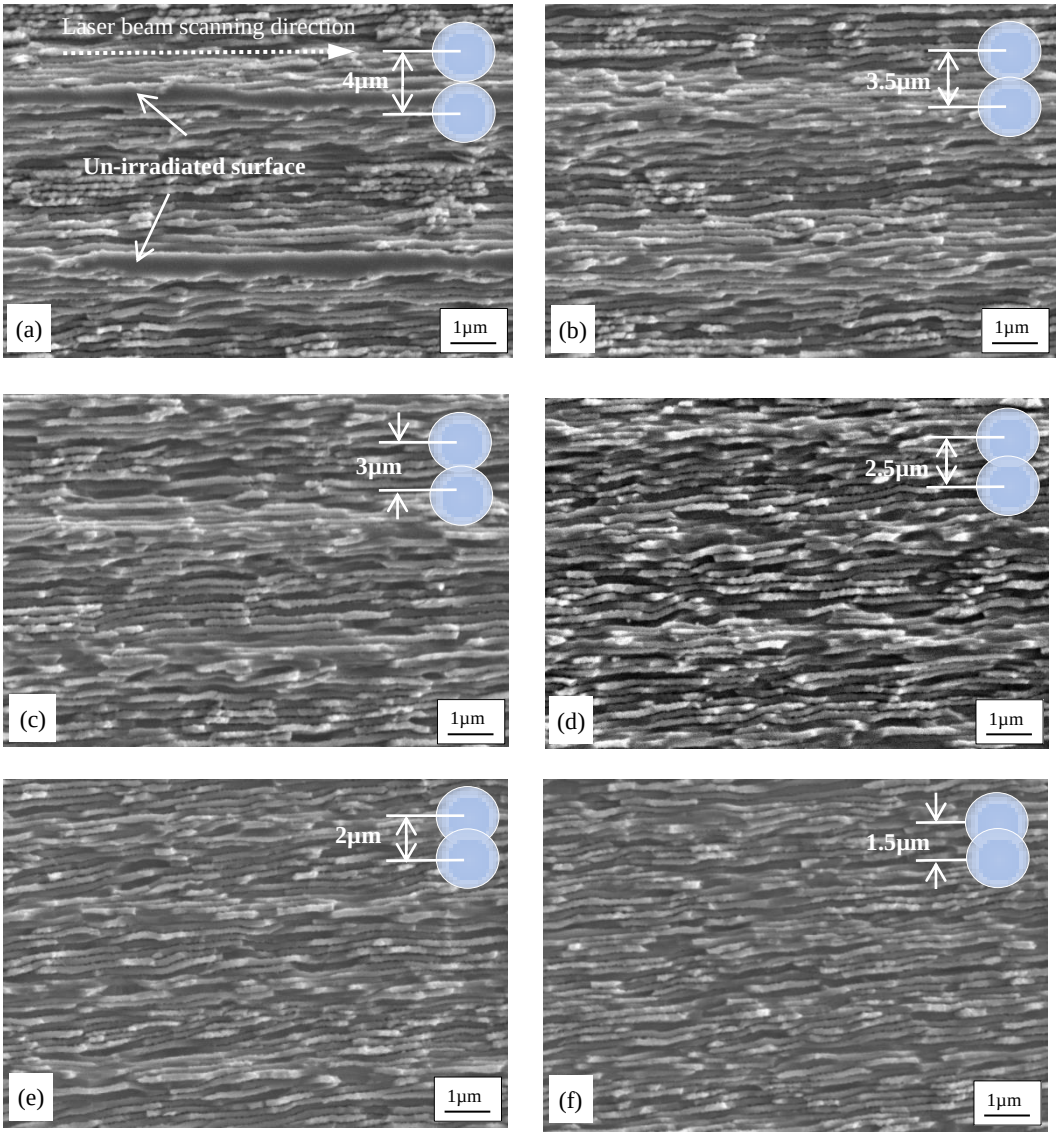

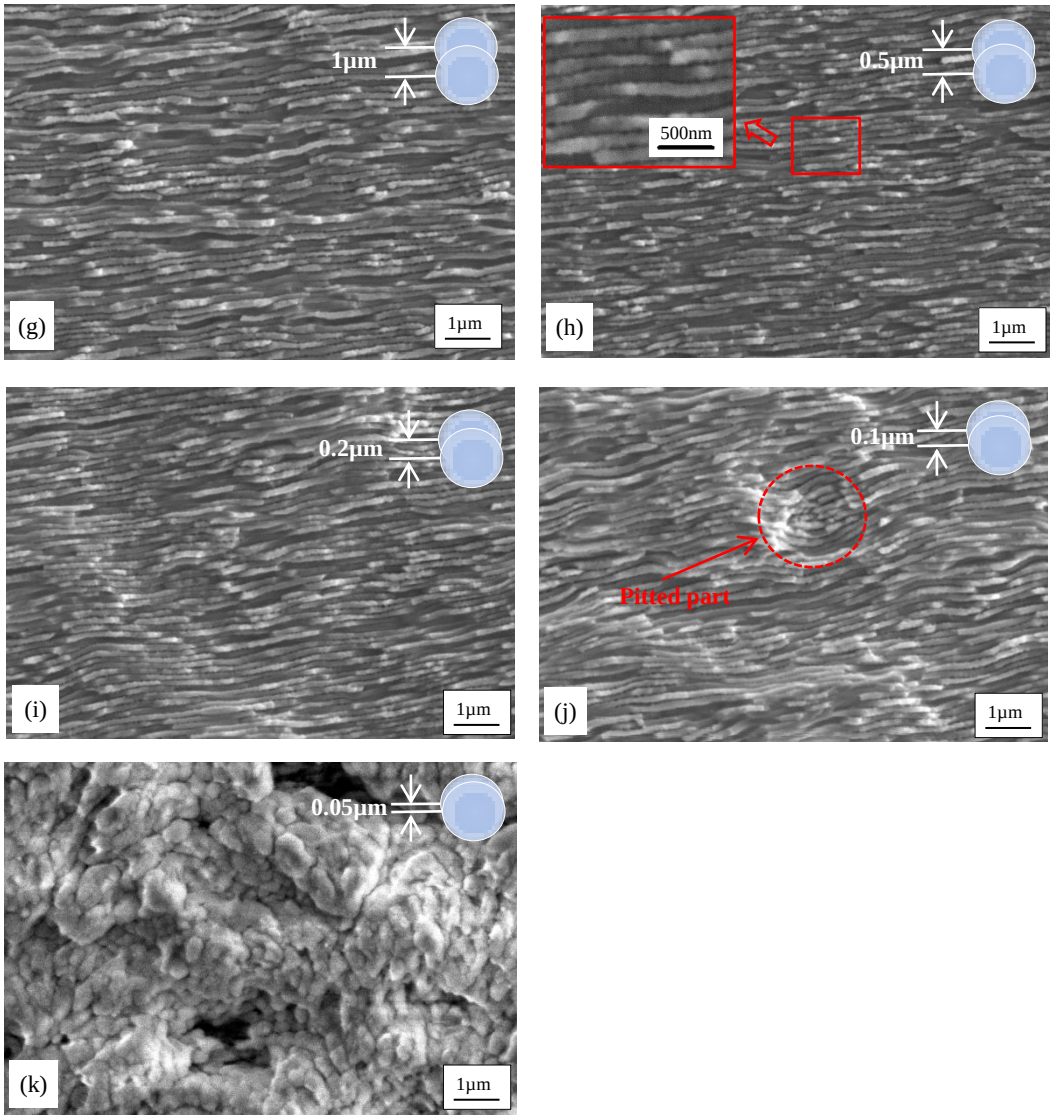

Fig.2.7 SEM images of femtosecond laser irradiated areas at different pitches with a fluence 0.44 J/cm^2. (a) 4μm; (b) 3.5μm; (c) 3μm; (d) 2.5μm; (e) 2μm; (f) 1.5μm; (g) 1μm; (h) 0.5μm; (i) 0.2μm; (j) 0.1μm; (k) 0.05μm.

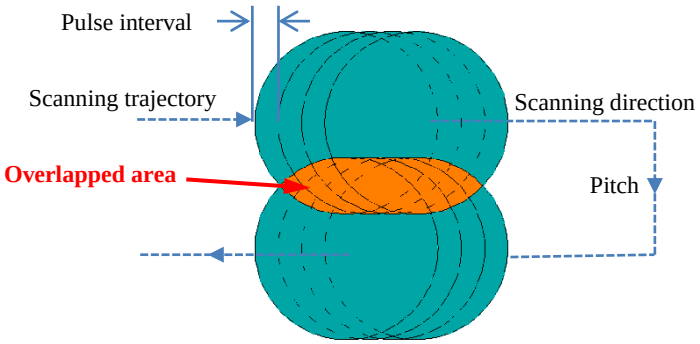

Fig.2.8. Schematic diagram of the overlapped area between two adjacent laser scanning trajectories

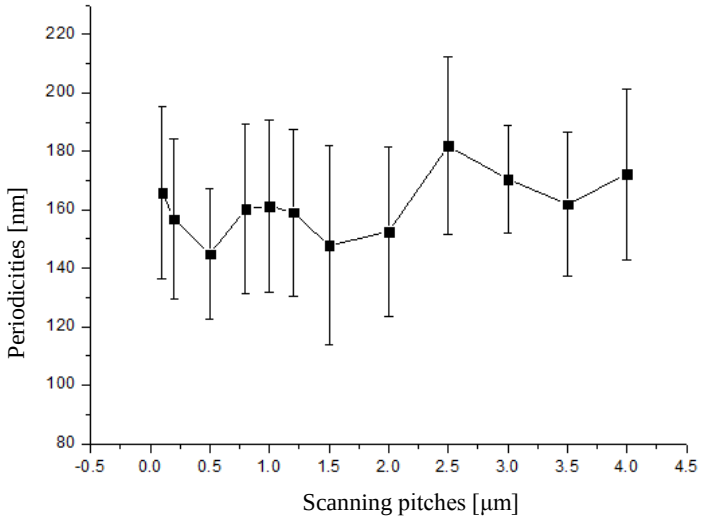

Fig.2.9 Dependence of spatial periodicity on scanning pitches for fine ripples on SiC Si-face

Fig.2.7 shows the evolution of periodic nanostructures induced by fs laser at different scanning pitches. All of these areas were irradiated by femtosecond laser with a pulse repetition frequency of 10 MHz, a fluence of 0.44 J/cm^2, and a scanning speed of 100mm/s in the same scanning direction with different scanning pitches of 4μm, 3.5μm, 3μm, 2.5μm, 2μm, 1.5μm, 1μm, 0.5μm, 0.2μm, 0.1μm, and 0.05μm,

respectively. Comparing SEM images of **Fig.2.7** (b) and **Fig.2.7** (c), it is found that the surfaces were wholly ablated, becoming much flatter than that of **Fig.2.7** (a) gradually, in which the surface of SiC was not wholly fabricated, remaining the un-ablated parts. It is proposed that smaller scanning pitch led the surfaces to be more repeatedly ablated due to larger overlapped area shown in **Fig.2.8**, in which the laser-induced ripples were refabricated. Dependence of spatial periodicity on laser scanning speed for the ripples shown in **Fig.2.9** indicates that the average periodicities of LIPSS structures range from 145nm to 181 nm. Even though the laser processes were carried out with different scanning pitches, the periodicity of periodic nanostructures didn't change greatly. Additionally, it should be noted that the periodic nanostructures with an average inclined angle of approximately 5°~10° were observed. Simultaneously, as shown in **Fig.2.7** (i), the periodic nanostructures started to become wave-like nonlinear patterns with inclined angle of about 10° after fs laser ablation with scanning pitch of 0.2μm. Some parts of the wave-like nonlinear nanostructures became discontinuous after fs laser ablation with scanning pitch of 0.1μm, accompanying with inclined ripples and the emergence of pitted part shown in **Fig.2.7** (j). This was presumed that the ablated surface affected the further formation of LIPSS structures [7]. During fs laser ablation, the previously laser-induced nanoscale ripples of the overlapped area were ablated repeatedly by higher laser intensity with smaller scanning pitches, resulting in newly-fabricated nanoripples with similar periodicities. The interaction of fs laser with the previously induced nanoripples has not been reported yet. It was presumed that harmonic

generation [5] would be also changed by the existing nanoripples when yielding new nanoripples. Different second harmonic generation and electric field redistribution were subsequently triggered by different laser energy distribution during different scanning process, which attributed for the wave-like nonlinear nanostructures and the emergence of pitted part. This was responsible for the significant distribution of surface morphologies during fs laser ablation. As shown in **Fig.2.7** (k), large amount of agglomeration come into being with no any periodic nanoscale patterns after fs laser ablation with scanning pitch of 0.05μm. Solid-gas-solid transformation and resolidification were assumed responsible for this phenomenon especially at extremely high pulse repetition rate of 10 MHz. During fs laser irradiation, fs laser energy was deposited instantly into the SiC surface by a host of pulses.

Comparing these experimental results, the scanning pitches during laser processing played an important role in fabricating the LIPSS structures during laser processing of smaller scanning pitches. As the scanning pitch was set bigger than (or similar with) the width of periodic nanostructure 160 nm, nanoscale structures could be formatted, as shown in **Fig.2.7** (a) **Fig.2.7** (b), **Fig.2.7** (c), **Fig.2.7** (d), **Fig.2.7** (e) **Fig.2.7** (f), **Fig.2.7** (g), **Fig.2.7** (h), **Fig.2.7** (i), **Fig.2.7** (j), and **Fig.2.7** (k); whereas if the scanning pitch was set far shorter than the width of periodic ripples, like that shown in **Fig.2.7** (k), nanostructures could not be successfully induced by femtosecond laser on SiC substrate surface. It is proposed that smaller scanning pitch (P=0.05μm) contributed for facilitating more frequent laser irradiation at higher fluence to the overlapped areas, accompanying with material solid-gas-solid

transformation, melt, resolidification on account of extremely high temperature and strong electric field at the focused laser beam spot.

Mie scattering from surface defects induced by laser irradiation on N-doped 4H-SiC (0001) accounted for High Special Frequency Periodic Ripples (HSFL) growth, simultaneously decreased the damage fluence in coordination with optical absorption [6]. However, in our experiments, the average periodicity of the periodic nanostructures induced by fs laser ranges approximately 160nm, which was far shorter than the wavelength (1030nm) of incident laser beam. Thus, it was conceivable that Mie scattering could not be induced by ripple structures at the over lapped areas according to its generation mechanism. According to literature [5], evolvement of 6H-SiC surface morphology fabricated by fs laser was elucidated. Linearly polarized lasers with different wavelengths such as 400 nm (0.9 μJ/pulse), 510 nm (1.0 μJ/pulse) and 800 nm (4.0 μJ/pulse) were respectively employed, aiming to prove the mechanism of second-harmonic generation during fs laser irradiation. LIPSS structures with spatial periodicities of 80, 100 and 150 nm were respectively triggered, revealing that the spatial periodicities of nanostructures were dependent on fs laser wavelengths. It was suggested that second-harmonic generation of the incident laser beam was dominant of periodic nanostructures formation on 6H-SiC crystal surface [5]. Moreover, harmonic generation was also presented to be able to scale down the size of highly oriented spherical nanoparticles induced on 3C-SiC by fs laser [3]. The periodicity (Λ) of parallel nanostructures was verified by formula $\Lambda=\lambda/2n$, where λ is the wavelength of incident laser, n is

refractive index. In literature [5], the periodicity of fs laser-induced nanoripples was about 1/5 of laser wavelength λ. Our serial experimental results especially shown in **Fig.2.9** indicated that the periodicities of nanoripples remain approximately 160nm, which were about 1/7~1/5.6 of the incident laser beam wavelength, suggesting that harmonic generation was a dominant factor of the nanoripples formation in these experiments.

2.3.3.2 The effect of different scanning speeds on surface morphology

As shown in **Fig.2.10**, different areas of SiC substrate were irradiated by femtosecond laser with a pulse repetition frequency of 10 MHz, a fluence of 0.44 J/cm^2, a scanning pitch of 2μm, and different scanning velocities ranging from 2 mm/s to 300 mm/s in the same scanning direction. The overlapped area of adjacent scanning trajectories (shown in **Fig.2.8**) remained the same owing to the same scanning pitch (2μm) and laser spot size, whereas the overlapped area between adjacent laser spots (shown in **Fig.2.11**) along each trajectory differed from each other on account of different scanning speeds. Even through all areas were fully irradiated by femtosecond laser, the surface morphologies differed greatly. As shown in **Fig.2.10** (a), the interval between adjacent pulses spots of each trajectory was 30nm, corresponding to the scanning trajectory of 300mm/s. From **Fig.2.10** (b) to **Fig.2.10** (f), it can also be clearly distinguished that inclined nanoscale ripples were induced. It is presumed that this was attributed to the bigger overlapped area of adjacent laser spots, which led to more energy deposition on SiC surface.

Dependence of spatial periodicity on laser scanning pitch for LIPSS structures induced on Si-faces shown in **Fig.2.12** indicates that the average periodicities of LIPSS structures range from 151nm to 181 nm. The surface morphologies didn't change greatly until the scanning speed decreased to 10mm/s. As can be seen from the evolvements revealed in **Fig.2.10** (g) and **Fig.2.10** (h), the agglomeration parts increased gradually with the decrease of scanning speeds which decreased the adjacent laser spots interval, suggesting that repeated irradiation during extremely short time in the overlapped areas contributed to more deposited energy which was responsible for solid-gas-solid transformation and re-solidification. Consequently, the surface was thoroughly covered with agglomerate substances during the lowest scanning velocity of 2mm/s, as shown in **Fig.2.10** (h).

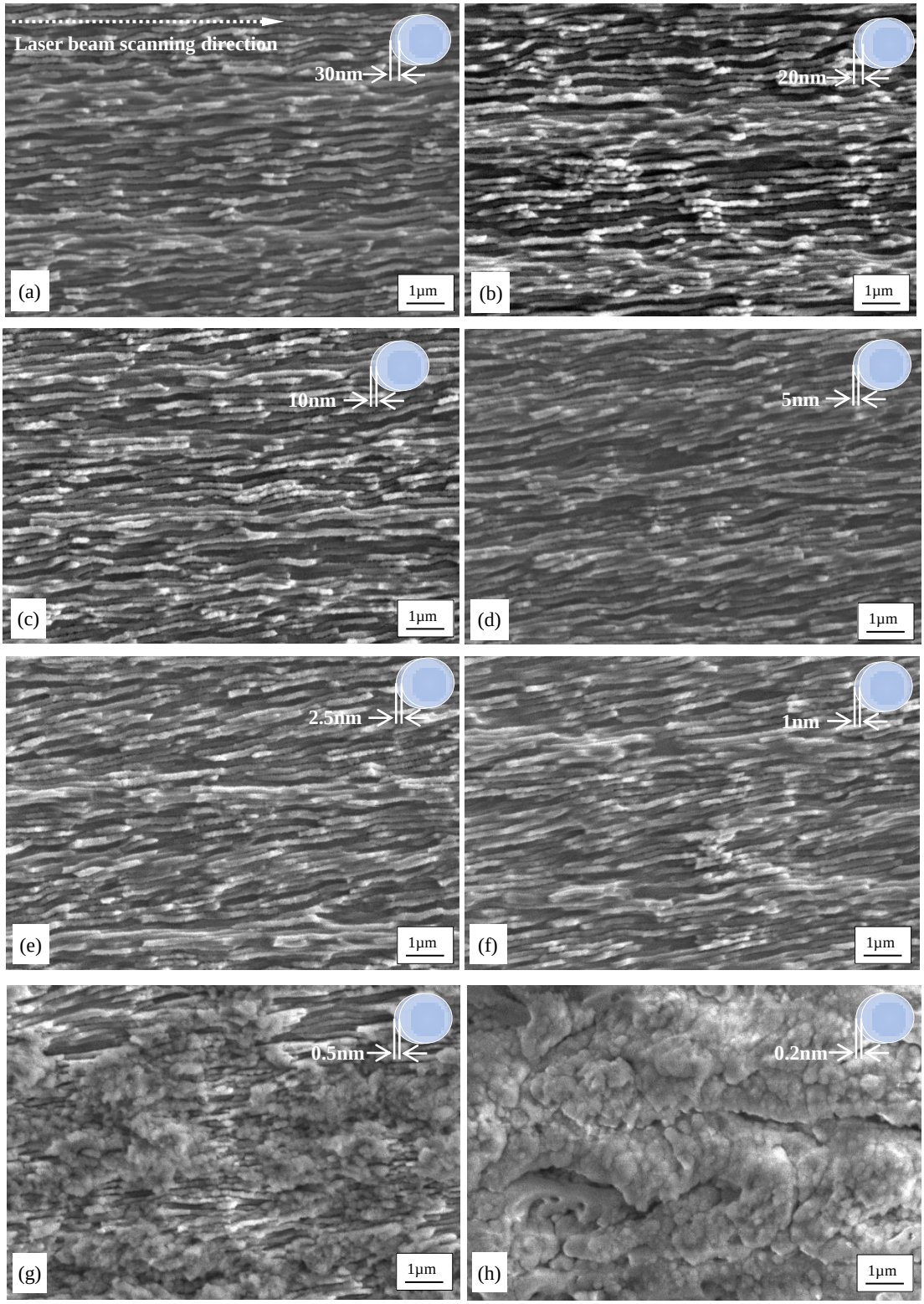

Fig.2.10. SEM images of femtosecond Laser irradiated areas at different speeds. (a)300mm/s; (b)200mm/s; (c)100mm/s; (d)50mm/s; (e)25mm/s; (f)10mm/s; (g)5mm/s; (h)2mm/s;

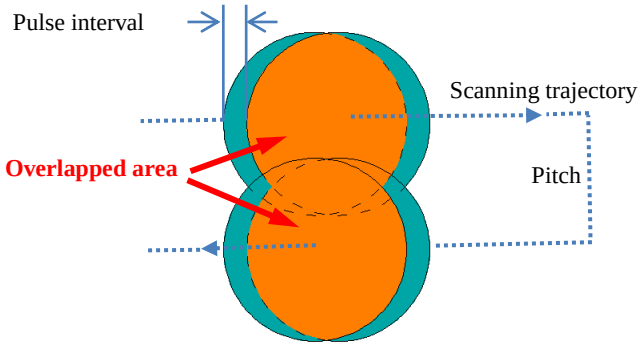

Fig.2.11. Schematic diagram of the overlapped area between two adjacent laser spots

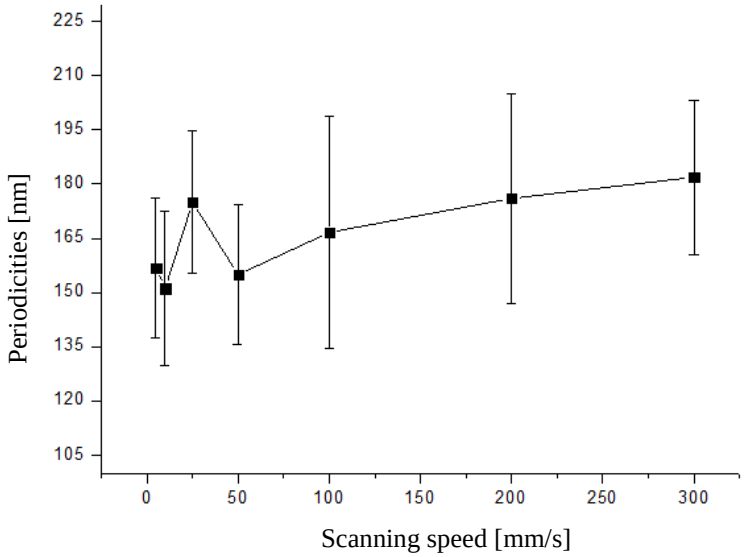

Fig.2.12. Dependence of spatial periodicity on scan speed for fine ripples on SiC Si-face

From the experimental results shown above, conclusion can be drawn that the surface morphology of 4H-SiC substrate surface could be greatly affected by different scanning speeds. Alternatively, the interaction of fs laser and materials differed greatly form different parameters. Differing from the results above, micro/nano scale patterns have been already successfully fabricated by fs laser at

much slower scanning speeds on other material surfaces. According to literature [8], low spatial frequency (LSFL) with a periodicity of 350~600 nm and high spatial frequency (HSFL) with a periodicity of 50~200 nm were induced on different metallic films surface during different ambient environment at scanning speed of V=1mm/s. Whereas literature [9] reported that microscale porous netlike structure and quasi-ordered holes ranging from 280 to 320 nm were induced on stain steel surface by fs laser with a scanning pitch of 2um, a laser fluence of 0.55 J/cm^2, and extremely slower scanning speed of 20μm/s and 320μm/s, respectively. Three basic surface topology types: nanoroughness, nanoripples (~500nm) and microspikes (1~10μm) were fabricated by a spatially asymmetrical fs laser beam (744 nm) on titanium surface at a velocity ranging from12.5 to 62.59 μm/s [10]. Microscale structures perpendicular to laser polarization with period more than two times of laser wavelength (800 nm) were induced on Si substrate after 0.25mm/s scanning [11]. Additionally, Parallel nanostructures induced by fs laser at extremely slow scanning speeds ranging from 10~50 μm/s and different fluence ranging from 0.1~1.86 Jcm^{-2} on 6H-SiC surface [12]. The authors referred that laser fluence played a critical role for obtaining the uniform and deep nanostructures. The mechanism should be studied further, toward to pulse number, scanning speed, material, and laser parameters, etc.

2.3.3.3 The effect of different repetition rates on surface morphology

As shown in **Fig.2.13**, different areas of SiC substrate Si-face were irradiated by fs laser with a scanning pitch of 1μm, different pulse repetition rates of 100 kHz, 500 kHz and 1 MHz, and a scanning speed of 100mm/s in the same scanning direction. From **Fig.2.13** (a) and **Fig.2.13** (d), it can be seen that nanoscale structures with average periodicity of approximately 440 nm were fabricated, mingling with small scale nanostructures with average periodicity of about 116 nm at pulse repetition rate of 100 kHz (1.69 J/cm^2). However, after fs laser irradiation of higher pulse repetition rate 500 kHz (1.92 J/cm^2), laser-inclined nanoscale ripples with average periodicity of about 196 nm were induced, as shown in **Fig.2.13** (b). Inclined nanoscale ripples of approximately 187 nm were further induced by fs laser after with 1MHz pulse repetition rate. According to **Fig.2.13** (a) and **Fig.2.13** (d), it should be noted that larger LIPSS structures were induced at a repetition rate of 100 kHz and a fluence of 1.69 J/cm^2. It was considered that lower fluence and bigger interval (shown in **Fig.2.11**) of adjacent pulses decreased the accumulation of laser energy deposition, further leading to weaker interaction between incident laser and crystal SiC substrate. Ripples formed by fs laser on ceramic [13], metal [14], dielectrics and semiconductors [15] exhibit periodicities following the formula (2.1).

$$\Lambda \approx \frac{\lambda}{\varphi \pm sin\theta} \quad with \ \ g \,||\, E \tag{2.1}$$

Where λ is the incident laser wavelength, $\varphi = \mathrm{Re}[\varepsilon/(\varepsilon+1)]^{1/2}$ is the real part of the effective refractive index for the surface plasmas mode, θ is laser beam

incidence angle, ε is the dielectric constant, g is grating vector, and E is the electrical field vector in incident laser beam. It is revealed that the period of laser-induced ripples rests with laser wavelength, incidence angle and effective refractive index. Formation appreciation of different LIPSS induced by fs lasers at different pulse numbers and wavelengths on the surfaces of semiconductors Si, InAs, Inp, and GaP were elucidated. In literature [16], the effects of fs laser (λ = 515 nm, τ = 250 fs, 100 kHz) pulse number were also investigated. It is found that fine ripples (roughly 120~155 nm (λ/4.3 – λ/3.3)) transformed into coarse ripples (about 420–520 nm) on 6H-SiC when the increased pulse number was over 10 at a fluence of 1.17 J/cm^2. The spatial periodicity of coarse ripples ranging from 600 to 760nm increased when laser pulse numbers decreased, whereas the periodicity was not subject to laser fluence. Fine ripples of approximately 140nm were formed on SiC surface with small pulse numbers N=25–100 and low fluence of about 0.2 J/cm^2~0.4 J/cm^2 by fs laser (λ = 800 nm, τ = 37 fs, 10 Hz) [17]. In document [5], periodic nanostructures with different periodicities (80, 100 and 150 nm) were induced corresponding to different wavelengths (400, 510 and 800 nm) of linearly polarized fs lasers (τ = 130 fs, 1 kHz) on 6H-SiC, indicating that the periodicity of nanostructures were dependent on fs laser wavelengths. A tend was found that the spatial periodicities of induced ripples increased with fs laser wavelengths [18].literature [11] reported that fs laser (λ = 800 nm, τ = 100 fs) induced microscale structures perpendicular to laser polarization as well as structures parallel to laser polarization, accompanying with periods more than two times of laser wavelength and periods close to laser

wavelength respectively on silicon surface at lower repetition rate 1kHz at fluence of 148 mJ/cm^2. The experimental results of our study indicated that the periodicities were also affected by fs laser fluence. It was expected to be a useful supplementary information to understand the effect of high repetition rates during fs laser irradiation on the formation of spatial ripple structures on semiconductor material 4H-SiC.

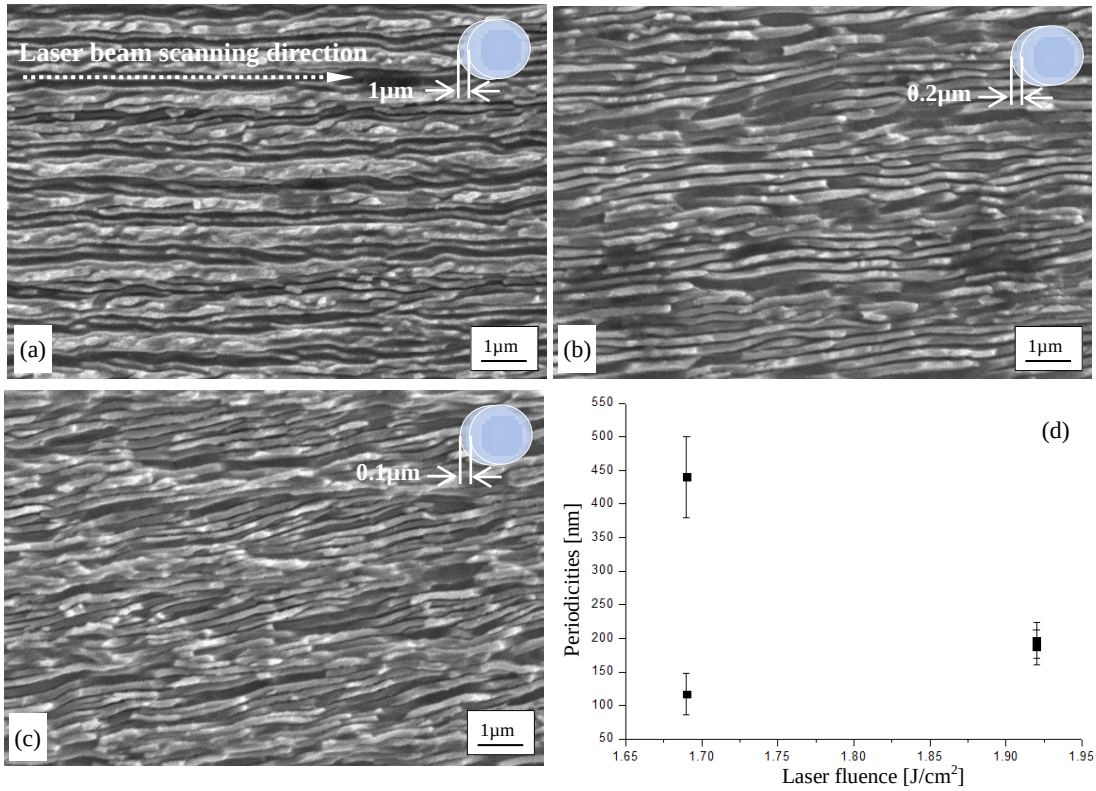

Fig.2.13. SEM images of femtosecond laser irradiated areas at different repetition frequency. (a) 100 kHz, 12mW, Φ=1.69 J/cm^2; (b) 500 kHz, 68mW, Φ=1.92 J/cm^2; (c) 1 MHz, 136mW, Φ=1.92 J/cm^2; (d) Dependence of spatial periodicity on laser fluence for LIPSS structures induced on Si-faces corresponding to (a), (b) and (c).

2.3.4 Surface morphology of Transverse irradiation mode and Cross-scan irradiation mode process

As shown in **Fig.2.14** (a), SiC substrate Si-face of SiC substrate was irradiated by fs laser with a scanning pitch of 0.5μm, a pulse repetition rate of 10MHz, and a laser fluence of 0.44 J/cm^2. Here we called it transverse irradiation mode process. After laser processing, the ablated substrate was cleaned by ultrasonic in deionized water for 1 hour to remove the surface debris and was then put on the XYZ axes system with an anticlockwise 90°rotation for further laser processing called Cross-scan irradiation mode here, as shown in **Fig. 2.14** (b). After this processing, the substrate was also cleaned for one hour and then rotated clockwisely for 90° to ensure the same angle of view with that of Transverse irradiation mode when observed by SEM. As can be seen in **Fig.2.14** (e), the horizontally oriented LIPSS structures induced during Transverse irradiation mode were newly fabricated into vertically oriented ripples after Cross-scan irradiation mode process. In addition, the orientation of LIPSS structures shown both in **Fig.2.14** (a) and **Fig.2.14** (e) were consistent with the scanning direction of linearly polarized laser beam. The polarization direction of incident laser was strictly responsible for the direction of these LIPSS structures [6]. Literature [19] has reported that parallel LIPSS structures of about 270 nm were induced on ZnO surface by fs laser beam (τ= 125 fs, 1 kHz, 3 J/cm^2) with a vertical polarization direction. Different from our experimental result, the LIPSS structures were fabricated into submicron periodic square structures with a spatial periodicity of 290 nm by another incident laser beam with a horizontal polarization direction. It

was presumed that the latter laser fluence was not strong enough to ablate the previously induced ripples structures thoroughly and form new LIPSS structures.

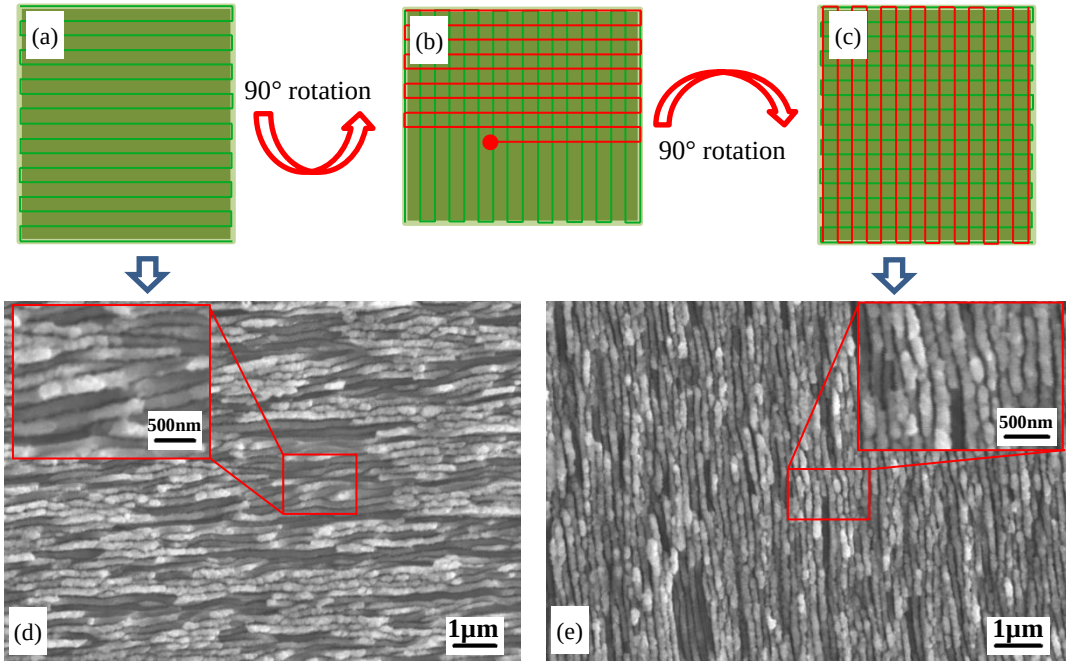

Fig.2.14 SEM images of SiC Si-face irradiated during (a) transverse irradiation mode and (b) cross-scan irradiation mode at laser fluence of 0.44 J/cm^2.

Fig.2.15 shows the images of SiC Si-face irradiated in cross-scan irradiation mode at the above experimental conditions. It can be seen that different surface pattern was formed by femtosecond laser. However, the surface was continuously irradiated by fs laser in vertical direction after horizontal direction irradiation without any surface cleaning. As reported in **Fig.2.5,** large amount of debris was induced after laser irradiation. Comparing to **Fig.2.14 (e)**, conclusion can be drawn that debris played an important role in surface formation.

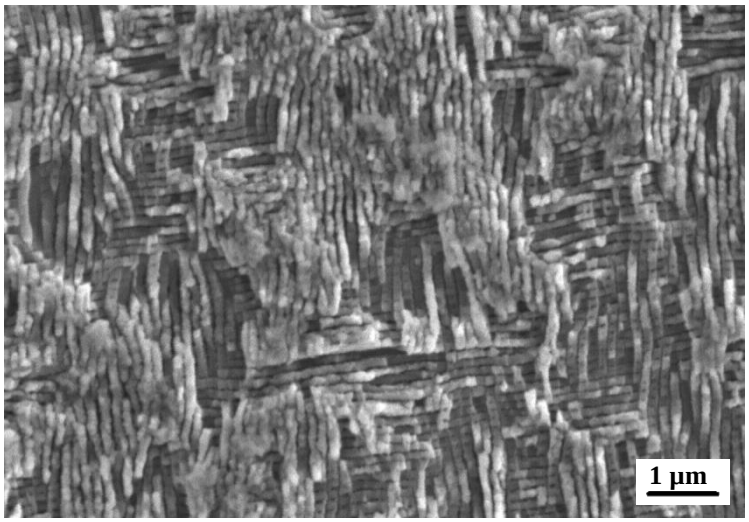

Fig.2.15 SEM images of SiC Si-face irradiated after cross-scan irradiation mode at laser fluence of 0.44 J/cm^2.

2.3.5 Femtosecond laser irradiation at near-threshold fluence

2.3.5.1 SEM observation of laser-irradiated areas at near threshold fluence

Fig.2.16 indicates the SEM images of SiC Si-face wholly irradiated by fs laser at a scanning pitch of 2μm, a pulse repetition rate of 10MHz, and a near-threshold

fluence of 0.25 J/cm^2, which was slightly higher than the ablation threshold. It can be clearly seen that small parts of the surface were lightly ablated, leading to the formation of LIPSS structures of about 160nm. During the initial stage of fs laser process at near threshold fluence, nonlinear effect [20] was excited during strong electromagnetic coupling fs laser irradiation, triggering multiphoton absorption which led to covalent chemical rupture. Ionization of valence band electrons and atomic migration further occurred, destroying SiC crystal structures eventually. During coulomb explosion [3, 21], the destroyed crystal lattice materials were sputtered instantaneously owing to the overwhelmingly high temperature and high pressure caused by strong electromagnetic coupling, forming nanovoids in SiC bulk [22-24], which was responsible for incubation effects [6] such as refractive index modification [6, 25, 26], collateral thermal damage [27], thermos elastic strain [28-30]. Incubation effects play an important role in triggering inhomogeneous accumulation of energy deposition which directly induced periodic ripples. Simultaneously, it was reported in literature [6] that Mie scattering attributed to laser-induced nanocraters was a cause of these special frequency periodic ripples at near threshold fluence of 0.4 J/cm^2 in a vacuum chamber.

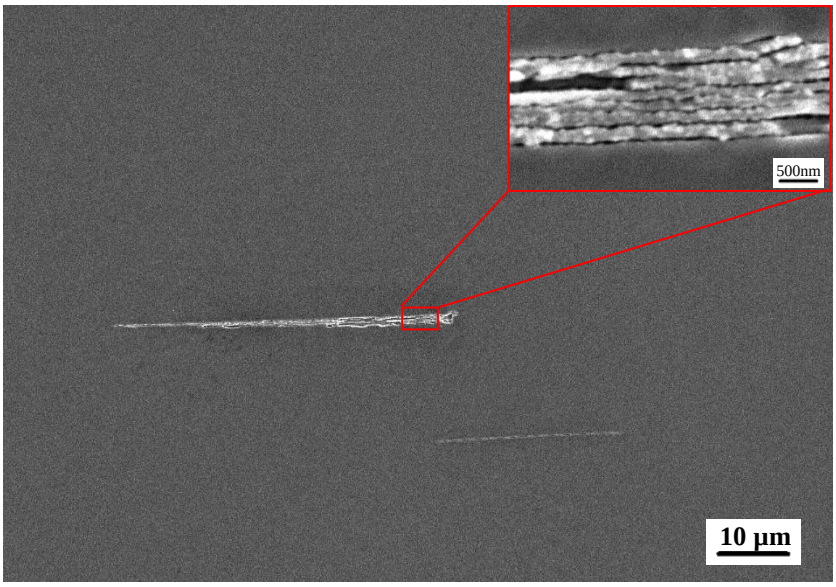

Fig.2.16 SEM images of Si-face wholly irradiated by fs laser at near-threshold fluence 0.25 J/cm^2.

Comparing with the previous experimental conditions shown in **Fig.2.13**, the laser fluence of this experiment decreased from 1.69 J/cm^2 (100 kHz) to 0.25 J/cm^2 (10MHz), substantially demonstrating that the threshold of laser ablation and surface modification depend on the number of laser pulses [31]. The following formula (2) consistent with our results clearly explained the relation between fluence and pulse numbers. This is a supplement for literature [32], which also summarized that the damage thresholds of laser irradiation were dependent on absorption, wavelength, beam spot size and pulse length. Additionally, defect formation [33] and defect density [34] were also reported as factors affecting surface damage threshold.

$$\Phi_{mod}(N) = \Phi_{mod}(1) \cdot N^{\varepsilon-1} \quad (2)$$

$\Phi_{\mathrm{mod}}(\mathrm{N})$ indicates the modification threshold fluence of femtosecond laser; N denotes the pulse numbers, and $\varepsilon(0 < \varepsilon < 1)$ is a coefficient related to material [35].

Nevertheless, the surface morphology of 4H-SiC irradiated by fs laser at near-threshold fluence in ambient atmosphere has been rarely reported. Its mechanism is still a matter of debate. More experimentally and theoretically study should be carried out in future.

2.3.5.2 Evaluation of surface morphology at near-threshold fluence

In order to further investigate laser ablation at near-threshold fluence, repeated irradiations were carried out at different combinations of scanning speeds and scanning times. As shown in **Fig.2.17** (a), **Fig.2.17** (b) and **Fig.2.17** (c), different parts of SiC substrate were irradiated by femtosecond laser at different combinations of scanning speeds and scanning times of respectively 10mm/s with 1 scan; 15mm/s with 1 scan; and 15mm/s with 5 scans. Comparing the irradiated morphologies shown in **Fig.2.17** (a) and **Fig.2.17** (b), it was observed that discontinuous ablated parts were induced by femtosecond laser. Whereas the discontinuous ablated areas (shown in **Fig.2.17** (a)) of 10mm/s laser irradiation was more than that of 15mm/s laser irradiation shown in **Fig.2.17** (b). Additionally, the amplified images of areas A, B, and C of **Fig.2.17** are respectively shown in **Fig.2.18**. The ablated area shown in **Fig.2.18** (a) _A was also bigger than that of **Fig.2.18** (a) _B, accompanying with parallel periodic nanoscale structures of approximately 150nm width, 1/6 of fs laser wavelength. As shown in **Fig.2.17** (a), the interval between adjacent laser pulses was 0.2μm in the case of scanning speed of 10mm/s, smaller than that (0.3μm) of **Fig.2.17** (b) corresponding with the scanning speed of 15mm/s.

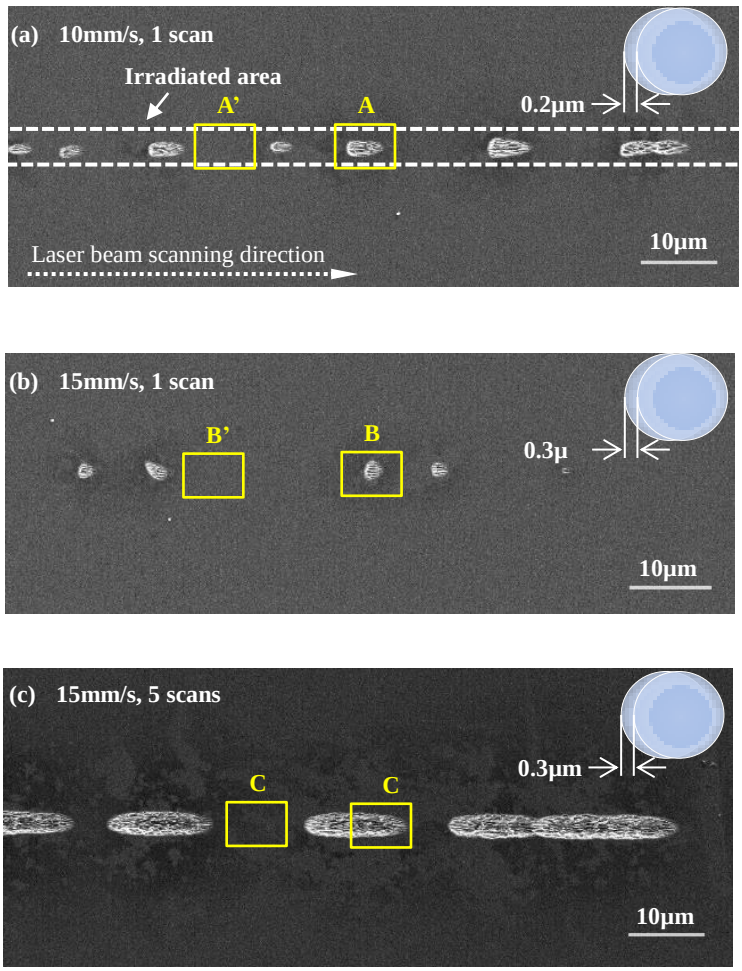

Fig.2.17 SEM images of femtosecond laser irradiated SiC surface at different scan speed and scanning times (a) 10mm/s, 1 scan; (b) 15mm/s, 1 scan; (c) 15mm/s, 5 scans.

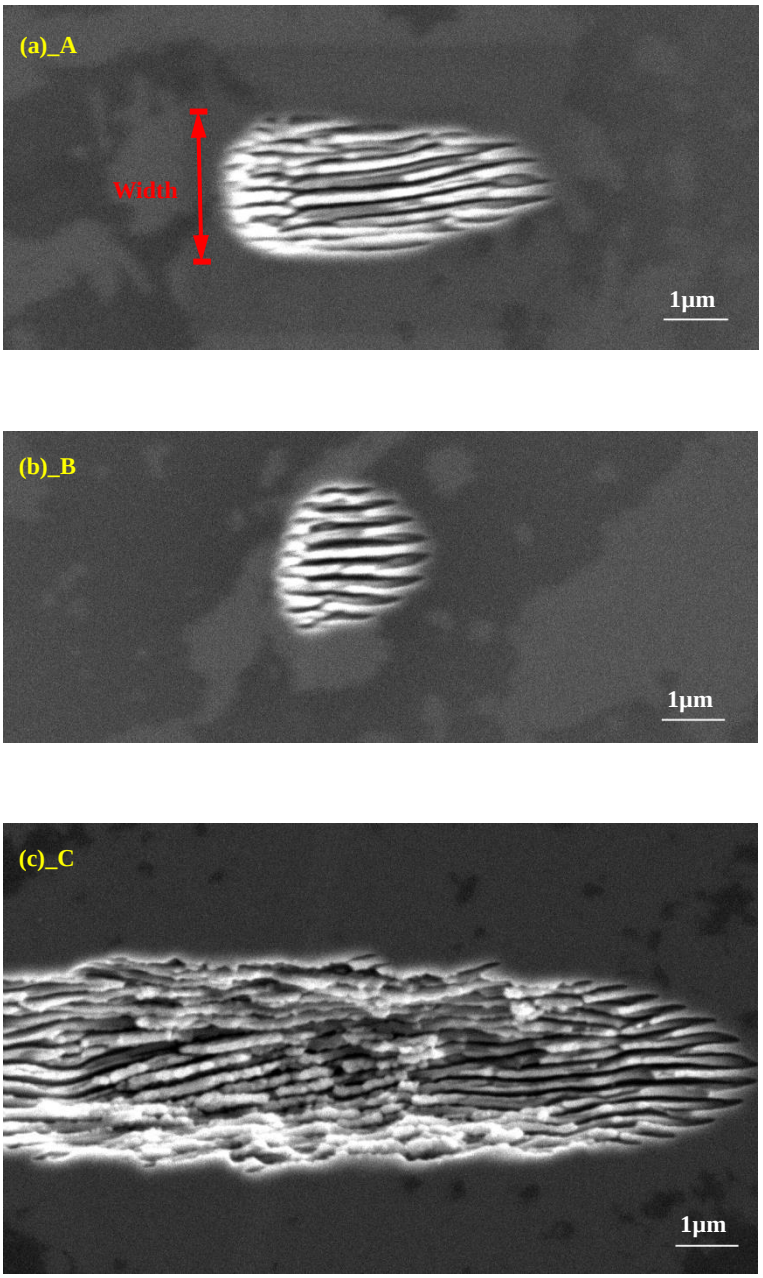

Fig.2.18 Amplified images of the marked-areas A, B, and C shown in **Fig**.2.17.

It was found that smaller interval of adjacent laser pulses led more areas to be ablated during laser irradiation. Furthermore, it was still puzzling and intriguing that no ablated ripples were observed in the areas marked A', B' and C' between the adjacent ablated areas, even though these surfaces were irradiated by femtosecond laser at the same conditions. Inhomogeneous accumulation of energy deposition effect of near-threshold fs laser was also supposed to be responsible for this phenomenon. It was presumed that an inhomogeneous laser beam profile, scratches, crystal defects, dust [31] and crystal lattice deformation [36] accounted for enhancing inhomogeneous energy deposition effect resulting in these discontinuous laser-ablated areas shown in **Fig.2.17**. It was known that smaller laser pulse interval and repeated irradiation led to stronger energy accumulation deposition effect, resulting in more and larger ablated spots, as shown in **Fig.2.17** (a), **Fig.2.17** (b), and **Fig.2.17** (c).

Owing to the extremely short pulse duration and high fluence of fs laser, nonlinear optical effect [20] was excited by strong electromagnetic coupling. Valence band electrons were ionized when absorbing photons during multiphoton ionization [37], accompanying with the release of surface electron, which led to the intensive change of electron density and electrostatic field of fs laser-irradiated areas. The covalent chemical bond of SiC crystal eventually fractured, attributing to the overwhelmingly high temperature and high pressure triggered by fs laser within an exceeding small spatial volume during coulomb explosion [3, 21]. Consequently, the destroyed crystal lattice material sputtered around instantaneously owing to high

temperature and high density expanding plasma concluding atomized and ionized particles, forming nanovoids in SiC bulk. Intensive shock and rarefaction waves generated by high pressure plasma further led to inhomogeneous electron density around these nanovoids [22, 23, 24]. Even through a host of physically microscopic phenomena of incubation effects such as refractive index modification [6, 25, 26, 38], collateral thermal damage [27], thermoelastic strain [28, 29, 30], microexplosion and void formation [23] formed by fs laser have been reported, but actual result of these phenomena during fs laser process have rarely been reported for 4H-SiC. The accumulation of incubation effect during fs laser irradiation can be seen more macroscopically and intuitively from the experimentally evolutions of surface morphologies formed by fs laser at near threshold fluence in **Fig.2.17**. As can be seen from the comparison of **Fig.2.17** (b) and **Fig.2.17** (c), larger laser-ablated areas with periodic structures of approximately 150nm were observed with the increase of scanning times. Stronger energy deposition accumulation effects caused by incubation effect led more areas to be ablated during repeated laser irradiation.

It was elucidated that high special frequency periodic ripples were fabricated during laser irradiation as a result of Mie scattering being attributed to laser-induced nanocraters which decreased threshold fluence by incubation effect [6]. This is illuminating and constructive for explaining the formation of ripples during the primary stage of fs laser processing. During further irradiation, the energy of fs laser was absorbed by plasma, causing plasma wave [39]. These laser-induced surface

defects such as color center reduced laser ablation threshold fluence [25]. Nevertheless, second harmonic generation was more rewarding for understanding the relationship between ripple periodicities and fs laser wavelengths as well as refractive index during subsequent stage during laser process, according to the experimental data and the formula $\Lambda=\lambda/2n$ in literature [5], where λ is the wavelength of incident laser, n is refractive index. Further study should be done to investigate the mechanism of this phenomenon.

2.3.5.3 AFM observation of laser-irradiated areas at near threshold fluence

In order to investigate the laser-irradiated surface where no ablation was induced, AFM was adopted. **Fig.2.19** shows the appearance of AFM measurement apparatus VECCO Dimension Icon. Its schematic diagram is shown in **Fig.2.20**. The surface morphology of specimen is recorded when using this measurement apparatus. The main principle of AFM is utilizing Van Der Waals Force between the atoms of the probe and specimen surface. The probe is firstly attached onto a fixed cantilever, and then it is gently pressed down onto the surface of specimen. During the scanning of Piezo-scanner, the probe moves upward and downward according to the asperity of specimen surface. The variation of cantilever is detected by optical lever type inclination detecting apparatus. The position aberration of cantilever in up-down direction is detected according to the intensity difference of laser reflected by cantilever to photo detector. The electric signal is sent to computer for further visualization after series of complicated signal processing.

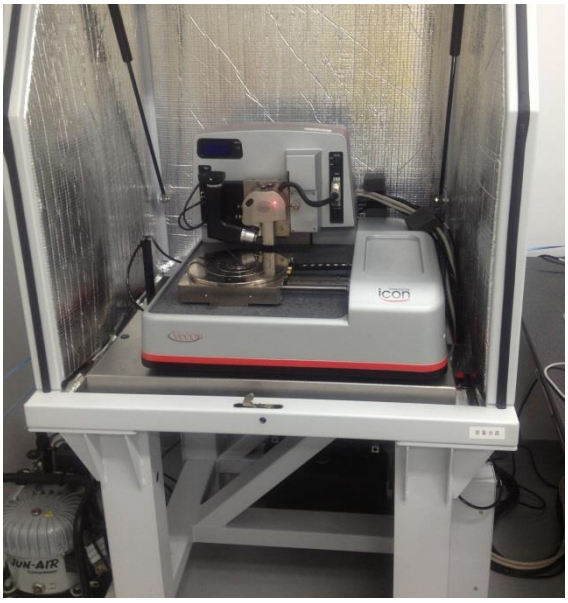

Fig.2.19 Appearance of measurement apparatus VEECO Dimension Icon

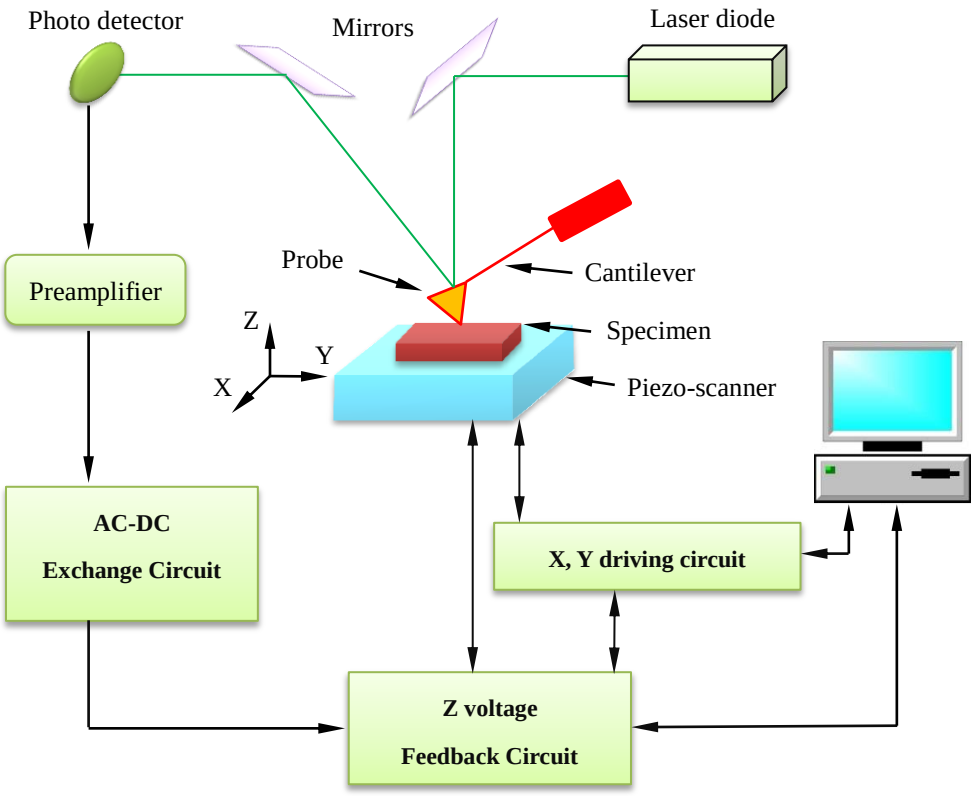

Fig.2.20 Schematic diagram of VEECO Dimension Icon

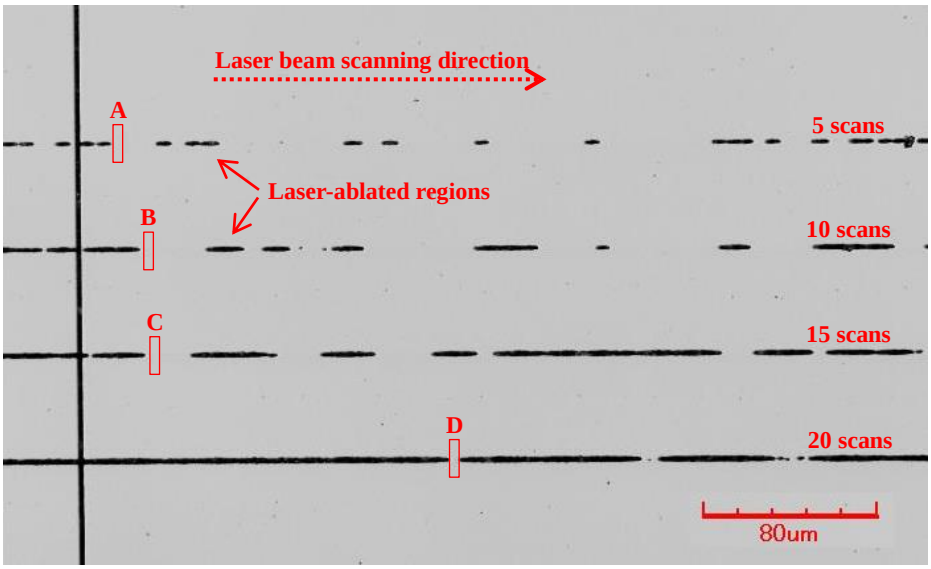

Fig.2.21 Confocal laser scanning microscopy image of SiC surface irradiated by fs laser at near-threshold fluence of 1.1 J/cm^2 and scanning speed of 15mm/s laser with different scanning times.

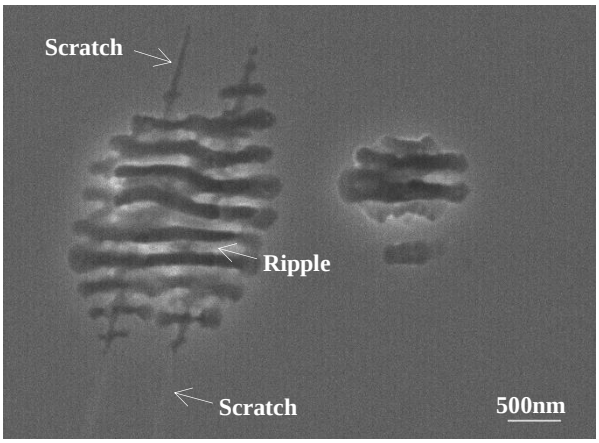

Fig.2.22 Si-face ablated by fs laser at a scan times of 5, a scan speed of 100mm/s and a fluence of 1.1 J/cm^2.

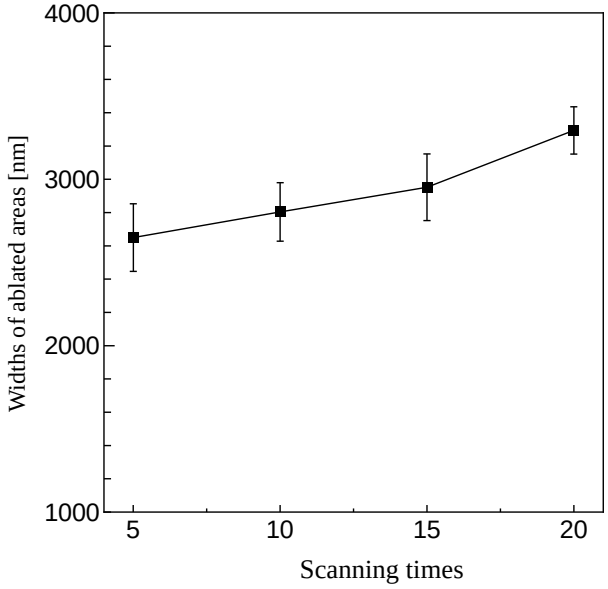

Fig.2.23 Relation between laser-ablated area width and scanning times at a scanning speed of 15mm/s and a fluence of 1.1 J/cm^2.

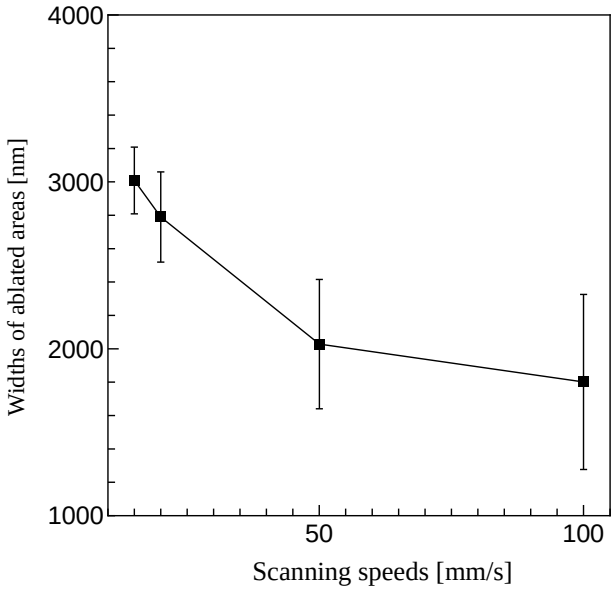

Fig.2.24 Relations of laser-ablated area width and scanning speed at scanning times of 5 and a fluence of 1.1 J/cm^2.

Fig.2.21 shows the confocal laser scanning microscopy image of SiC surface irradiated by near-threshold fluence laser irradiation with different scanning times. Four parts of SiC substrate Si face were repeatedly irradiated by fs laser at a repetition rate of 50 kHz, near-threshold fluence 1.1 J/cm^2 and the same scanning speed of 15mm/s in the same scanning direction. As shown in **Fig.2.21**, the scanning times were respectively 5, 10, 15, and 20. After laser ablation, discontinuous irradiated areas were fabricated. More continuous fabricated areas were observed with the increase of fs laser scanning times, inferring that stronger accumulation of energy deposition effect caused by incubation effect played an important role for the increasing ablated areas. As presumed previously, this was attributed to enhanced absorption due to mechanical stress (scratch, crystal defect) [31] etc, yielding inhomogeneous energy deposition accumulation on SiC surface during fs laser scanning. As shown in **Fig.2.22**, the areas with scratches on Si-face were ablated in advance of its ambient parts, demonstrating that the scratches enhanced the absorption of laser energy. Incubation effect of surface morphology changes were gradually induced during repeated laser irradiation on SiC surface, accounting for the increase of fs laser-irradiated areas. As are shown in **Fig.2.23** and **Fig.2.24**, the widths (shown in **Fig.2.18** (a) _A) of laser-ablated areas changed at different scanning times and scanning speeds, indicating that more energy deposition would be accumulated with more scanning times and slower scanning speeds. For further understanding of the surface morphology change where no laser-ablated areas were observed between adjacent ablated areas, Atomic Force Microscope (AFM)

measurement was employed for detailed surface observations. As shown in **Fig.2.21**, areas A, B, C, and D marked by red dashed frame were measured by AFM. The corresponding results were shown in **Fig.2.25**, respectively. As can be seen in **Fig.2.25** A, **Fig.2.25** B, **Fig.2.25** C, and **Fig.2.25** D, no obvious differences were found between the ablated irradiated area and the un-irradiated area, revealing that no surface morphology changes were yielded by femtosecond laser in spite of increasing laser scanning times. Consequently, these results suggested that the surface morphology ablation was firstly from the inside of SiC substrate, deeper insight of incubation effect induced by fs laser in internal change of SiC sub-surface should be taken into account. To investigate the effect of near-threshold fluence femtosecond laser irradiation on SiC substrate systematically, we carried out CMP polishing in chapter 3.

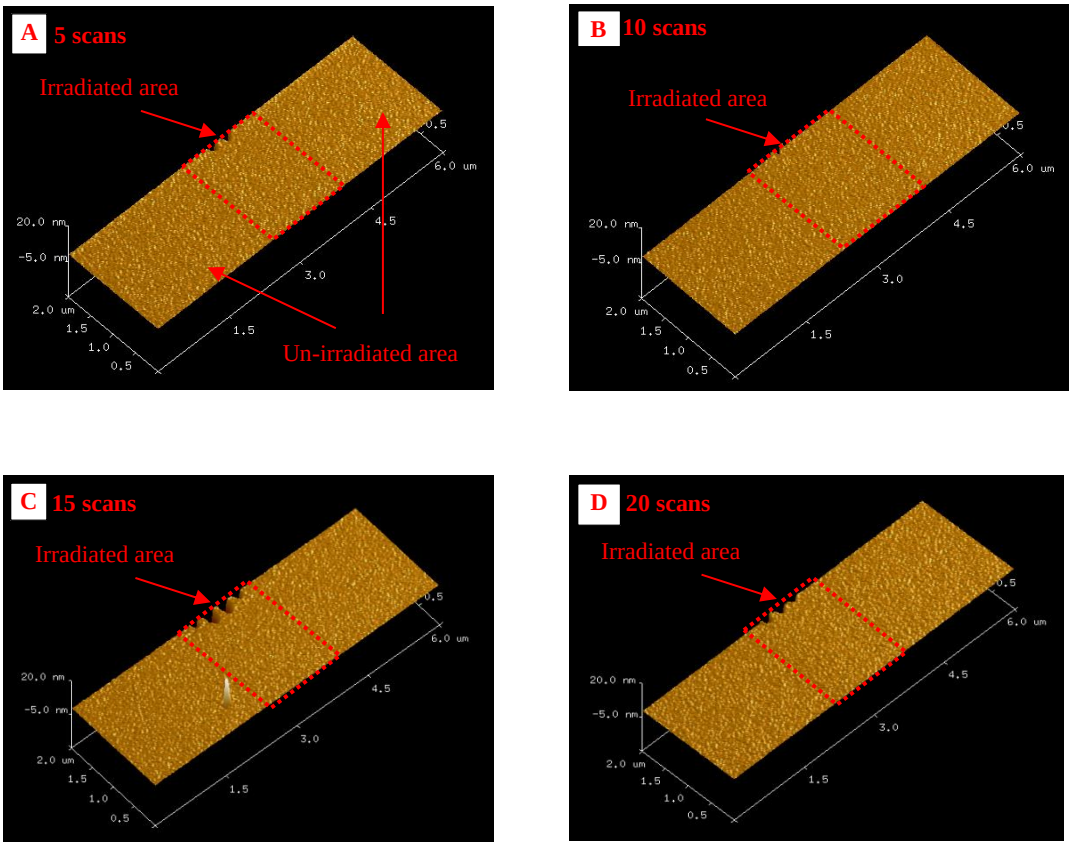

Fig.2.25 AFM images of SiC surfaces between adjacent ablated areas irradiated by fs laser at near-threshold fluence with different scanning times corresponding to **Fig**.2.21.

2.4 Summary

In this study, the effect of fs laser processing on SiC surface morphology was investigated. Si-faces of as-polished silicon carbide (SiC) substrate were irradiated by femtosecond laser at different laser scanning pitches, different scanning speeds, and different pulse repetition rates at near-threshold fluence or higher fluence. The evolutions of surface morphologies were reviewed for detailed surface morphology investigation. It was found that femtosecond laser-irradiated morphologies on SiC substrate surface changed dramatically with different laser processing parameters. At higher laser repetition rate (500 kHz, 1 MHz, 10 MHz), ripples with average spatial periodicities of 145~196nm were induced. Whereas for lower repetition rate (100 kHz), coarse ripples (roughly 440nm) and fine ripples (about 117nm) were simultaneously formed at fluence of 1.69 J/cm^2 by fs laser, It was considered that lower fluence and bigger interval of adjacent pulses decreased the accumulation of laser energy deposition, further leading to weaker interaction between incident laser and crystal SiC substrate. Approximately 5°~10° inclined ripples were fabricated during laser ablation. Meanwhile, large amount of laser-induced agglomeration was fabricated during laser process with scanning pitch of 0.05μm and scanning speed $\leq$ 5mm/s. Decrease of scanning velocity also gradually contributed to the increase of agglomeration parts. After near-threshold fluence of 0.25 J/cm^2, LIPSS structures were partly induced. The accumulation of energy deposition was presumed to be responsible for these surface morphology changes. LIPSS structures induced in Transverse irradiation mode process were further ablated during Cross-scan

irradiation mode process, newly fabricating similar LIPSS structures of about 160nm parallel with the scanning direction of laser beam. Laser-induced debris played an important role on ripples formation. More theoretical analysis and experimental work needed to be done to investigate the formation mechanism of periodic inclined ripples. It is expected that the interaction between femtosecond laser and semiconductor materials 4H-SiC could be further understood.

The effect of fs laser irradiation at near-threshold fluence on 4H-SiC surface morphology was also investigated. Different laser scanning speeds and scanning times resulted in discontinuous laser-ablated areas at near-threshold fluence of 1.1 J/cm^2. Decreasing laser scanning speed and increasing scanning times as well as surface scratches increased the ablated areas. It was considered that enhanced absorption due to incubation effect caused by fs laser-induced defects in the subsurface of SiC crystal yielded inhomogeneous energy deposition. Spatial ripple structures with periodicities substantially shorter than the incident laser wavelength have been observed. Similar ripples were formed by repetitious laser irradiation.

Reference

[1] A. Rousse, C. Rischel, S. Fourmaux, I. Uschmann, S. Sebban, G. Grillon, Ph. Balcou, E. Förster, J.P. Geindre, P. Audebert, J.C. Gauthier & D. Hulin, Non-thermal melting in semiconductors measured at femtosecond resolution, Nature 410, 65-68 (1 March 2001)

[2] Ben Pecholt & Monica Vendan & Yuanyuan Dong & Pal Molian, Ultrafast laser micromachining of 3C-SiC thin films for MEMS device abrication, Int J Adv Manuf Technol (2008) 39:239–250

[3] Yuanyuan Dong and Pal Molian, Coulomb explosion-induced formation of highly oriented nanoparticles on thin films of 3C–SiC by the femtosecond pulsed laser, Appl. Phys. Lett. 84, 10 (2004)

[4] Laude, L. D. Cohesive Properties of Semiconductors Under Laser Irradiation. (NATO ASI Series Martinus Nijhoff Vol. 69, The Hague, 1983).

[5] X.J. Wu, T.Q. Jia, F.L. Zhao, M. Huang, N.S. Xu, H. Kuroda, Z.Z. Xu, Formation mechanisms of uniform arrays of periodic nanoparticles and nanoripples on 6H-SiC crystal surface induced by femtosecond laser ablation, Appl. Phys. A 86, 491–495 (2007)

[6] Go Obara, Hisashi Shimizu, Taira Enami, Eric Mazur, Mitsuhiro Terakawa, and Minoru Obara, Growth of high spatial frequency periodic ripple structures on SiC crystal surfaces irradiated with successive femtosecond laser pulses, Optics Express Vol. 21, Issue 22, pp. 26323-26334 (2013)

[7] Takuro Tomita, Keita Kinoshita, Shigeki Matsuo, and Shuichi Hashimoto, Effect of surface roughening on femtosecond laser-induced ripple structures, APPLIED PHYSICS LETTERS 90, 153115 2007

[8] Catalina Albua, Adrian Dinescu, Mihaela Filipescu, Magdalena Ulmeanu, Marian Zamfirescu, Periodical structures induced by femtosecond laser on metals in air and liquid environments, Applied Surface Science 278 (2013) 347–351

[9] Xiaodong Xu, Ningyi Yuan, Jianhua Qiu, Jianning Ding ,Formation of conductive copper lines by femtosecond laser irradiation of copper nitride film on plastic substrates, Materials Research Bulletin 65 (2015) 68–72

[10] A.Y. Vorobyev, V.S. Makin, C. Guo, Periodic ordering of random surface nanostructures induced by femtosecond laser pulses on metals, Journal of Applied Physics 101 (2007) 034903.

[11] Chengyun Zhang, JianwuYao, ShengLan, VyacheslavA.Trofimov, TatianaM.Lysak, Effects of plasma confinement on the femtosecond laser ablation of silicon, Optics Communications 308(2013)54–63

[12] Sung Hoon Kim · Ik-Bu Sohn · Sungho Jeong, Fabrication of uniform nanogrooves on 6H-SiC by femtosecond laser ablation, Appl Phys A (2011) 102: 55–59

[13] Youqiang Xing, Jianxin Deng, Yunsong Lian, Kedong Zhang, Guodong Zhang, Jun Zhao, Multiple nanoscale parallel grooves formed on Si_3N_4/TiC ceramic by femtosecond pulsed laser, Applied Surface Science 289 (2014) 62–71

[14] F. Garrelie, J. P. Colombier, F. Pigeon, S. Tonchev, N. Faure, M. Bounhalli, S. Reynaud, and O. Parriaux, Evidence of surface plasmon resonance in ultrafast laser-induced ripples, Optics Express Vol. 19, Issue 10, pp. 9035-9043 (2011)

[15] M. Huang, F. Zhao, Y. Cheng, N. Xu, Z. Xu, Origin of laser-induced near-subwavelength ripples: interference between surface plasmons and incident laser, ACS Nano 3 (2009) 4062–4070.

[16] S. H. Kim, K. H. Byun, I. B. Sohn, S. H. Jeong, Progressive formation of fine and coarse ripples on SiC surface by repeated irradiation of femtosecond laser pulses, Appl. Phys. B (2013) 113:395–402

[17] Laura Gemini, Masaki Hashida, Masahiro Shimizu, Yasuhiro Miyasaka, Shunsuke Inoue, Shigeki Tokita, Jiri Limpouch, Tomas Mocek, Shuji Sakabe, Periodic nanostructures self-formed on silicon and silicon carbide by femtosecond laser irradiation, Appl. Phys. A (2014) 117:49–54

[18] Haugen, Subwavelength ripple formation on the surfaces of compound semiconductors irradiated with femtosecond laser pulses, Appl. Phys. Lett. 82 (2003) 4462–4464.

[19] M Huang, F L Zhao, T Q Jia, Y Cheng, N S Xu and Z Z Xu, A uniform 290 nm periodic square structure on ZnO fabricated by two-beam femtosecond laser ablation, Nanotechnology 18 (2007) 505301 (6pp).

[20] Yuqiang Jiang, Tetsuya Narushima & Hiromi Okamoto, Nonlinear optical effects in trapping nanoparticles with femtosecond pulses, Nature Physics 6, 1005–1009 (2010)

[21] T. DITMIRE, J. W. G. TISCH, E. SPRINGATE, M. B. MASON, N. HAY, R. A. SMITH, J. MARANGOS & M. H. R. HUTCHINSON, High-energy ions produced in explosions of superheated atomic clusters, Nature 386, 54 - 56 (06 March 1997).

[22]Saulius Juodkazis, Hiroaki Misawa, Tomohiro Hashimoto, Eugene G. Gamaly and Barry Luther-Davies, Laser-induced microexplosion confined in a bulk of silica: Formation of nanovoids, Appl. Phys. Lett. 88, 201909 (2006)

[23] Eugene G. Gamaly, Saulius Juodkazis, Koichi Nishimura, Hiroaki Misawa, Barry Luther-Davies, Ludovic Hallo, Philippe Nicolai, and Vladimir T. Tikhonchuk, Laser-matter interaction in the bulk of a transparent solid: Confined microexplosion and void formation, Phys. Rev. B 73, 214101 – Published 6 June 2006

[24] Hisashi Shimizu, Shuhei Yada, Go Obara, and Mitsuhiro Terakawa, Contribution of defect on early stage of LIPSS formation, OPTICS EXPRESS, Vol. 21, No. 22, 26323-26325 (2013).

[25] S.-H. Cho, H. Kumagai, K. Midorikawa, and M. Obara, “Fabrication of double cladding structure in optical multimode fibers using plasma channeling excited by a high-intensity femtosecond laser,” Opt. Commun. 168(1-4), 287–295 (1999).

[26] X.r.zhang, X. xu, A.M.rubenchik, Simulation of microscale densification

during femtosecond laser processing of dielectric materials, Appl. Phys. A 79, 945–948 (2004)

[27] Ben Pecholt, Monica Vendan, Yuanyuan Dong, Pal Molian, Ultrafast laser micromachining of 3C-SiC thin films for MEMS device fabrication, Int J Adv Manuf Technol (2008) 39:239–250

[28] Nadezhda M. Bulgakova, Rarefaction shock wave: Formation under short pulse laser ablation of solids, PHYSICAL REVIEW E, VOLUME 63, 046311

[29] A. Borowiec, D. M. Bruce, Daniel T. Cassidy, and H. K. Haugen, Imaging the strain fields resulting from laser micromachining of semiconductors, Appl. Phys. Lett. 83, 225 (2003)

[30] F. S. Krasniqi, S. L. Johnson, P. Beaud, M. Kaiser, D. Grolimund, and G. Ingold, Influence of lattice heating time on femtosecond laser-induced strain waves in InSb, PHYSICAL REVIEW B 78, 174302 (2008)

[31] J. Bonse, S. Baudach, J. Krüger, W. Kautek, M. Lenzner, Femtosecond laser ablation of silicon–modification thresholds and morphology, Appl. Phys. A 74, 19–25 (2002)

[32] R. M. WOOD, Laser induced damage thresholds and laser safety levels. Do the units of measurement matter, Optics & Laser Technology; Vol. 29, No. 8, pp. 517-522, 1997

[33] N. Bloembergen, "Role of cracks, pores, and absorbing inclusions on laser induced damage threshold at surfaces of transparent dielectrics," Appl. Opt. 12(4), 661–664 (1973).

[34] L. G. DeShazer, B. E. Newnam, and K. M. Leung, Role of coating defects in laser-induced damage to dielectric thin films, Appl. Phys. Lett. 23 (11), 607–609 (1973).

[35] Yong Jee, Michael F. Becker, and Rodger M. Walser, Laser-induced damage on single-crystal metal surfaces, Journal of the Optical Society of America B Vol. 5, Issue 3, pp. 648-659 (1988)

[36] Logan DesAutels, Christopher Brewer, Peter Powers, Mark Walker,David Tomlin, Albert Fratini, Shane Juhl, Weibin Chen, Femtosecond index change mechanisms and morphology of SiC crystalline materials, Physics Letters A 373 (2009) 583–591

[37] G Mainfray and G Manus, Multiphoton ionization of atoms, Rep. Prog. Phys. 1991, 54 (10) 1333~1372.

[38] Hengchang Guo, Hongbing Jiang, Ying Fang, Chao Peng, Hong Yang, Yan Li and Qihuang Gong, The pulse duration dependence of femtosecond laser induced refractive index modulation in fused silica, Journal of Optics A: Pure Appl. Opt.2004, 6 787

[39] Ajit P. Joglekar, Hsiao-hua Liu, Edgar Meyhöfer, Gerard Mourou, and Alan J. Hunt, Optics at critical intensity: Applications to nanomorphing, PNAS April 20, 2004 vol. 101 no. 16 5856-5861

CHATER 3

POLISHINIG PROPERTIES INVESTIGATION FOR FEMTOSECOND LASER-IRRADIATED SIC SUBSTRATES

3.1 Introduction

As an extremely important process in the manufacture of semiconductor devices, CMP (Chemical Mechanical Polishing) plays a decisive role. Its principle can be described as: the wafer surface is firstly oxidized by the additions in slurry, resulting in an oxidation film. After the polishing of mechanical action, the oxidation film was removed, exposing new surface. By the repeated cycle of these steps, high material removal rate (MRR), high planarization, and ultra-smooth surface without sub-surface damage can be obtained at adaptable conditions. However, the effect of CMP process is greatly affected by the physical properties of polishing pad [1, 2], slurry [2-6], polishing environment [7-10], and mechanical condition, etc. The research team of Toshiro Doi has studied CMP technique for many years. Detailed contents of polishing technique are systemically introduced in their monographs [11, 12]. In recent years, they developed new polishing apparatus [13-16] for CMP process. Polishing of hard-to-process materials, such as GaN [17-20], SiC [18, 21-23], Diamond [24], Sapphire [18], has been studied in varies of experimental conditions. However, the material remove rate still should be further improved to meet industrial needs. New technique should be studied, aiming for higher MRR and better surface.

In recent years, some new methods for improving the MRR of SiC wafer were proposed. A novel plasma-assisted polishing technique, combined with the

irradiation of atmospheric pressure water vapor plasma and polishing using soft abrasives, has been proposed [25]. By using this polishing technique, an atomically flat surface was obtained. It was inferred that the MRR of this process must be much higher than 2.7nm/min. Si-face of as-polished SiC wafer was polished by using slurry with extremely strong oxidant KMnO4 [26]. The MRR was reported as 1695nm/h (=28nm/min). However, large amount of slurry will be consumed in as-lapped SiC substrate polishing. In addition, potential environment pollution will also be probably caused by the discharged slurry which was added with strong oxidant $KMnO_4$. Nevertheless, few studies of how to improve C-face MRR of SiC have been reported, especially the MRR of as-lapped SiC C-face has been rarely reported. Lapping as well as polishing technique is quite indispensable in semiconductor process. The so called as-lapped SiC substrate means that the SiC substrate was machined in lapping process by microscale abrasives and eventually achieved a rough surface with many tiny cracks. It is time-consuming and costly to polish as-lapped SiC wafer by CMP process directly to obtain as-polished surface with high level surface roughness and high material removal rate on account of its high chemical instability and high hardness. So it is significant to take femtosecond laser into account for SiC surface micromachining before CMP process, aiming for laser-fabricated surface which contributes for CMP process. In this study, femtosecond laser was considered as a novel pre-process without any pollution for SiC substrate before CMP process.

In chapter 2, we investigated the evolution of surface morphologies induced by

femtosecond laser at near threshold ablation fluence on 4H-SiC surface. Discontinuous laser-ablated areas were found on SiC surface. It was put forward that incubation effect occurred in ablated SiC subsurface triggered inhomogeneous energy absorption which was responsible for the discontinuous ablated areas. It was revealed that laser-induced seed defects induced by multiphoton absorption attributed to nanocraters in the early stage of laser irradiation and finally resulted in LIPSS structures on SiC surface [27, 28]. Literature [29] has revealed that nano-voids were induced by shock and rarefaction waves at fs laser pulse power lower than threshold of self-focusing in the bulk of silica. Residual strain induced during fs laser micromachining of semiconductors has also been studied in [30]. It was stated that the sign of the stress could sensitively depend on laser processing conditions. It was also suggested that the initial strain wave dynamics depended crucially on the lattice heating time [31] of semiconductor material. Laser-induced strain field was also presented to trigger the localized change of the index of refraction of glass bulk by simulation [32]. However, polishing behaviors have rarely reported for SiC (Si-face) surface after inhomogeneous energy absorption.

In the first part, we firstly carried out CMP process to investigate the polishing behaviors of femtosecond laser-irradiated SiC (Si-face) surface at different output powers as well as the effect of accumulation effect of energy deposition at near-threshold fluence on CMP process. After fs laser irradiation, some areas were thoroughly ablated, triggering an ablation depth of 0.4μm as well as the edges of some areas were oxidized. After CMP polishing, the oxidized parts showed higher

MRR than the non-irradiated areas and the areas irradiated at relatively low laser power which could not induce laser ablation.

In the second part, we introduced the irradiation results of femtosecond laser on C-face of SiC in different modes as well as the effects on CMP process. As-lapped C-face of SiC substrate was treated by the femtosecond laser in Transverse irradiation mode and Cross-scan irradiation mode. The surface morphology changes were analyzed before and after laser ablation by scanning electron microscope (SEM). The effects of surface morphology changes before and after each CMP process were also reviewed to evaluate the surface planarization and the MRR. A white-light interferometer was used to measure three-dimensional surface roughness of non-irradiated and irradiated SiC substrates polished during each CMP process. An electronic balance with a resolution of 0.01mg was used to weigh substrate's weight change before and after CMP process for MRR evaluation. We found that lower surface roughness and higher MRR were realized after laser-assisted CMP process. Finally, X-ray diffraction analysis and X-ray photoelectron spectroscopy were carried out to explain the mechanism of laser-assisted CMP process.

3.2. The effect of laser irradiation at different laser output powers on CMP process

3.2.1 Experimental conditions

In this part of our experiments, we carried out CMP process to investigate the polishing behaviors of each area irradiated at different femtosecond laser output powers as well as effect of accumulation effect of energy deposition on CMP process. The linearly polarized laser beam was delivered through an optical mirror system and finally travelled through a 0.42 NA (50x) microscope objective lens with a working distance of 17mm. Then the focused stationary laser beam with a calculated spot size of about 3μm in ambient air was irradiated perpendicularly onto as-polished SiC Si-face mounted on a computer-controlled stage. Firstly, The SiC wafer was irradiated by femtosecond laser at scanning speed of 10mm/s, a repetition rate of 10MHz and scanning pitch of 0.5μm. The output powers of femtosecond laser were respectively set as 154mW, 144 mW, 130 mW, 120 mW, 108 mW, and 95 mW, containing higher fluence and near-threshold fluence. Each area was designed as a 3mm×3mm square. Considering the impact of XYZ stage inclination during its operation, we designed a symmetrical distribution of irradiating areas and the output power. For example, area A_1 and area A_1' were irradiated at symmetrical position but with the same conditions, the rest was done in the same manner, as shown in **Fig.3.1.** Zigzag scanning pattern shown in **Fig.3.2** ensured that the designed areas were irradiated respectively and thoroughly by utilizing a special program by which the focused laser spot was irradiated on SiC surface with a

scanning pitch of 0.5μm during laser irradiation.

After femtosecond laser irradiation, SiC substrates were rinsed in an ultrasonic cleaner with deionized water for 1 hour. Debris induced by fs laser was removed from the substrate surface to ambient water during ultrasonic cleaning process. The polishing conditions are shown in **Table 3.1**. A contacting surface roughness meter SE-30K (Kosaka Laboratory Ltd.) and a non-contacting optical interference surface roughness measurement apparatus Wyko NT3300 (Veeco Inc.) were utilized for surface morphology investigations.

Table 3.1 Experimental conditions of CMP process

Work piece		Single crystal 4H-SiC wafer Si-face Φ50.8mm
Polishing machine		LAPMASTER-15
Rotational speed [min^{-1}]		50
Polishing pad		Polyurethane foamed pad (IC1000)
Polishing pressure [kPa]		24.5
Slurry		Colloidal silica (COMPOL-80)
	Concentration of slurry [%]	8
	Abrasive size [nm]	70
	pH	11
	Flow rate [mL/min]	5
Processing atmosphere		Air
Processing time [s]		60s, 60s, 60s, 60s

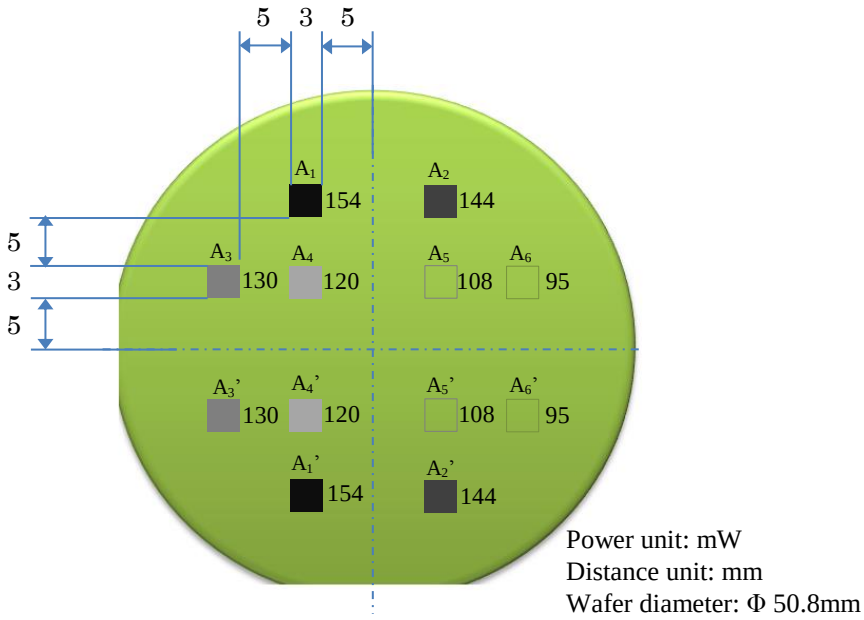

Fig.3.1 Design of femtosecond laser irradiation at different power on SiC (Si-face)

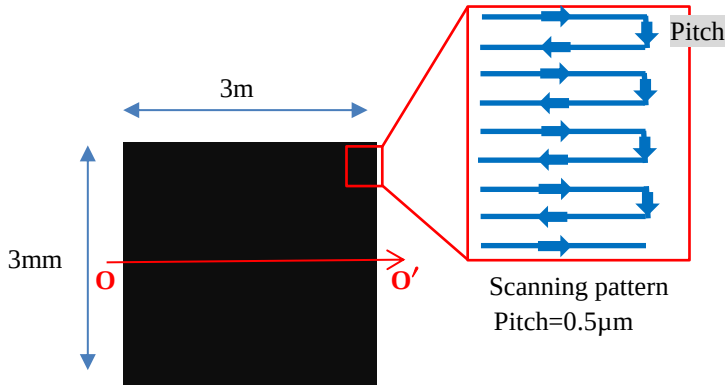

Fig.3.2 Zigzag scanning pattern of femtosecond laser focused spot

3.2.2 Distribution of femtosecond laser irradiation

After femtosecond laser irradiation, the SiC wafer surface was cleaned in deionized water by ultrasonic. As is seen in **Fig.3.3**, area A_1, area A_2 and their symmetrical areas A_1' A_2' were thoroughly ablated by higher output powers. Whereas areas A_3, A_4, A_3' and A_4' just were partly ablated by femtosecond laser, attributing to the lower output powers. Areas A_5, A_6, A_5' and A_6' were almost not ablated by femtosecond laser at lower powers.

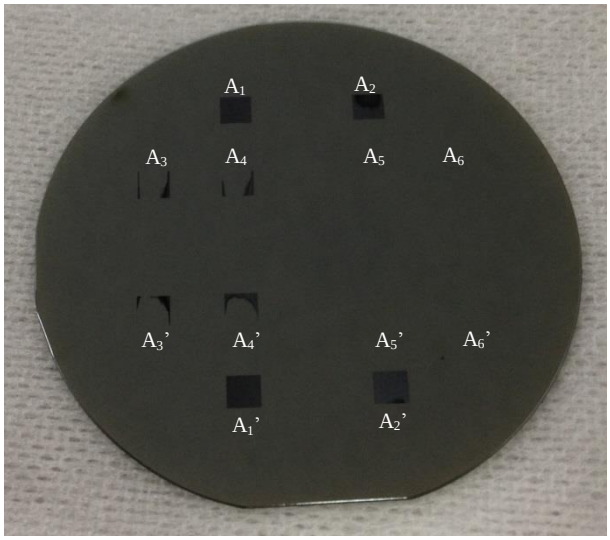

Fig.3.3 Femtosecond laser-irradiated SiC wafer (Si-face)

3.2.3 Investigation for laser-irradiated wafer by AY-41

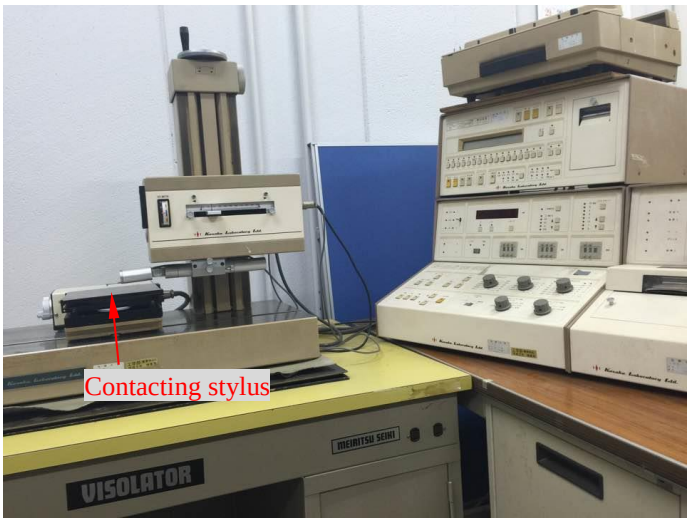

Fig.3.4 Appearance of SE-30K produced by Kosaka Laboratory Ltd.

Table 3.2 Main specification of SE-30K

Magnification	Longitudinal direction	Lateral direction
	50～100,000	1～1000
Stable	150（W）×150（D）mm	
contacting stylus	R5μm 90°	Diamond

Fig.3.5 Appearance of contacting stylus

In order to measure the cross section of laser-irradiated areas for profile investigation, a contacting surface roughness meter (produced by Kosaka Laboratory Ltd) was utilized. Its appearance is shown in **Fig.3.4**. The main specification is shown in **Table 3.2**. In this measurement apparatus system, a contacting stylus (as is shown in **Fig.3.5**) with a radius of 5μm was adopted onto a detector. The contacting head was controlled to scan each irradiated area from their center line O-O' (as shown in **Fig.3.2**) at a feeding rate of 0.5 mm/s, a horizontal magnification of 40, and a vertical magnification of 5000. **Fig.3.6** shows the cross section profiles of areas A_1', A_2' and A_3'. **Fig.3.6** (a) and **Fig.3.6** (b) shows that areas A_1'and area A_2' were ablated with depths of 0.4μm and 0.3μm respectively by femtosecond laser at high power. Whereas almost no ablated part was found from the center section profile of area A_3' except for the both ends, as is shown in **Fig. 3.6** (c).

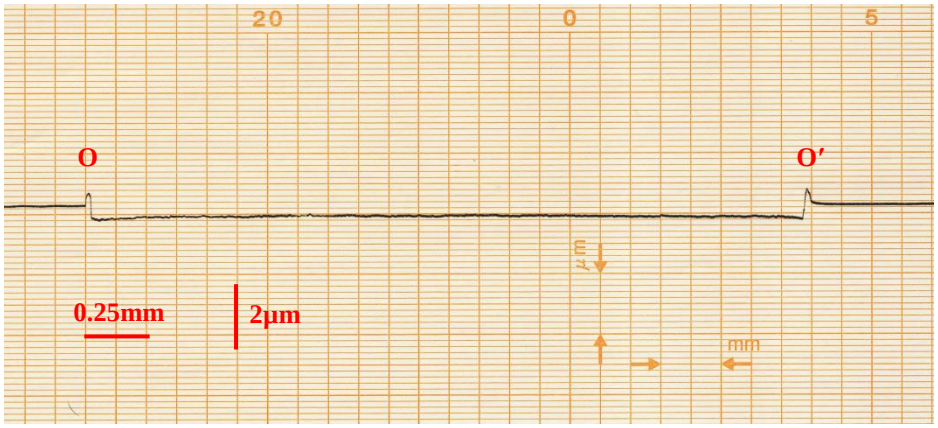

(a) Area A_1'

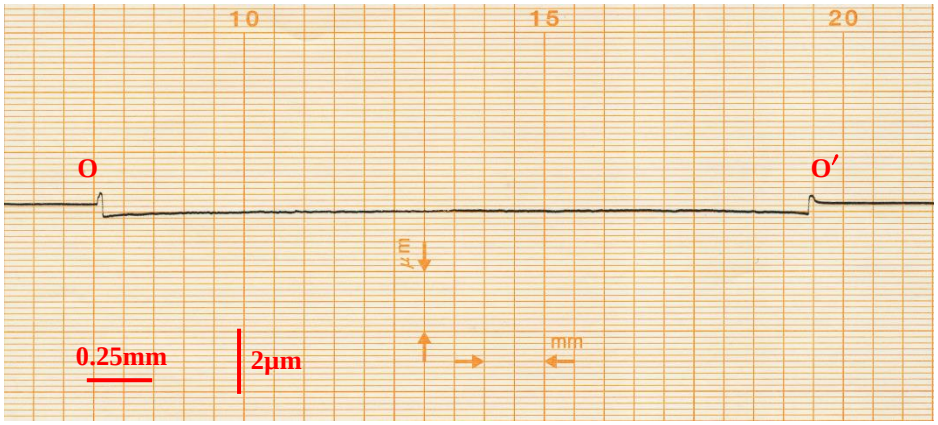

(b) Area A_2'

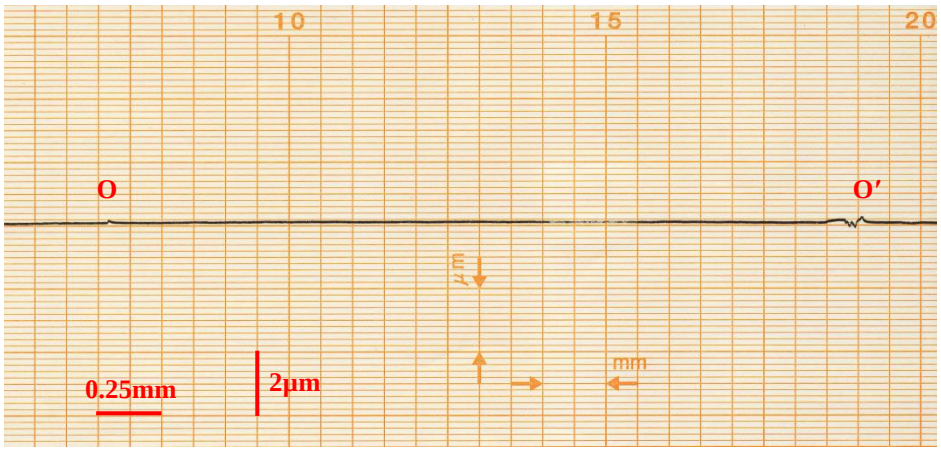

(c) Area A_3'

Fig.3.6 Cross section profiles of laser-irradiated areas at different output power

3.2.4 Investigation for laser-irradiated wafer by VEECO NT 3300

As the apparatus AY-41 is mainly used to evaluate the change of surface morphology by two dimensional measurements, it is not satisfactory for three dimensional surface morphology evaluations in this part. Subsequently, we carried out non-contacting optical interference surface roughness measurement apparatus Wyko NT3300 (Veeco Inc.) shown in **Fig.3.7** for the evaluation of three-dimensional surface morphology change before and after CMP process. Its schematic diagram is shown in **Fig.3.8**. The main principle of this apparatus is utilizing the interference of the light reflected from specimen surface and reference mirror for surface morphology measurement, as shown in **Fig.3.9**. The light path length difference of these two white light beams can sensitively lead to the movement of interference fringe, which is used for surface measurement of specimen. By Optical interference modes containing Phase Shift Interferometry (PSI) and Vertical Scan Interferometry (VSI), high resolution of respectively 1 Å and 1nm can be obtained, as is shown in **Table 3.3**. PSI mode is usually used to measure smooth surface at high roughness, while VSI mode is usually used to measure the surface of comparative roughness.

For CMP process, the experimental conditions are set as **Table 3.1**. It was carried out in air atmosphere. Especially, it should be noted that the polishing time during CMP process was set as 60s. After each polishing process, the wafer was cleaned in deionized water by ultrasonic for measurement and next polishing.

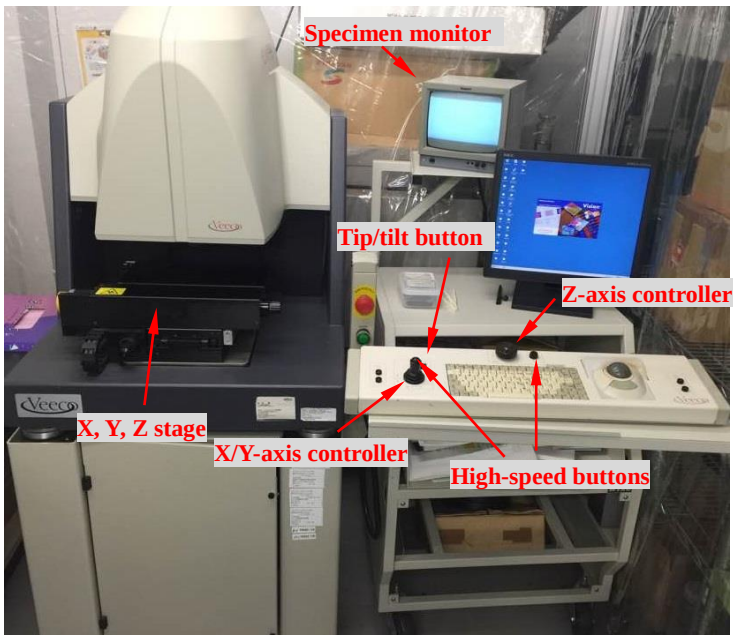

Fig.3.7 Appearance of measurement apparatus VEECO NT 3300

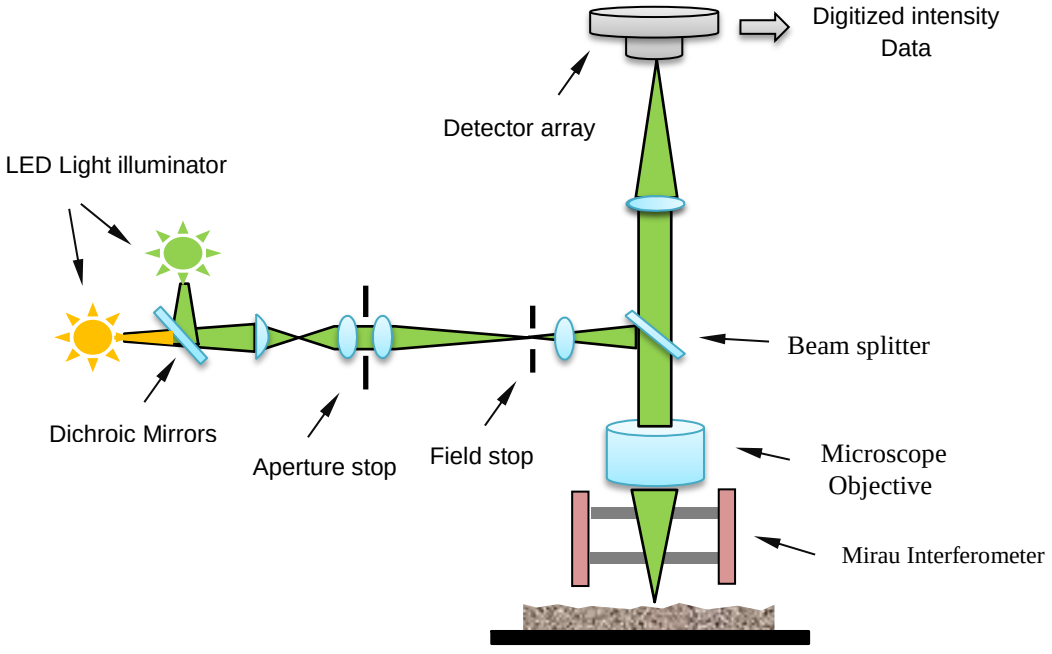

Fig.3.8 Schematic diagram of VEECO NT 3300

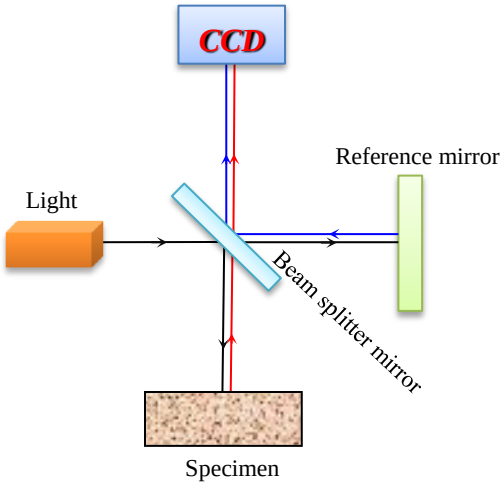

Fig.3.9 Phase shifting interferometry

Table 3.3 Measurement mode of VEECO NT 3300

Principle	Optical interference mode	
	PSI	VSI
Resolution	1 Å	1nm
Measurement range	1 Å-160nm	1nm-1mm

As is shown in **Fig.3.10** (a), the top left corner of area A_3' was observed and amplified by confocal laser scanning microscopy (CLSM) at a magnification of 20× before CMP process. The areas A and B marked with red frame in **Fig.3.10** (a) were further amplified at a magnification of 100× and shown in **Fig.3.10** (b) and **Fig.3.10** (c) respectively. In **Fig.3.10** (b), the area marked with red-dotted frame indicates the formation of large amount of oxide agglomeration induced by laser irradiation. The area on the right side of this red-dotted frame is laser-ablated zone, in which Laser Induced Periodic Surface Structures (LIPSS) were formed by fs laser. Nevertheless, even though the whole area shown in **Fig.3.10** (c) was horizontally irradiated by femtosecond laser beam spot with a scanning pitch of 0.5μm, the black oxidized parts were not fully distributed, which was quite a confusing experimental phenomenon. We call this laser-irradiated shape as dendritic pattern here. More experimental efforts and theoretical analysis will be done for its formation mechanism.

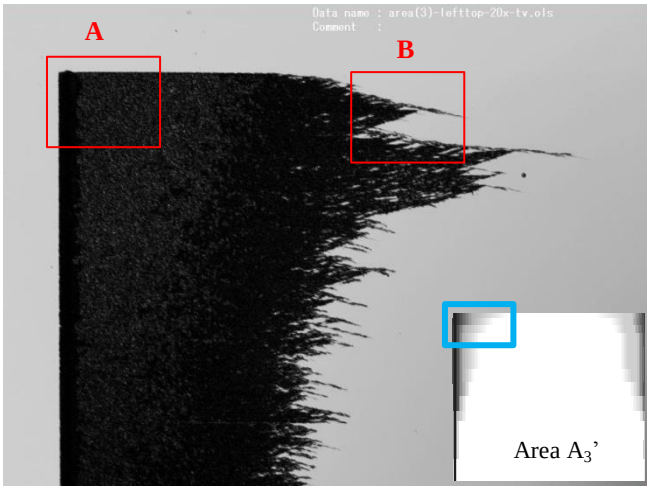

(a) CLSM image of area A3' (20 x)

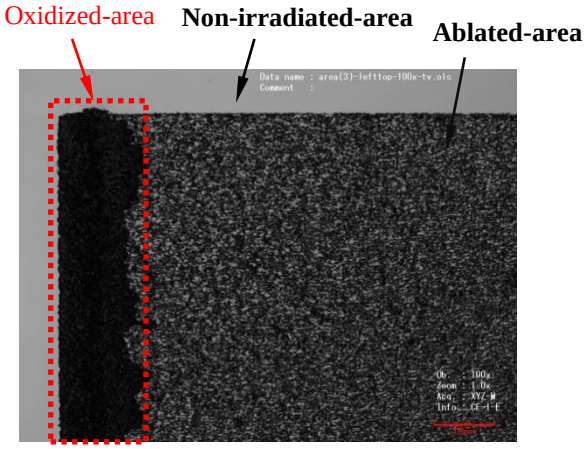

(b) Amplified image (100x) of area A

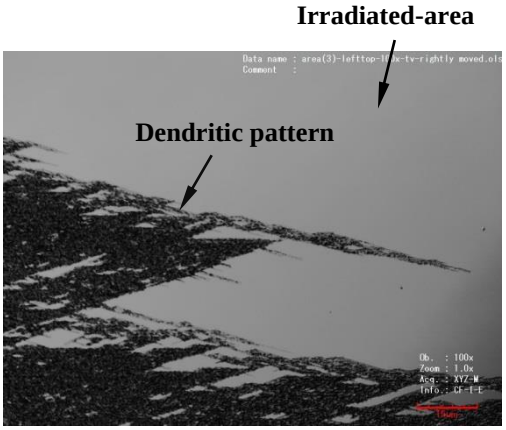

(c) Amplified image (100x) of area B

Fig.3.10 Top left corner of laser-irradiated area A3', Before CMP process

Fig.3.11 and **Fig.3.12** show the effect of CMP process on femtosecond laser-irradiated areas corresponding to **Fig.3.10** (a) and **Fig.3.10** (b), respectively. As shown in **Fig.3.11** (b) and **Fig.3.12** (b), the oxidized area and dendritic-pattern area were partly removed after 120s CMP process. The surfaces further changed more drastically after 240s CMP polishing. However, it is dramatic that no change was observed at the non-irradiated area shown in **Fig.3.11** (a) and the irradiated area shown in **Fig.3.12** (a) after 240s CMP process, even though they were simultaneously polished at the same conditions. In the final, we demonstrated the profile changes of the section marked as A-A' in **Fig.3.13** (a). From **Fig.3.13** (b) we found that the relative difference in height is approximately 0.6μm. As is shown in **Fig.3.14** (a), the lower left corner of laser-irradiated area A_3' was also investigated before and after CMP process. A relative difference in height ranging from 0.18μm to 0.72μm at cross section B-B emerged after 240s CMP polishing, demonstrating that the oxidized areas were quite easier to be polished. It should be noted that the oxidized areas were fast removed in CMP process, which is illuminating for our further study.

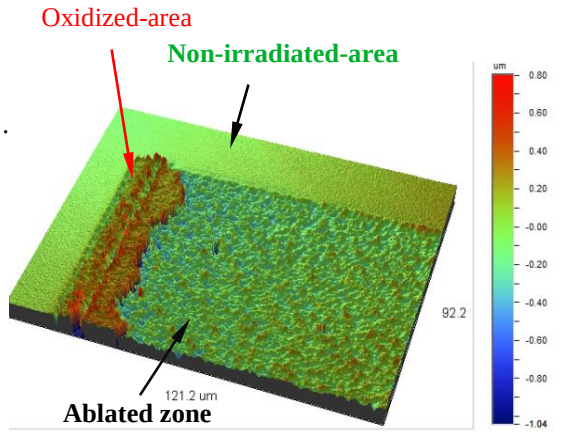

(a) Before CMP polishing

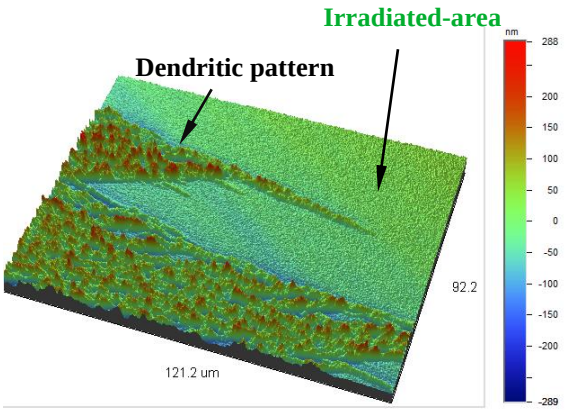

(a) Before CMP polishing

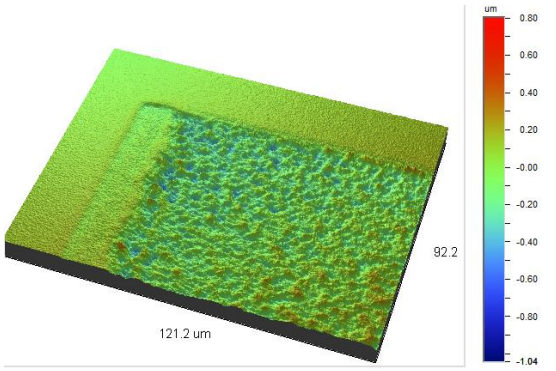

(b) After 120s CMP polishing

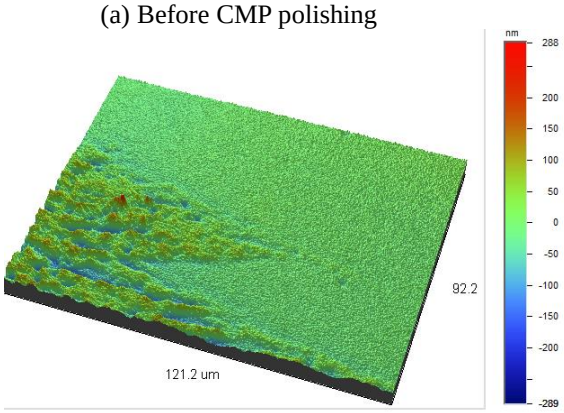

(b) After 120s CMP polishing

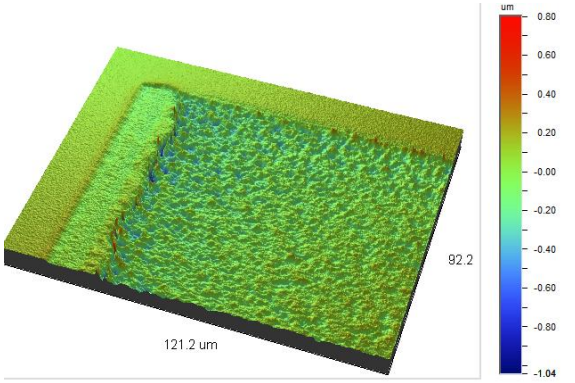

(c) After 240s CMP polishing

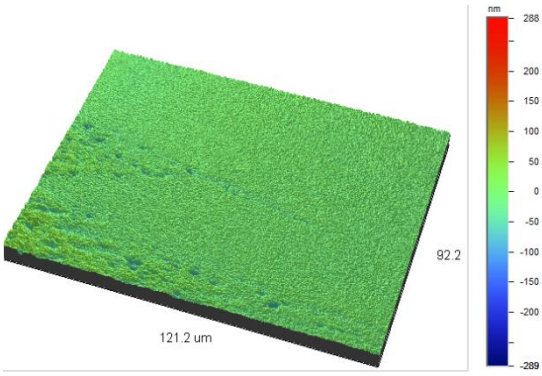

(c) After 240s CMP polishing

Fig.3.11 Effect of CMP polishing on area A

Fig.3.12 Effect of CMP polishing on area B

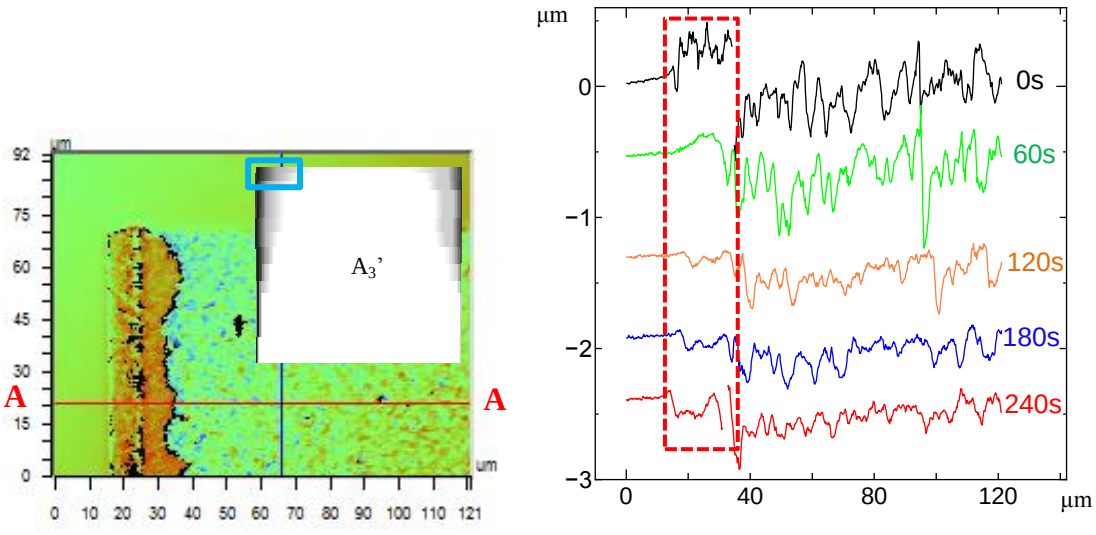

(a) Measuring section position A-A (b) Section profiles of A-A after CMP process

Fig.3.13 Effect of CMP process on top left area A

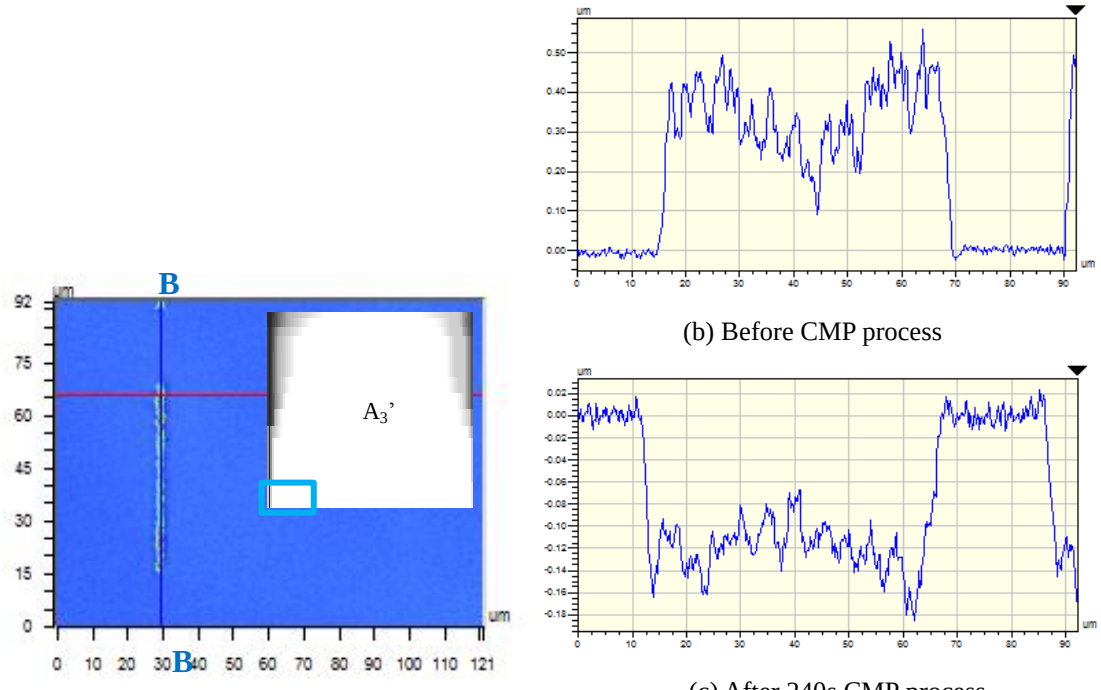

(a) Measuring section position B-B

(b) Before CMP process

(c) After 240s CMP process

Fig.3.14 Effect of CMP process on lower left corner of area A_3'

After 240s CMP processing, the oxidized area shown in **Fig.3.15** (b) was thoroughly removed from SiC surface. However, no change was observed at the irradiated area shown in **Fig.3.15** (d) after CMP process.

During laser ablation, its peak intensity can reach extremely high power (10^{12} W~10^{15} W), due to the short pulse duration (10^{-15}s). Electrons will be directly emitted from atom or molecule of the surface [33], accompanying with material melt [34], coulomb explosion [35, 36], etc. According to literature [37], low-laser-fluence was considered as an important condition for laser coulomb explosion; under near-threshold laser irradiation, lattice of SiC crystal was heated by laser irradiation, subsequently leading to so called "cold ablation" coulomb explosion and lattice vibration which was responsible for final lattice reconfiguration. Simultaneously, atomic bonds were partly ionized during coulomb explosion, leading to lattice disorder of SiC lattice [37]. Lattice reconfiguration and defects due to lattice disorder were activated during laser irradiation, seed defects were induced by fs laser irradiation in 4H-SiC at near-threshold fluence [27]. Sub-surface micro cracking and defect accumulation [38] of SiC crystal in the subsurface are regarded as dominating ablation mechanisms of these experimental incubation effects which induced inhomogeneous energy deposition. This was considered as the main reason of the emergence of the irregular dendritic pattern area shown in **Fig.3.10** (c). In addition, it was demonstrated that laser-induced sub-surface micro cracks and defects could not lead to obvious surface material remove during CMP process, as shown in **Fig.3.15**. This was attributed to the intensely high Mohs hardness and

chemical stability as well as compact atomic structure of SiC substrate.

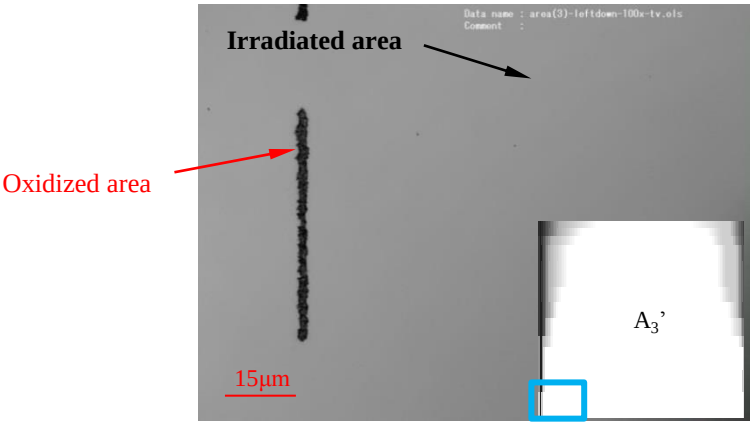

(a) Lower left corner of laser-irradiated area A3', CLSM image (100x), Before CMP process

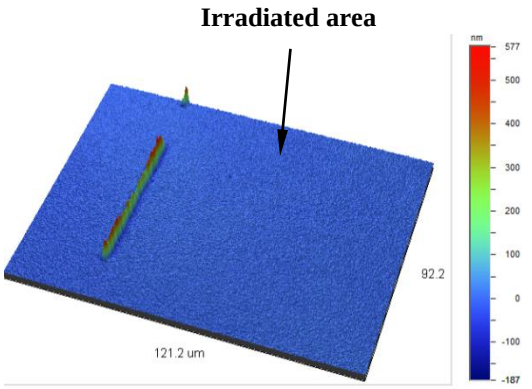

(b) Before CMP polishing

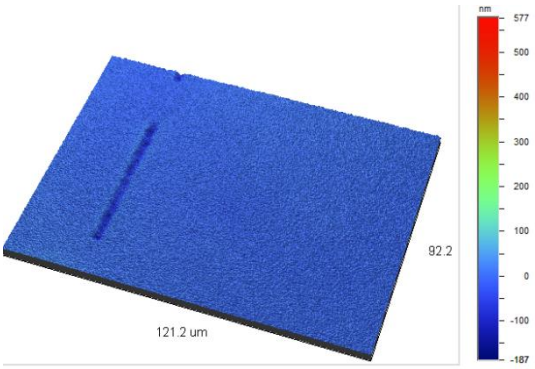

(c) After 120s CMP polishing

(d) After 240s CMP polishing

Fig.3.15 Three dimentional effect of CMP process on lower left corner of area A_3'

3.3 Polishing properties of laser-irradiated SiC (C-face)

3.3.1 Experimental conditions

In this part, C-face of SiC substrates were irradiated by femtosecond laser at a width of 373fs, a wavelength of 1030nm, a repetition rate of 10MHz and a fluence of 0.44 J/cm^2. A special zigzag pattern controlling program was designed for femtosecond laser scanning, ensuring that every interval between adjacent trajectories was 0.5μm. With the help of this control program, C-face of single crystal 4H-SiC (0001) substrate with a thickness of about 430μm was wholly irradiated on the three-dimensional XYZ stage. Transverse model irradiation and Cross-scan model irradiation were carried out on SiC substrates to investigate the surface morphologies and their effects on CMP process. The SiC substrates were irradiated at a scanning speed of 100mm/s by linearly polarized femtosecond laser beam with a focused spot of 3μm in diameter. All the experiments were done in normal air atmosphere. After femtosecond laser irradiation, the SiC substrates were cleaned by ultrasonic for 1 hour by using deionized water.

After femtosecond laser irradiation, the irradiated SiC substrates and the non-irradiated SiC substrate were fixed by a thin plate shown in **Fig.3.16** and polished simultaneously CMP process in CMP process. The experiment conditions of CMP process are set as: colloidal silica slurry (COMPOL-80, from Fujimi Incorporated), a polishing pressure of 120 kPa, and rotational speed of 50min^{-1} in air atmosphere. The average size of abrasive grains was 80nm; the slurry flow rate was 5mL/min, the concentration and pH of slurry was 7.5% and 11 respectively. During CMP process,

each polishing time interval was set to 60s, except that the last two polishing time intervals were set as 300s to confirm the effect of CMP process finally. A white-light interferometer and a scanning electron microscope (SEM) were used to investigate the surface morphologies of laser-irradiated and non-irradiated SiC substrates before and after each CMP process. High resolution (0.01mg) electric balance was used to weigh the change of the substrate's weight before and after CMP process for the evaluation of MRR. Finally, X-ray diffraction analysis and X-ray photoelectron spectroscopy were carried out to explain the mechanism of laser-assisted CMP process.

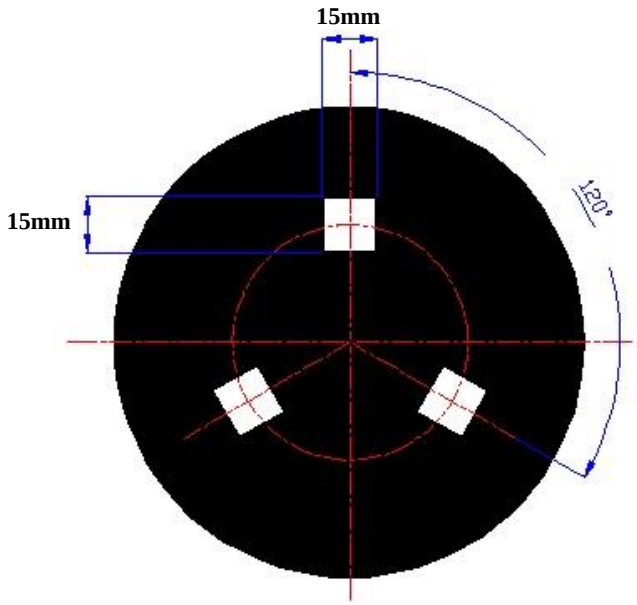

Fig.3.16 Fixing plate used in CMP process

3.3.2 Results and discussion

Fig.3.17 (a) indicates non-irradiated as-lapped C-face of SiC substrate before CMP process. The rough surface with irregular tiny cracks and indentations can be seen clearly in **Fig.3.17 (a)**. Comparing **Fig.3.17 (a)** with **Fig.3.17 (a)**, it is found that the irregular as-lapped surface morphology was fabricated into periodic rippled morphology with spatial periodicity of approximately 150nm induced by laser irradiation. **Fig.3.18 (a)** and **Fig.3.19 (a)** respectively show transversely-irradiated substrate (**Fig.3.20 (a)**) and cross-scan irradiated substrate (**Fig.3.20 (b)**) with periodic patterns fabricated by femtosecond laser with a fluence of 0.44J/cm^2. **Fig.3.20 (a)** shows the schematic diagram of transverse laser scanning model. In this model, after each X direction horizontal scan, laser beam was fed with a 0.5μm pitch in vertical (Y) direction for another horizontal scan carried out in the opposite horizontal (X) direction. This process was continuously cycled until the substrate surface was fully irradiated. **Fig.3.20 (b)** shows another type of laser process model. In this model, SiC substrate irradiated by fs laser in transverse irradiation model (**Fig.3.20 (a)**) was cleaned by ultrasonic in deionized water and further mounted on the XYZ stage with a rotation angle of 90° for further fs laser irradiation at the same laser conditions. This trajectory-crossed laser process is called as cross-scan irradiation model here (**Fig.3.20 (b)**). After femtosecond laser irradiation, the irradiated substrates (**Fig.3.18 (a)** and **Fig.3.19 (a)**) were cleaned by ultrasonic for 1 hour using deionized water and were observed by SEM. The cross-scan irradiated substrate was observed at the same observation perspective with that of the

transversely irradiated one, as shown in **Fig.3.18 (a)** and **Fig.3.19 (a)**. In transverse irradiation model, nanoscale parallel periodic patterns were induced from the irregular rough as-lapped C-face during fs laser irradiation. These laser-induced periodic patterns were further fabricated into compactly distributed periodic nanostructures shown in cross-scan irradiation model (**Fig.3.19 (a)** and **Fig.3.20 (b)**) during trajectory-crossed laser process.

Many studies have been carried out to understand the formation mechanism of those kinds of ripples. It is found that the nanostructures depend strongly on wavelength, laser polarization and laser beam incidence angle [39, 40]. Some researchers reminded that interference of incident laser light and scatter waves [41], the generation of second-harmonic [42], self-organization [43] and surface plasmon polarizations are responsible for the formation of periodic ripples. Other researchers also investigated laser-induced periodic surface structures on ceramic material Si_3N_4/TiC. They found that the femtosecond laser-induced ripples depended strongly on the pulse energy, scanning speed and number of repeated scans [44]. In recent years, laser-induced ripples on SiC substrate were also widely studied. In reference [45], morphology formation evolution induced by femtosecond laser (515nm, 250fs, 100 kHz) on SiC targets was investigated by increasing femtosecond laser pulses with fluence of 1.17J/cm^2. The authors pointed out that the single-pulse ablation threshold of the low surface roughness (<20nm) SiC sample was 1.07J/cm^2. Fine and coarse ripples were fabricated by femtosecond laser on SiC substrate, and it is found that initial surface roughness plays a remarkable effect for the formation of

fine ripples [46]. This was attributed to that the roughened surface reduced threshold fluence. In literature reference [27], it is elucidated that Mie scattering from the surface defect was a cause of high special frequency periodic ripples (HSFL) induced by fs laser in SiC surface; in addition, the number of HSFL was enhanced with increasing pulse numbers. In our study, the laser with fluence of 0.44 J/cm^2 was irradiated onto as-lapped rough SiC surface with lots of cracks. Regardless of that the fluence was far below than that of [45], regular periodical ripples were induced on SiC surface. This is assumed that the thermalization of electrons and lattice defects existing in rough and irregular surface cracks was extremely fast during laser irradiation, contributing to laser-induced ripples formation on as-lapped SiC C-face. **Fig.3.17 (b)**, **Fig.3.18 (b)** and **Fig.3.19 (b)** respectively denote the polished surface morphologies of **Fig.3.17 (a)**, **Fig.3.18 (a)** and **Fig.3.19 (a)**. After 1560s CMP polishing, both the irregular morphology and the periodic ripples were removed mostly. Nevertheless, in comparison with **Fig.3.19 (b)**, residual indentations and ripples were still respectively observed on the surface of non-irradiated substrate and transversely-irradiated substrate, as shown in **Fig.3.17 (b)** and **Fig.3.18 (b)**. Conclusion can be drawn that different laser processes with different surface morphologies may lead to improvements for surface quality during CMP process by comparing the polished surface morphology shown in **Fig.3.17 (b)**, **Fig.3.18 (b)** and **Fig.3.19 (b)**; in addition, cross-scan irradiation model contributes to better surface after CMP process. To confirm this conclusion, white light interferometer measurement was carried out.

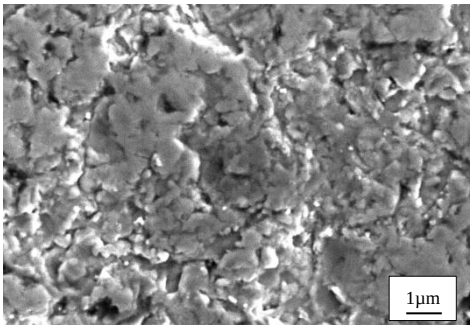

Fig.3.17 (a) Non-irradiated substrate (0s) before CMP

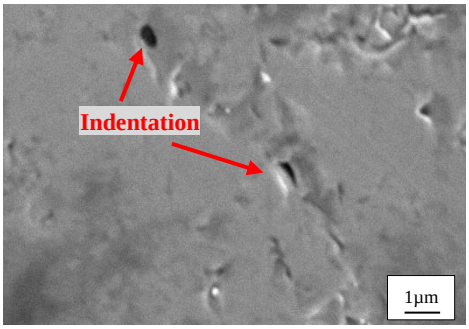

Fig.3.17 (b) Non-irradiated substrate (1560s) after CMP

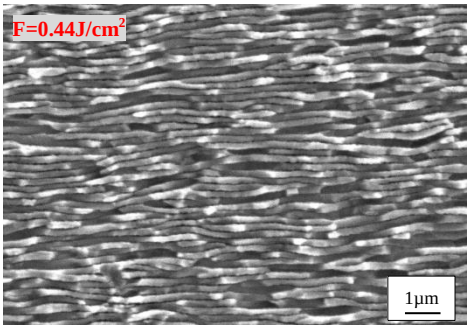

Fig.3.18 (a) Transversely-irradiated substrate (0s) before CMP

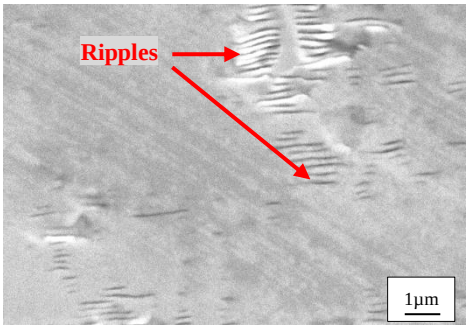

Fig.3.18 (b) Transversely-irradiated substrate (1560s) after CMP

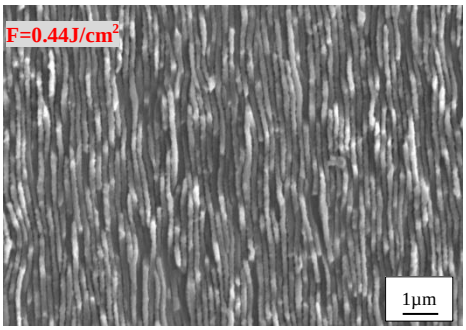

Fig.3.19 (a) Cross-scan irradiated substrate (0s) before CMP

Fig.3.19 (b) Cross-scan irradiated substrate (1560s) after CMP

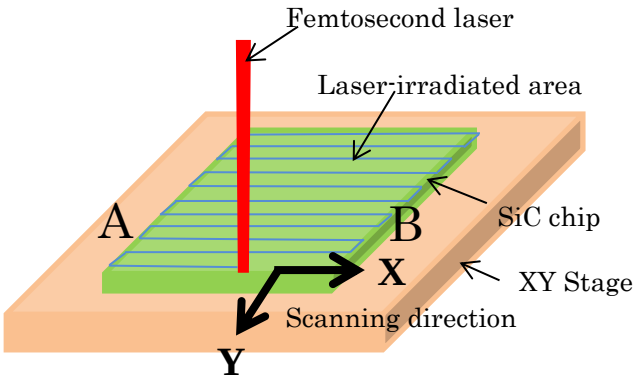

Fig.3.20 (a) Transverse irradiation model

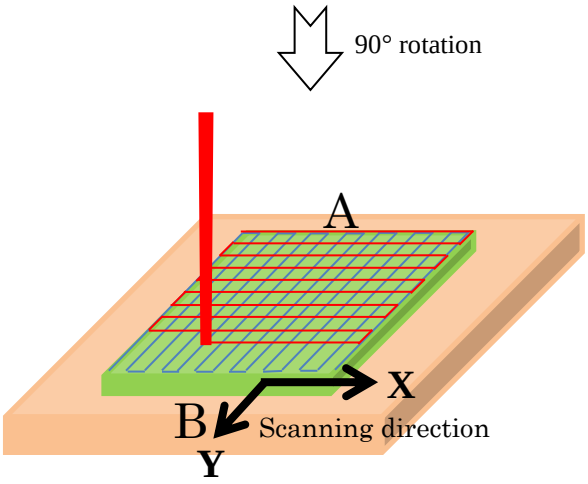

Fig.3.20 (b) Cross-scan irradiation model

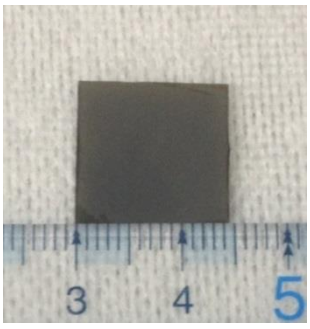

Fig.3.21 Image of SiC C-face after fs laser irradiation

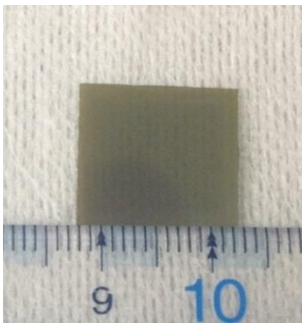

Fig.3.22 Image of SiC C-face after 1560s CMP process

The authors have previously carried out femtosecond laser irradiation experiment for a diamond substrate regarded as the hardest material on the earth. The subsequent cross section of diamond captured by TEM observation displayed that a thin amorphous layer with depth of approximately 10nm was induced by femtosecond laser [24]. Diamond and SiC are both considered as hard-to-process semiconductor materials. A continuous amorphous layer of about 10~50nm thick was fabricated by fs laser on a 4H-SiC single-crystal surface [47]. It is conceivable that amorphous layer was induced on C-face of SiC substrate by fs laser. **Fig.3.21** and **Fig.3.22** respectively show the images of SiC substrate irradiated in Transverse Irradiation Model before and after CMP process. After 1560s CMP process, the substrate seems to be transparent as initial before laser irradiation. It is assumed that femtosecond laser-affected layer was mostly removed from SiC substrate surface.

Fig.3.23 (a), Fig.3.24 (a), Fig.3.25 (a) and **Fig.3.26 (a)** show the birds-eye images and surface roughness of non-irradiated as-lapped SiC substrate center zone before and after CMP process. **Fig.3.23 (b), Fig.3.24 (b), Fig.3.25 (b)** and **Fig.3.26 (b)** show the birds-eye images of that in transverse irradiation model substrate (**Fig.3.20 (a)**). **Fig.3.23 (c), Fig.3.24 (c), Fig.3.25 (c)** and **Fig.3.26 (c)** show the birds-eye images of that in cross-scan irradiation model substrate (**Fig.3.20 (b)**). The numbers in every bracket attached to those images show polishing times of each CMP process. **Fig.3.23 (a)** and **Fig.3.23 (b)** was juxtaposed with **Fig.3.23 (c)** to show the difference of surface morphology among non-irradiated substrate, transverse irradiation model substrate and cross-scan irradiation model substrate

before CMP polishing. The rest can be deduced by analogy. Ra being used as the most common type of average surface roughness is defined as arithmetic mean of the roughness profile. Rq is root mean square roughness. Rt is defined as the maximum height of profile. Surface features were described by those roughness parameters for the substrate center positions. From the comparison of the birds-eye images of **Fig.3.23 (a), Fig.3.23 (b)** and **Fig.3.23 (c)**, it is found that Ra and Rq of non-irradiated substrate (**Fig.3.23 (a)**) were approximately the same with that of laser-irradiated substrate (**Fig.3.23 (b)**), but Rt became larger than that of non-irradiated substrate after laser irradiation. This is supposed to be attributed to that larger indentations among periodic ripples were induced by fs laser (shown in **Fig.3.18 (a)**), giving rise to rougher surface after laser ablation. However, it was difficult to compare and evaluate the surface roughness for cross-scan irradiation substrate (shown in **Fig.3.23 (c)**) due to the unsatisfactory measurement of white light interferometer. It is supposed that substantial oxidation fabricated by laser in the cross-scan irradiation substrate blocked the formation of interference patterns in white light interferometer detector. According to comparison of surface roughness after CMP process, it is found that surface quality improved well with each CMP process; surface of cross-scan irradiation model substrate is considerably flat comparing to non-irradiated substrate and transverse irradiation model substrate. Very smooth surface was realized in cross-scan irradiation model substrate after 1560s CMP process, as shown in **Fig.3.26 (c)**. Roughness decrease trends were found by comparison of **Fig.3.24 (a), Fig.3.25 (a), Fig.3.26 (a)** and **Fig**.**3.24 (c),**

Fig.3.25 (c), Fig.3.26 (c); whereas the surface roughness was found with a slight decrease by comparing **Fig.3.24 (b)** and **Fig.3.25 (b)**, differing from the slight surface roughness increase shown from **Fig.3.25 (b)** to **Fig.3.26 (b)**. As shown in **Fig.3.17 (a)** and **Fig.3.17 (b)**, large asperities on the non-irradiated surface were polished, remaining a matrix surface with tiny indentations and cracks after 1560s polishing process. This is considered responsible for the roughness reduction tendency of the non-irradiated surface with CMP process. While the trend shown in **Fig.3.24 (b)**, **Fig.3.25 (b)** and **Fig.3.26 (b)** is assumed that after the nanoscale patterns on the surface were removed during CMP process, an amorphous layer started to be polished, giving birth to lower roughness surface (**Fig.3.25 (b)**); eventually SiC matrix with tiny cracks appeared (as shown in **Fig.3.18 (b)**), resulting in a rougher surface shown in **Fig.3.26 (b)**. After repeated laser ablation in cross-scan irradiation (**Fig.3.20 (b)**), the surface with tiny indentations and cracks) were further ablated by fs laser, inducing compactly distributed periodic patterns. With CMP process, a smooth surface with lower roughness surface was gradually obtained, resulting in the roughness decrease trend shown in **Fig.3.24 (c), Fig.3.25 (c)** and **Fig.3.26 (c)**.

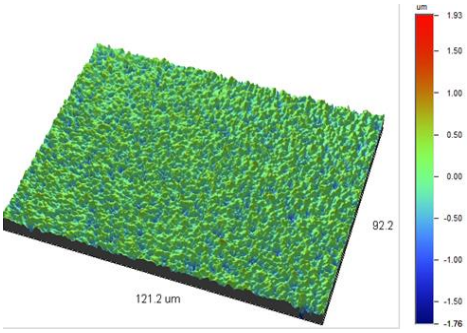

Fig.3.23 (a) Non-irradiated chip (0s)
Ra=187nm, Rq=237nm, Rt=2430nm

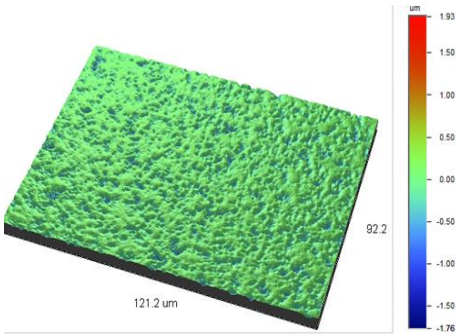

Fig.3.24 (a) Non-irradiated chip (420s)
Ra=87nm, Rq=119nm, Rt=1620nm

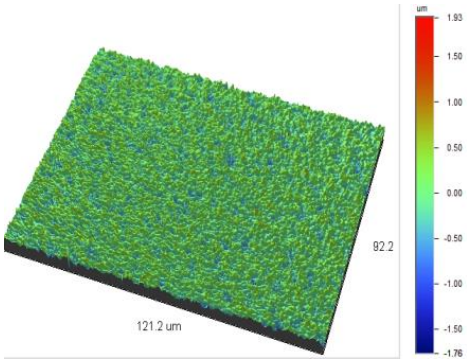

Fig.3.23 (b) Transversely-irradiated chip (0s)
Ra=184nm, Rq=233nm, Rt=3560nm

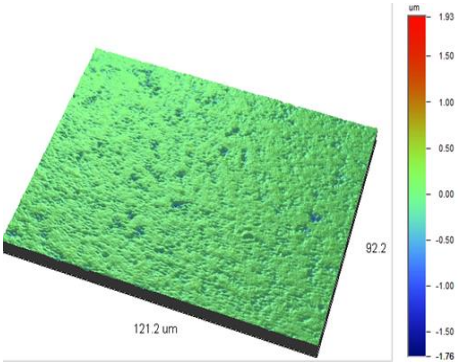

Fig.3.24 (b) Transversely-irradiated chip (420s)
Ra=41nm, Rq=61nm, Rt=1130nm

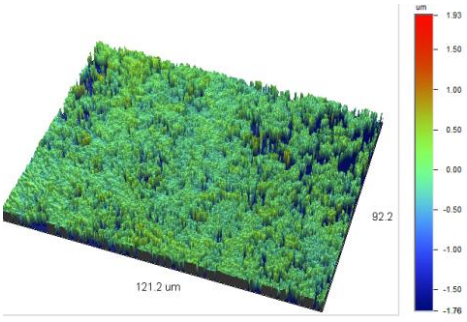

Fig.3.23 (c) Cross-scan irradiated chip (0s)
(partly range over)

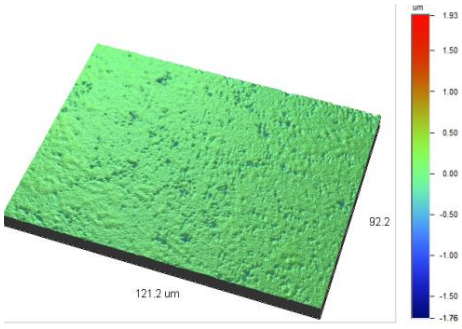

Fig.3.24 (c) Cross-scan irradiated chip (420s)
Ra=30nm, Rq=48nm, Rt=930nm

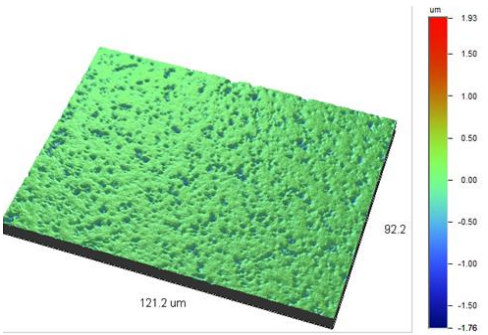

Fig.3.25 (a) Non-irradiated chip (960s)
Ra=58nm, Rq=90nm, Rt=1060nm

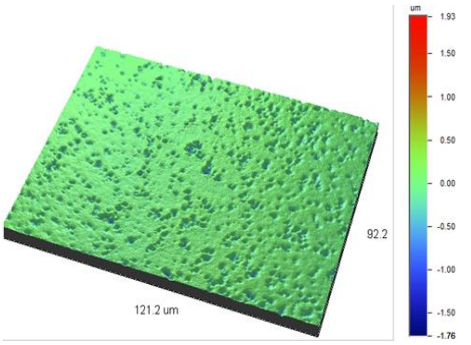

Fig.3.26 (a) Non-irradiated chip (1560s)
Ra=51nm, Rq=78nm, Rt=1110nm

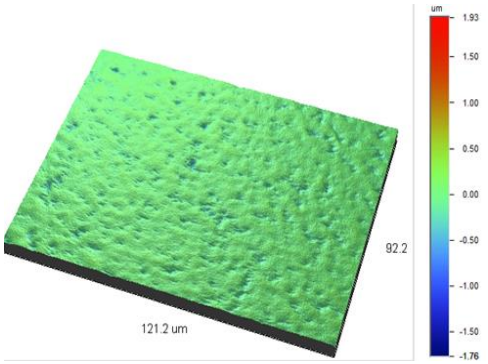

Fig.3.25 (b) Transversely-irradiated chip (960s)
Ra=38nm, Rq=52nm, Rt=695nm

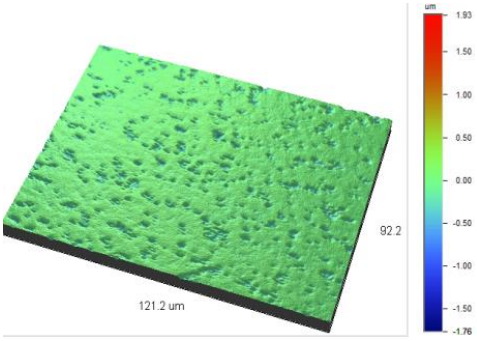

Fig.3.26 (b) Transversely-irradiated chip (1560s)
Ra=45nm, Rq=67nm, Rt=819nm

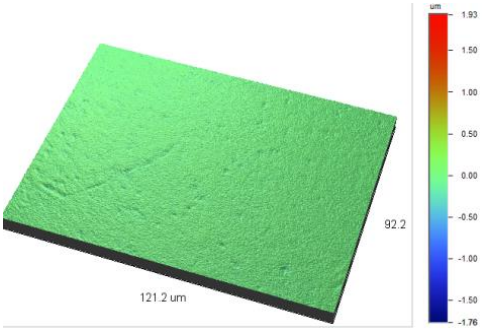

Fig.3.25 (c) Cross-scan irradiated chip (960s)
Ra=13nm, Rq=17nm, Rt=339nm

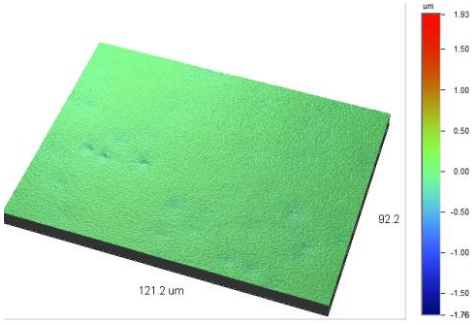

Fig.3.26 (c) Cross-scan irradiated chip (1560s)
Ra=17nm, Rq=22nm, Rt=267nm

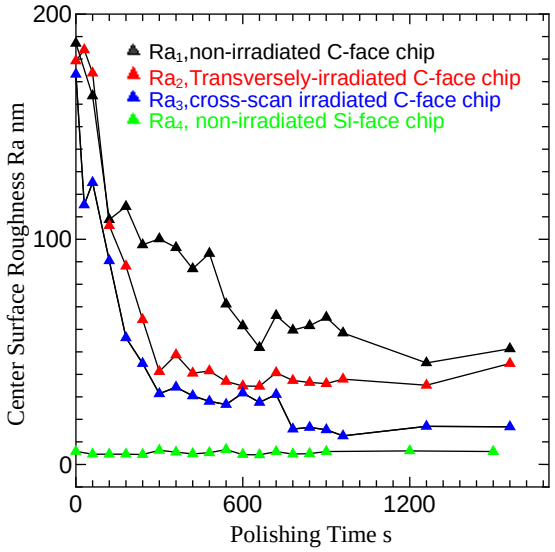

Fig.3.27 Relation between Ra and polishing time

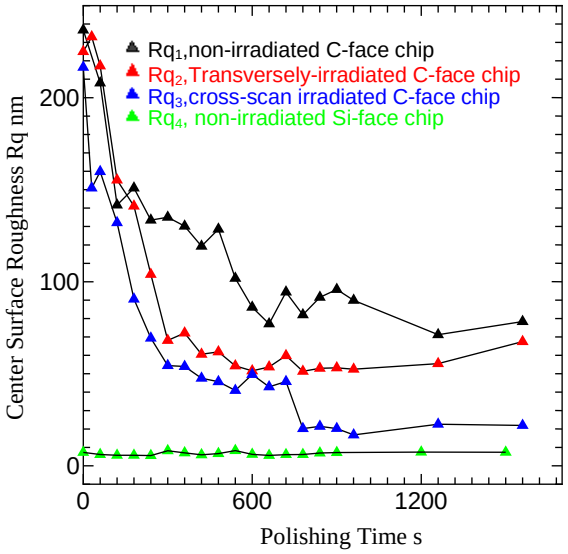

Fig.3.28 Relation between Rq and polishing time

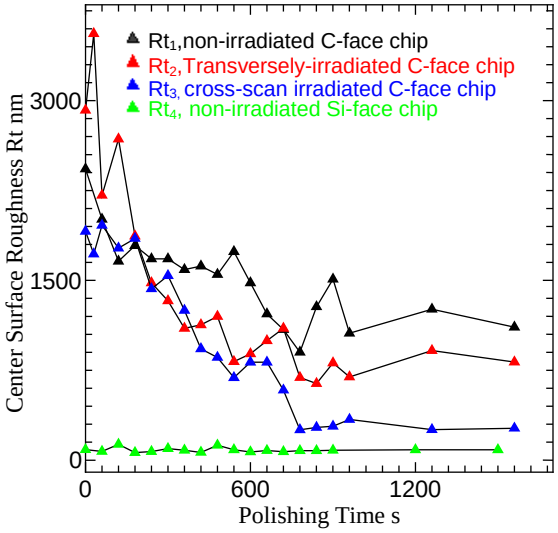

Fig.3.29 Relation between Rt and polishing time

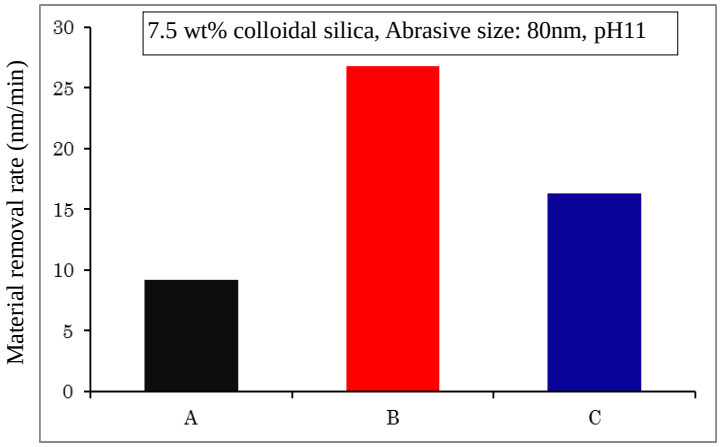

A: non-irradiated chip, B: transversely-irradiated chip, C: cross-scan irradiated chip

Fig.3.30 Comparison of MRR of femtosecond laser-irradiated chip and non-irradiated chip

The roughness measured by white light interferometer of each substrate before and after each CMP process was plotted in accordance with the polishing time, as shown in **Fig.3.27**, **Fig.3.28** and **Fig.3.29**. Surface roughness of non-irradiated substrate, transverse irradiation model substrate and cross-scan irradiation model substrate was obviously decreased with CMP process. Ra_1, Rq_1, and Rt_1 mean the surface roughness of non-irradiated substrate, Ra_2, Rq_2, and Rt_2 mean the surface roughness of transverse irradiation model substrate, and Ra_3, Rq_3, and Rt_3 mean the surface roughness of cross-scan irradiation model substrate respectively.

Before femtosecond laser ablation, the original surface roughness Ra_1, Rq_1 and Rt_1 of non-irradiated SiC substrate were respectively 187nm, 237nm and 2430nm (**Fig.3.26 (a)**). After transverse irradiation model process and cross-scan irradiation model process, Ra and Rq changed slightly. The coherent and homogenously distributed nanoscale parallel periodic patterns (**Fig.3.18 (a)** and **Fig.3.19 (a)**) induced by femtosecond laser on SiC substrate were supposed to give rise to similar Ra and Rq (**Fig.3.27** and **Fig.3.28**) to that of the non-irradiated substrate. However, as shown in **Fig.3.29**, Rt increased substantially after transverse irradiation, comparing with the slight change of Rt after cross-scan irradiation. As shown in **Fig.3.18 (a)**, substantial indentations among periodic patterns were observed, this is assumed as the reason of the remarkable increase of Rt shown in **Fig.3.19**. The periodic patterns induced in transverse irradiation process were repeatedly irradiated by fs laser during the cross-scan irradiation process, leading to compactly distributed periodic patterns without large indentations (**Fig.3.19 (a)**). As shown in **Fig.3.27, Fig.3.28** and **Fig.3.29**,

during polishing time interval of 0~240s, the periodic patterns fabricated by laser were gradually polished during CMP process, bringing about a prompt decreasing tendency of surface roughness; during polishing time interval of 240s~960s, surface roughness decreased relatively slowly, revealing that laser-induced amorphous layer was partly and gradually removed during CMP process after the elimination of periodic ripples; the curve between polishing time interval of 960s~1560s shows that the surface roughness changed hardly regardless of increasing polishing time. It is supposed that the emerged matix of SiC preventing further polishing after long time polishing. The final roughness after CMP process of cross-scan irradiation model substrate was Ra_3=17nm, Rq_3=22nm, and Rt_3=267nm. Comparing the images of **Fig.3.26 (a), Fig.3.26 (b)** and **Fig.3.26 (c)**, it is clearly found that quite small surface roughness was realized after CMP process of cross-scan irradiation model laser-fabricated substrate. As-polished Si-face of SiC substrate was also polished during CMP process at the same conditions simultaneously. However, according to the roughness tendencies shown in **Fig.3.27, Fig.3.28** and **Fig.3.29**, it was found that the roughness of as-polished Si-face hardly changed during present CMP process. The results shown in **Fig.3.27, Fig.3.28** and **Fig.3.29** indicate that the slurry abrasive SiO_2 at present conditions could polish laser-induced layer but couldn't polish as-polished Si-face or the original matrix of C-face further. **Fig.3.30** shows MRR of the polished SiC substrates. It reveals that the MRR of the transverse irradiation model substrate is about 3 times higher than that of cross-scan irradiation model substrate; meanwhile, the MRR of cross-scan irradiation model substrate is about 1.8 times higher than that

of non-irradiated substrate. It is concluded that periodic ripples and amorphous layer (schematically shown in **Fig.3.18**, and **Fig.3.19**) were also induced by repeated femtosecond laser machining process of SiC substrate. The polishing of periodical nanoscale parallel patterns and amorphous layer led to better surface roughness and higher MRR than the substrate which was not irradiated by fs laser.

Owning to the fact that few studies with regard to as-lapped SiC C-face irradiated by femtosecond laser have been done, more studies should be further implemented to understand the formation mechanism of the ripples induced in SiC C-face substrate. In further, reasonable experimental conditions related to femtosecond laser, such as laser fluence, wavelength, polarization, scan speed, laser beam trajectory interval, surface roughness and the number of repeated scans, must be thoroughly investigated to understand the effect of fs laser on as-lapped SiC C-face. TEM observation should also be carried out to investigate the amorphous layer fabricated in transverse irradiation model and cross-scan irradiation model. Appropriate experimental parameters will be arranged for satisfactory surface morphology which can bring high efficiency and high planarization for CMP process.

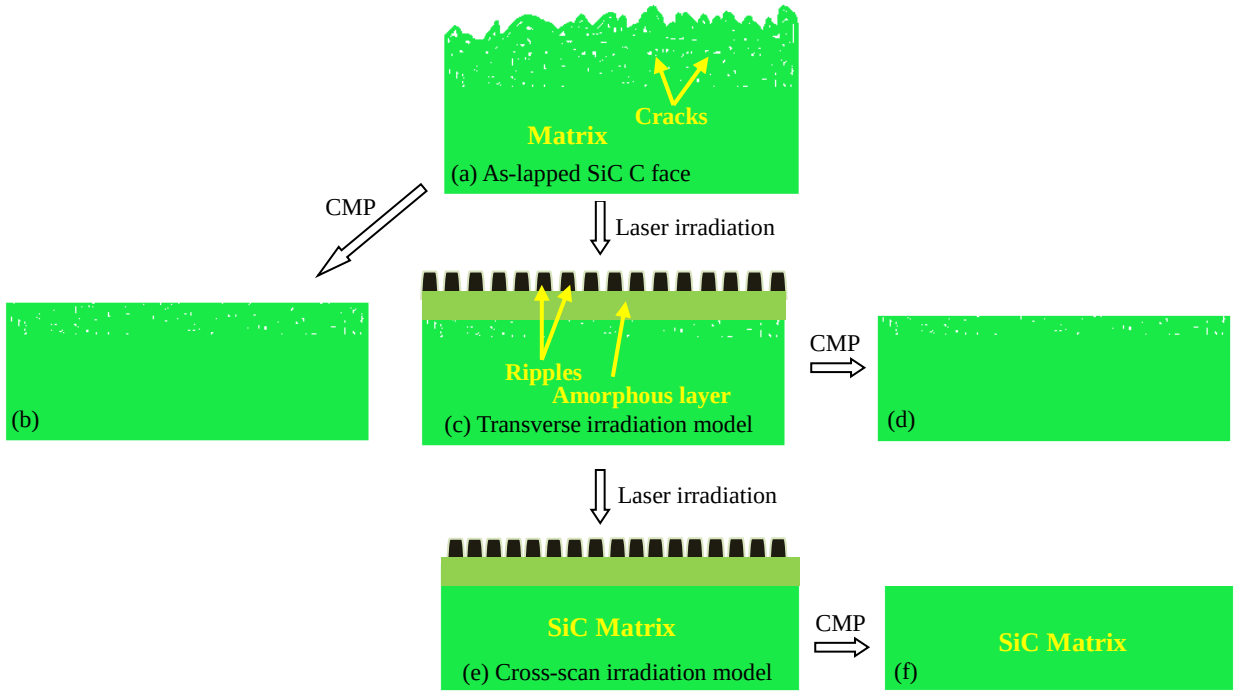

Fig.3.31 Schematic diagram for comparing common CMP and femtosecond laser-assisted CMP for SiC substrate C-face

According to the experimental results shown in SEM and white light interferometer images above, a schematic diagram of conventional CMP and fs laser-assisted CMP process was proposed in **Fig.3.31** for detailed explanation. **Fig.3.31 (a)** corresponding to **Fig.3.17 (a)** shows the schematic section of as-lapped SiC substrate accompanying with a rough surface with many indentations and tiny cracks after lapping process. As shown in **Fig.3.31 (b)**, although it was polished in CMP process for 1560s, indentations shown in **Fig.3.17 (b)** was still found remained in the polished SiC surface. **Fig.3.31 (c)** and **Fig.3.31 (e)** show the schematic cross sections perpendicular to ripples distribution direction of transverse irradiation model substrate (**Fig.3.18 (a)** and **Fig.3.20 (a)**) and cross-scan irradiation model substrate (**Fig.3.19 (a)** and **Fig.3.20 (b)**) respectively. It is assumed that amorphous layer was induced below the periodic structures in the subsurface of SiC substrate. As shown in **Fig.3.31 (c)**, a layer with residual cracks was not fully ablated in spite of laser irradiation, resulting to a relatively rough surface shown in **Fig.3.18 (b)** and **Fig.3.26 (b)** corresponding to **Fig.3.31 (d)** after CMP process. As the laser-irradiated surface of transverse model was mounted on XYZ stage again with a 90° rotation and further fabricated by fs laser, compactly distributed periodic structures with amorphous layer were induced by fs laser (**Fig.3.19 (a)** and (**Fig.3.31 (e)**). Because the residual indentations and cracks were hardly found on the polished surface after CMP process in **Fig.3.19 (b)** and **Fig.3.26 (c)** corresponding to **Fig.3.31 (f)**, it is notably assumed that the layer with residual cracks could be mostly removed from SiC surface by repeated laser ablation. In

addition, in literature [48], oxygen concentration detected by energy dispersive X-ray spectroscopy increased with laser pulse energy, revealing that some interaction between fs laser and SiC material was triggered. Chemical reaction between slurry and laser-irradiated SiC surface and physical characteristics were inspected in the following, aiming for further detailed understanding of the mechanism of femtosecond laser-assisted CMP process.

3.3.3 Investigation according to X-ray diffraction analysis

To understand the effect of laser irradiation of CMP process, X-ray diffraction analysis (XRD) was implemented. XRD measurement is considered as an effective method for investigating crystalline material and some amorphous structures. As shown in **Fig.3.32** (a), the crystal material is made up of parallel equidistant atomic planes A, B, C, etc. After X-rays were irradiated to the crystal surface, the incident X-ray beams will be reflected by atoms present in the atomic plans. Some of these reflected beams will reinforce into each other if they are in phase, leading to the maximum intensity of the reflected beam. While some of them are out of phase, the intensity of reflected beams will be weakened, result in the minimum intensity. Especially, if the following Bragg equation is met, maximum intensity of reflected beam will be obtained. Phase analysis, containing qualitative analysis and quantitative analysis, is the main analysis of X-ray diffraction. According to XRD measurement, crystal orientation analysis, crystallite size, micro crystal stress, material macro stress, lattice parameters as well as crystallinity can be obtained by

XRD analysis. In this experiment, "2-theta (θ)" measurement mode was utilized for the laser-irradiated SiC substrate. As shown in **Fig.3.31 (b)**, the X-ray tube was fixed. The incident angle ω is between the X-ray beam and the sample. It is always 1/2 of the detector angle 2θ. During measurement, the sample was rotated slowly as well as that the reflected X-ray beams were detected by a removable detector. As the measurable depth is approximately 1nm~1μm, "2-theta (θ)" measurement mode is mainly used for thin film.

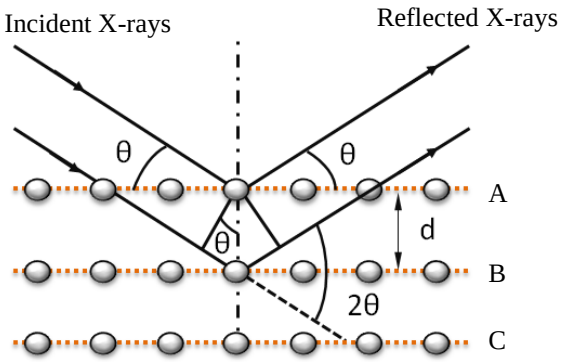

Fig.3.32 (a) X-rays diffraction

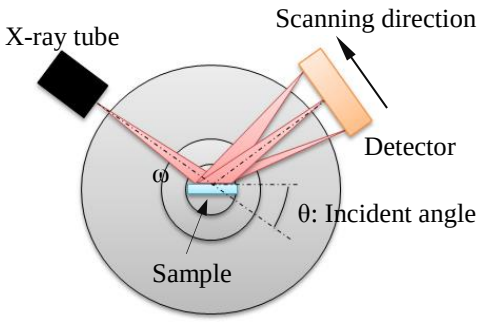

Fig.3.32 (b) Schematic diagram "2θ" mearsurement

Bragg's equation:

$2d\sin\theta = n\lambda$

n: integer revealing the order of the diffraction peak.

λ: wavelength of the x-ray

d: inter-plane distance of (i.e atoms, ions, molecules)

θ: scattering angle

3.3.3.1 Results of X-ray diffraction analysis

Fig.3.33 shows the results of X-ray diffraction for non-irradiated SiC substrate (a) and laser-irradiated substrate (b). From **Fig.3.33 (a)**, with the increase of incidence angle, the peaks become stronger at the same angle position, revealing that the crystallinity of as-lapped SiC surface was slightly weaker than the subsurface. It was considered that the lapping process of semiconductor material affected the crystallinity. In comparison, as shown in **Fig.3.33 (b)**, no obvious peaks were found at curves of incident angles 0.5°, 1°, and 1.5°, demonstrating that the surface of laser-induced ripple structures shown in **Fig.3.18 (a)** was of poor crystallinity. It is assumed that the hardness also decreased after laser irradiation. This physical performance change is important for understanding why the irradiated surface was easier to be polished with higher material remove rate.

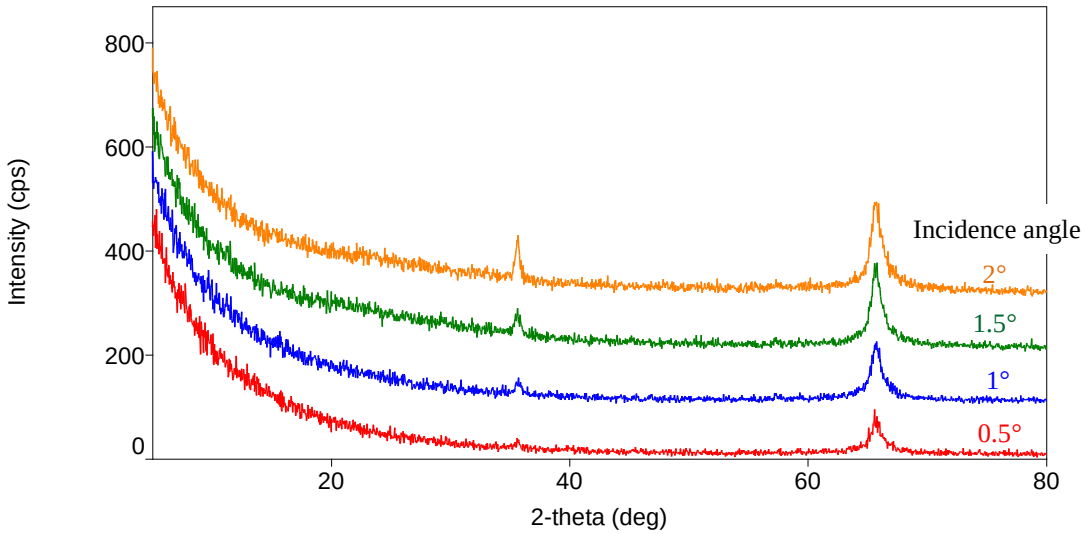

Fig.3.33 (a) X-ray diffraction for non-irradiated SiC surface

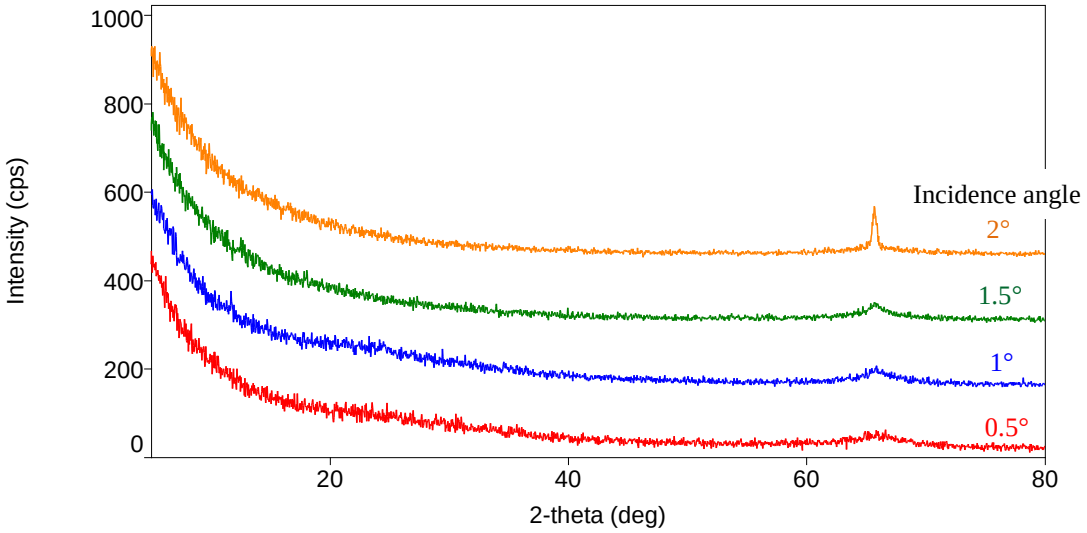

Fig.3.33 (b) X-ray diffraction for laser-irradiated SiC surface

3.3.4 Investigation according to XPS analysis

To understand the chemical characteristic of femtosecond laser-irradiated SiC substrate and the effect on CMP process, we carried out XPS (X-ray photoelectron spectroscopy) analysis. The principle of x-ray photoelectron spectroscopy is based on a single photon in/electron out process, as shown in **Fig.3.34**. When the photon of X-rays is absorbed by an atom in a molecule, ionization and the ejection of electrons are triggered. It is utilized for identifying component element in qualitative analysis and judging the element valence state as well as relative concentration in quantitative analysis, by detecting the Binding energy of ejected characteristic electrons. In addition, functional group structure of chemical compounds is also be identified by XPS analysis. For XPS analysis, the experimentally detected energies of the ejected photoelectrons are given by: $E_k = h\nu - E_b - \Phi$. Where, E_k is the kinetic energy of emitted photoelectrons; E_b is binding energy; the monochromatic X-ray energy sources $E=h\nu$ are often set as Al Kalpha (1486.6eV) or Mg Kalpha (1253.6eV); Φ is the work function of the spectrometer. **Table 3.4** shows the detailed experimental conditions of this XPS analysis for SiC substrate.

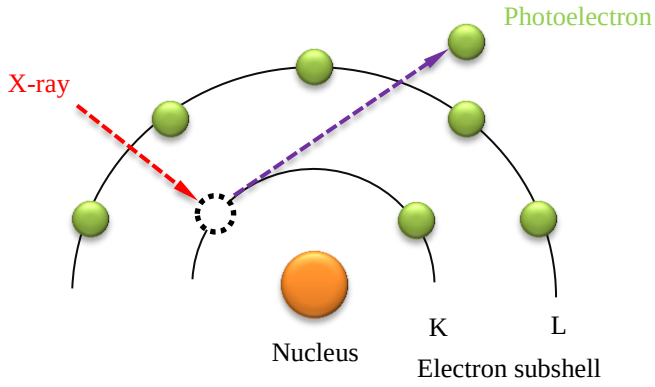

Fig.3.34 Schematic diagram of XPS

Table 3.4 XPS measurement conditions

Measurement apparatus	ESCA-3400
X-ray resource	Mg (Emission:10 mA, Accel HT:10 kV)
Etching	Emission: 10 mA, Accel HT:2.0 kV
Etching time(s)	0, 5, 10, 30, 30, 60, 60, 60, 120, 120, 120
Sweep times	5
Measured elements	C 1s, O 1s, Si 2p, Si 2s
Substrate surface	C-face (SiC)

3.3.4.1 Results of XPS analysis

Fig.3.35 shows the results of depth direction XPS analysis carried out for non-irradiated SiC substrate and laser-irradiated SiC substrate, both of which were dipped in the alkaline slurry for 5mins and 60s respectively before analysis. It can be clearly seen from the comparison that the intensities of ejected photoelectrons from O 1s differed greatly, inferring that femtosecond laser irradiation played an important role for increasing the concentration of element O in the slurry. The reason was considered as: (1) the surface materials of laser-irradiated SiC substrate were assumed to react with the chemical substance of the slurry in alkaline atmosphere more easily. (2) laser-induced ripple structures led to a larger ratio surface which helped the chemical reaction in the slurry. In brief, the product of chemical reaction in the dipped surface promoted the polishing of CMP process.

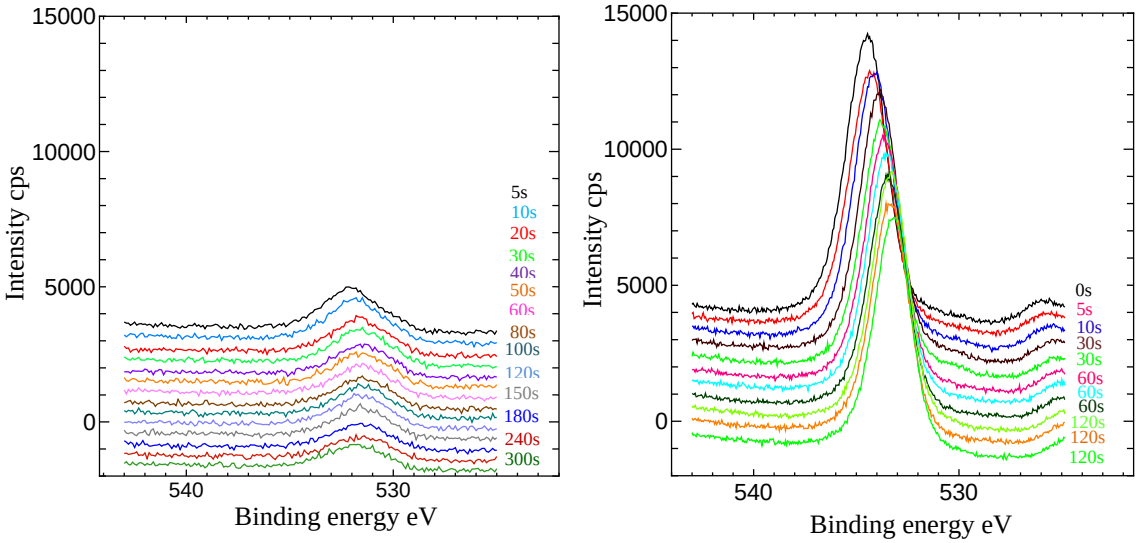

(a) O 1s (b) O 1s

Fig.3.35 XPS analysis in depth direction after dipping in slurry
(a) Non-irradiated substrate and (b) Laser-irradiated substrate

3.4 Summery

Changes of femtosecond laser-induced surface morphologies were investigated on the surface of as-lapped SiC C-face by scanning electron microscope (SEM). Periodical nanoscale parallel patterns were observed after femtosecond laser ablation. The formation mechanism of periodical ripples on femtosecond laser-induced SiC surface was reviewed. Secondly, CMP process was carried out for non-irradiated substrate, transversely irradiated substrate and the substrate of cross-scan irradiation model. The final surface morphology was measured by white-light interferometer and SEM. We found that better surface and higher material removal rate (MRR) of laser-irradiated substrate than that of non-irradiated substrate were realized in the experiment. The MRR of transverse irradiation model is 27 nm/min, which is about 3 times higher than that of non-irradiated substrate. The MRR of cross-scan irradiation model is 16nm/min, smaller than that of transverse irradiation model but have much better surface roughness. Reasonable combination of femtosecond laser parameters will be clearly found for higher polishing efficiency and higher surface planarization in the future studies. X-ray diffraction (XRD) and X-ray Photoelectron Spectroscopy (XPS) was further employed for illuminating the mechanism of femtosecond laser process of SiC. The poor crystallinity and being easily oxidized in colloidal SiO_2 slurry of the laser-induced ripple structures as well amorphous layer were considered to improved CMP process for SiC substrate.

Reference

[1]Toshiro K Doy, Kiyoshi Seshimo, Keisuke Suzuki, Ara Philipossian, and Masaki Kinoshita, Impact of Novel Pad Groove Designs on Rate and Uniformity of Dielectric and Copper CMP, Journal of The Electrochemical Society, 151(3) G196-G199 (2004), 2004.03.

[2]Syuhei KUROKAWA, Toshiro DOI, Tsutomu YAMAZAKI, Yoji UMEZAKI, Osamu OHNISHI, Yoji MATSUKAWA, Kiyoshi SESHIMO, Yasuhide YAMAGUCHI, and Yasunori KAWASE, Impact of Reduction in CeO2 Slurry Consumption for Oxide CMP ---Approach from Alternative Slurries and Pad Groove Patterns---,Proc. of International Conference on Planarization/CMP Technology 2010,244-247,pp.244-247,2010.11.

[3] T.K.Doy, T.Hara, T.Tomizawa, T.Kurosu, Chemical Mechanical Polishing of Polyarylether Low Dielectric Constant Layers by Manganese Oxide Slurry, Journal of J. of Electrochemical Society,146,6(1999)pp.2333-2336,1999.06.

[4] Syuhei KUROKAWA, Toshiro DOI, Tsutomu YAMAZAKI, Yoji UMEZAKI, Osamu OHNISHI, Yoji MATSUKAWA, Kiyoshi SESHIMO, Yasuhide YAMAGUCHI, and Yasunori KAWASE, Impact of Reduction in CeO2 Slurry Consumption for Oxide CMP ---Approach from Alternative Slurries and Pad Groove Patterns---,Proc. of International Conference on Planarization/CMP Technology 2010,pp.244-247,pp.244-247,2010.11.

[5]Kazusei TAMAI, Hitoshi MORINAGA, Toshiro DOI, Syuhei KUROKAWA, and Osamu OHNISHI, Analysis of Chemical and Mechanical Factors in CMP Processes for Improving Material Removal Rate, Journal of the Electrochemical Society, 158, 3, H333-H337, Vol.158, No.3, pp.H333-H337, 2011.01.

[6]Toshiro K. DOI, Tsutomu YAMAZAKI, Syuhei KUROKAWA, Yoji UMEZAKI, Osamu OHNISHI, Yoichi AKAGAMI, Yasuhide YAMAGUCHI, and Sadahiro KISHII, Study on the Development of Resource-Saving High Performance Slurry ---Polishing/CMP for Glass Substrates in a Radical Polishing Environment, Using Manganese Oxide Slurry as an Alternative for Ceria

Slurry---, Advances in Science and Technology, 64, 65-70, Vol.64, pp.65-70, 2010.10.

[7]Toshiro Doi, Ara Philipossian and Koichiro Ichikawa, Design and Performance of a Controlled Atmosphere Polisher for Silicon Crystal Polishing, Electrochemical and Solid-State Letters, 7(8) G158-G160 (2004), 2004.08.

[8]Ji ZHANG, Syuhei Kurokawa, Terutake Hayashi, Eiji ASAKAWA, Chengwu WANG, Processing Characteristics of SiC Wafer by Consideration of Oxidation Effect in Different Atmospheric Environment, Proc. of the International Conference on Planarization/CMP Technology, ICPT2014,pp.279-282 ,2014.11.

[9]Toshiro DOI and Syuhei KUROKAWA,CMP of SiC Wafers as a Post-Si Power-Device (Bell-Jar shaped CMP machine assisted by photocatalitic reactions under high pressure oxygen gas and CMP characteristics of functional materials),Proc. of the 1st International Conference on Surface and Interface Fabrication Techonologies (ICSIF),168-174,pp.168-174,2009.07.

[10]Toshiro K. DOI, and Syuhei KUROKAWA,CMP of SiC Wafers as a Post-Si Power-Device -Photocatalitic reaction assisted Bell-Jar shaped CMP Machine under high pressure oxygen gas-,Proc. of International Conference on Planarization/CMP Technology 2008,pp.2-7,2008.11.

[11]Toshiro Doi, Ioan D. Marinescu, Syuhei Kurokawa, Advances in CMP Polishing Technologies [M], 1st Edition, Elsevier, 2011

[12]Toshiro Doi, Ioan D. Marinescu and Eckart Uhlmann, Handbook of Ceramics Grinding and Polishing [M], Elsevier, 2014

[13]Toshiro K.Doi, Shigeru Watanabe, Hideyuki Doy, Shin Sakurai, Daizo Ichikawa, Impact of Novel Bell-jar type CMP Machine on CMP Characteristics of Optoelectronics Materials, International Journal For Manufacturing Science & Technology,Vol.9,Nr.1(2007),pp5-10,2007.09.

[14] Toshiro K Doi, hideyuki Doy, Shin Sakurai, Daizo Ichikawa, Impact of Novel Bell-jar type CMP Machine on CMP characteristics of Optoelectronics

Materials, International Journal For Manufacturing Science & Technology ,p.5-10,2007.01.

[15]Toshiro Karaki Doi, Yasuhisa SANO, Syuhei Kurokawa, Hideo AIDA, Osamu OHNISHI, Michio UNEDA, Koki OHYAMA, Novel Chemical Mechanical Polishing/Plasma-Chemical Vaporization Machining(CMP/P-CVM) Combined Processing of Hard-to-Process Crystals Based on Innovative Concepts, Sensors and Materials, Vol. 26, No. 6, pp 403-415,2014.06.

[16]Kousuke SHIOZAWA, Yasuhisa SANO, Toshiro Karaki Doi, Syuhei Kurokawa, Hideo AIDA, Koki OYAMA, Tadakazu MIYASHITA, Haruo SUMIZAWA, Kazuto YAMAUCHI, Development of Basic-Type CMP/P-CVM Fusion Processing System (Type A) and Its Fundamental Characteristics, Proc. of the International Conference on Planarization/CMP Technology, ICPT2014,pp.275-278,2014.11.

[17] Current Status and Future Prospects of GaN Substrates for Green Devices, T. Doi, Sensors and Materials, Vol.25, No.3 (2013) 141-154

[18] Hideo Aida, Toshiro Doi, Hidetoshi Takeda, Haruji Katakura, Seong-Woo Kim, Koji Koyama, Tsutomu Yamazaki, Michio Uneda, Ultraprecision CMP for sapphire, GaN, and SiC for advanced optoelectronics materials, Current Applied Physics, Volume 12, Supplement 2, September 2012, Pages S41-S46

[19] Hideo Aida, Hidetoshi Takeda, Seong-Woo Kim, Natsuko Aota, Koji Koyama, Tsutomu Yamazaki, Toshiro Doi, Evaluation of subsurface damage in GaN substrate induced by mechanical polishing with diamond abrasives, Applied Surface Science, Volume 292, 15 February 2014, Pages 531-536

[20]Yasuhisa SANO, Toshiro Karaki Doi, Syuhei Kurokawa, Hideo AIDA, Osamu OHNISHI, Michio UNEDA, Kousuke SHIOZAWA, Yu OKADA, Kazuto YAMAUCHI, Dependence of GaN Removal Rate of Plasma Chemical Vaporization Machining on Mechanically Introduced Damage, Sensors and Materials, Vol. 26, No. 6, pp 429-434,2014.06.

[21] Toshiro DOI and Syuhei KUROKAWA, CMP of SiC Wafers as a Post-Si

Power-Device (Bell-Jar shaped CMP machine assisted by photocatalitic reactions under high pressure oxygen gas and CMP characteristics of functional materials), Proceedings of the 1st International Conference on Surface and Interface Fabrication Techonologies (ICSIF),Vol. 2009 (Invited), No. July, pp. pp.168-174, 2009.07.

[22] Guomei Chen, Zifeng Ni, Laijun Xu, Qingzhong Li, Yongwu Zhao, Performance of colloidal silica and ceria based slurries on CMP of Si-face 6H-SiC substrates, Applied Surface Science, Volume 359, 30 December 2015, Pages 664-668

[23] Yan Zhou, Guoshun Pan, Xiaolei Shi, Suman Zhang, Hua Gong, Guihai Luo,Effects of ultra-smooth surface atomic step morphology on chemical mechanical polishing (CMP) performances of sapphire and SiC wafers,Tribology International, Volume 87, July 2015, Pages 145-150

[24]Syuhei Kurokawa, Toshiro Karaki Doi, Chengwu W. WANG, Yasuhisa SANO, Hideo AIDA, Koki OYAMA, Kunimitsu TAKAHASHI,Approach to High Efficient CMP for Power Device Substrates, ECS Transactions,Vol.60, Issue1, pp.641-646,2014.03.

[25] Hui Deng & Masaki Ueda & Kazuya Yamamura, Characterization of 4H-SiC (0001) surface processed by plasma-assisted polishing, Int J Adv Manuf Technol (2014) 72:1–7

[26] Tao Yin , Toshiro Doi, Syuhei Kurokawa, Osamu Ohnishi, Tsutomu Yamazaki, Zhida Wang, Zhe Tan, The Effects of Strong Oxidizing Slurry and Processing Atmosphere on Double-sided CMP of SiC Wafer, Advanced Materials Research Vols. 591-593 (2012) pp 1131-1134

[27] Go Obara, Hisashi Shimizu, Taira Enami, Eric Mazur, Mitsuhiro Terakawa, and Minoru Obara, Growth of high spatial frequency periodic ripple structures on SiC crystal surfaces irradiated with successive femtosecond laser pulses, Optics Express Vol. 21, Issue 22, pp. 26323-26334 (2013)

[28] Hisashi Shimizu, Shuhei Yada, Go Obara, and Mitsuhiro Terakawa,

Contribution of defect on early stage of LIPSS formation, OPTICS EXPRESS, Vol. 21, No. 22, 26323-26325 (2013)

[29] Saulius Juodkazis, Hiroaki Misawa, Tomohiro Hashimoto, Eugene G. Gamaly and Barry Luther-Davies, Laser-induced microexplosion confined in a bulk of silica: Formation of nanovoids, Appl. Phys. Lett. 88, 201909 (2006)

[30] A. Borowiec, D. M. Bruce, Daniel T. Cassidy, and H. K. Haugen, Imaging the strain fields resulting from laser micromachining of semiconductors, Appl. Phys. Lett. 83, 225 (2003)

[31] F. S. Krasniqi, S. L. Johnson, P. Beaud, M. Kaiser, D. Grolimund, and G. Ingold, Influence of lattice heating time on femtosecond laser-induced strain waves in InSb, PHYSICAL REVIEW B 78, 174302 (2008)

[32] X.r.zhang, X. xu, A.M.rubenchik, Simulation of microscale densification during femtosecond laser processing of dielectric materials, Appl. Phys. A 79, 945–948 (2004)

[33] N.Haustrup, G.M. O'Connor, Impact of laser wavelength on the emission of electrons and ions from thin gold films during femtosecond laser ablation, Applied Surface Science 302 (2014) 1–5

[34] Yusaku Izawa, Shigeki Tokita, Masayuki Fujita, Takayoshi Norimatsu, Yasukazu Izawa, Ultrafast melting process in femtosecond laser crystallization of thin a-Si layer, Applied Surface Science 255 (2009) 9764–9769

[35] W. G. Roeterdink, L. B. F. Juurlink, O. P. H. Vaughan, J. Dura Diez, M. Bonn, and A. W. Kleyn, Coulomb explosion in femtosecond laser ablation of Si (111), Appl. Phys. Lett. 82, 4190 (2003)

[36] E.M. Snyder, S. Wei, J. Purnell, S.A. Buzza, A.W. Castleman Jr, Femtosecond laser-induced Coulomb explosion of ammonia clusters, Chemical Physics Letters 248 (1996) 1-7

[37] Y.Y. Dong, P. Molian, Coulomb explosion-induced formation of highly oriented nanoparticles on thin films of 3C–SiC by the femtosecond pulsed laser,

Appl. Phys. Lett., 84 (2004), p.10

[38] E. Leveugle, D.S. Ivanov, L.V. Zhigilei, Photomechanical spallation of molecular and metal targets: molecular dynamics study, Appl. Phys. A 79, 1643–1655 (2004)

[39] A.Y. Vorobyev, C.L. Guo, Femtosecond laser structuring of titanium implants, Appl. Surf. Sci. 253 (2007) 7272–7280.

[40] M. Huang, F. Zhao, Y. Cheng, N. Xu, Z. Xu, Origin of laser-induced near-subwavelength ripples: interference between surface plasmons and incident laser, ACS Nano 3 (2009) 4062–4070.

[41] Miyazaki, J. Kiuchi, Femtosecond-laser-induced nanostructure formed on hard thin films of TiN and DLC, Appl. Phys. A 76 (2003) 983–985.

[42] Haugen, Subwavelength ripple formation on the surfaces of compound semiconductors irradiated with femtosecond laser pulses, Appl. Phys. Lett. 82 (2003) 4462–4464.

[43] J. M. Li, J. T. Xu, Self-organized nanostructure by a femtosecond laser on silicon, Laser Phys. 19 (2009) 121–124.

[44] Y.Xing, J.Deng, et al. multiple nanoscale parallel grooves formed on Si_3N_4/TiC ceramic by femtosecond pulsed laser, Applied Surface Science. 289(2014)62-71

[45] S. H. Kim, K. H. Byun,I. B. Sohn,S. H. Jeong, Progressive formation of fine and coarse ripples on SiC surface by repeated irradiation of femtosecond laser pulses, Appl. Phys. B (2013) 113:395–402

[46] Takuro Tomita, Keita Kinoshita, Shigeki Matsuo, and Shuichi Hashimoto, Effect of surface roughening on femtosecond laser-induced ripple structures, APPLIED PHYSICS LETTERS 90, 153115, 2007

[47] Okada, T, Kawahara, H, Ishida, Y, Kumai, R, Tomita, T, Matsuo, S, Hashimoto, S, Kawamoto, M, Makita, Y,

[48] Vanthanh Khuat, Yuncan Ma, Jinhai Si, Tao Chen, Feng Chen, Xun Hou,

Fabrication of through holes in silicon carbide using femtosecond laser irradiation and acid etching, Applied Surface Science 289 (2014) 529– 532

CHAPTER 4

FEMTOSECOND LASER PROCESSING FOR DIAMOND: FORMATION AND EVALUATION OF QUASI-RADICAL SITE

4.1 Introduction

Diamond, regarded as new substrate material for next generation power device substrate, is the hardest material on the earth. For the sake of energy conservation, studies and developments of power devices are being promoted actively. Studies relevant to crystal of single-crystal diamond growth, crystal defect evaluation, have already been carried out in several fields and perspectives. Due to the high Mohs hardness and chemical stability, the ultra-precision machining technique of how to polish the surface of substrate material diamond to gain mirror-like precision efficiently should be established as rapidly as possible. However, studies on ultra-precision machining of hard-to-polish materials are still untouched. Consequently, the study of how to polish semiconductor diamond to gain mirror-like precision efficiently is significant.

Due to its outstanding characteristics, such as ultra-short pulse duration, high pulse repetition rate and high fluence, femtosecond laser is being used for various fields. In this experiment, as a pre-process, fs laser was utilized to irradiate the surface of single crystal diamond substrate, aiming to investigate the surface change for further CMP process.

In pre-process, quasi-radical site was formed after using femtosecond laser irradiation on the surface of single-crystal diamond substrate. Quasi-radical site collectively defined as the change of nanostructure, formation of fine defects and

amorphous was expected to improve the CMP removal rate of diamond substrate. Raman spectral analysis and TEM (Transmission electron microscopy) observation were carried out to investigate laser-induced ultra-micro-defect on diamond single crystal substrate.

4.2 Principle of Raman spectral analysis and TEM

Phenomena such as reflection, refraction, absorption as well as scattering will be triggered when substance is illuminated by light, on account of the reaction of material and light. Scattered light which has the same frequency rate (ν_o) with incident light is called Rayleigh scattering. The light with different frequency rate ($\nu_o \pm \nu$) with the incident light by molecular vibration is called Raman scattering, as shown in **Fig.4.1**. Raman spectrum is usually detected by passing the scattered light in a spectroscope in which high monochromaticity laser is used as an excitation light source. Raman spectrum analysis is mainly applied in organic chemistry for qualitative and quantitative analysis, analyzing molecular structure, functional group and its content.

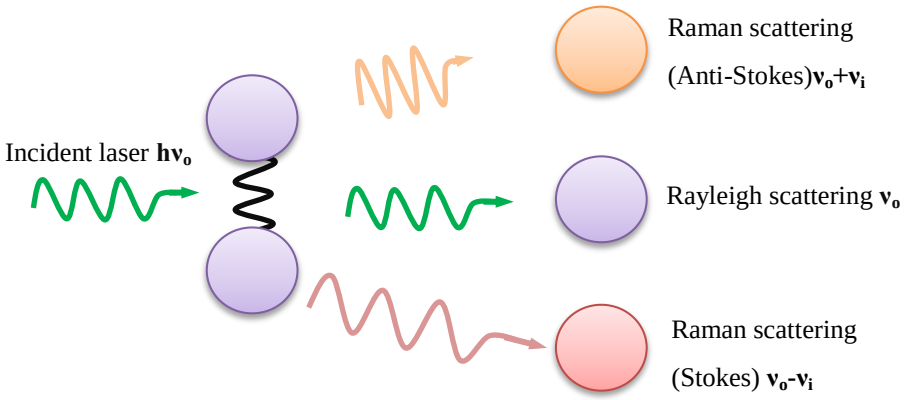

Fig.4.1. Raman scattering and Rayleigh scattering

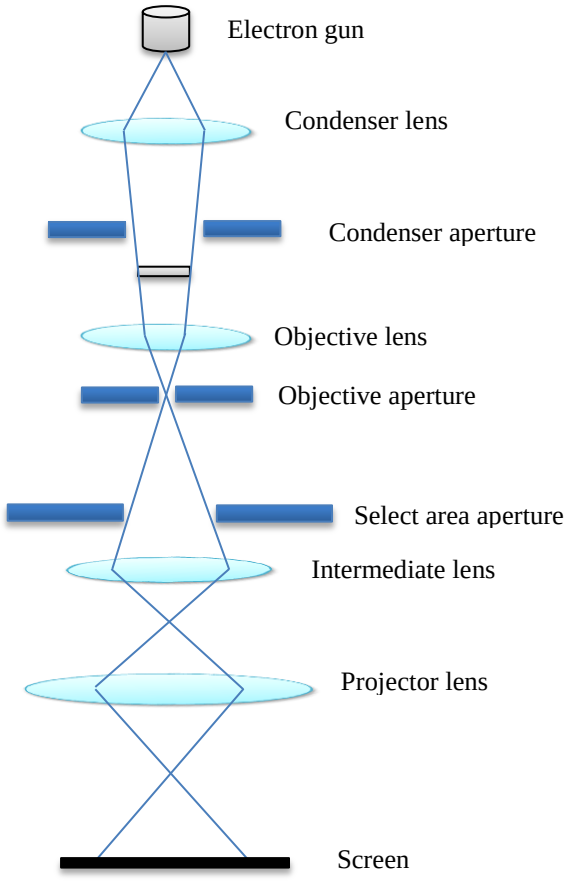

Fig.4.2 Main constitutions of electronic optical system in TEM

Transmission Electron Microscope (TEM) is widely used for ultra-micro-structure observation at high resolution (0.1～0.2nm) by partly amplifying objective image at tens of thousands times ~ one million times. It usually consists of highly stabilized power supply system, vacuum pumping system, cooling water system, controlling system and operation system. The main constitutions of electronic optical system in TEM are shown in **Fig.4.2**. The focused electron beam was accelerated in electromagnetic lens system and projected onto extremely thin specimen. After the collision of electron with atom, the direction of electron will be changed, giving rise to stereo angle scattering which is related to the density and thickness of specimen. The transmitted electron beam will be finally focused and projected onto fluorescent screen, formatting an amplified image of an extraordinary tiny structure in the specimen. Crystallization defect of semiconductor structure, surface and distribution of micro grains of material science and biology science can be effectively observed and investigated by TEM.

4.3 Experiments

The pulse duration of femtosecond (10^{-15}s) laser is extremely short, less than 1 picosecond. By focusing extremely short pulse beams, its peak intensity can reach from terawatt (10^{12}) to petawatt (10^{15}). Electron will be directly torn off from atom or molecule of the surface irradiated by the result of the electric field of extremely high intensity laser. The irradiation will be finished within extremely short time without thermal diffusion to the surround. To form quasi-radical site on the surface layer of diamond substrate is the pre-process of this study. TEM cross-section observation was carried out to verify whether crystal structure changes or not at lower output power than that can cause laser ablation in preliminary experiment. The output power was set as 1/5 of that can cause laser ablation. Diamond single crystal substrate (100) was irradiated by fs laser whose wave length is 1045nm. Raman spectral analysis was carried out to investigate the change of crystal.

As shown in **Fig.4.3**, the reverse side of diamond substrate was firstly irradiated by femtosecond laser in air atmosphere, aiming to format four marks in four different areas respectively. These marks were used for easily distinguishing the laser-irradiated areas in the obverse side of diamond substrate, which was partly irradiated by femtosecond laser at output power of 747mW, 594mW, 472mW, 375mW and 206mW, as shown in **Fig.4.4**. During laser scanning process, interval between adjacent trajectories called pitch here was set as 2 μm in the zigzag pattern shown in **Fig.4.5**.

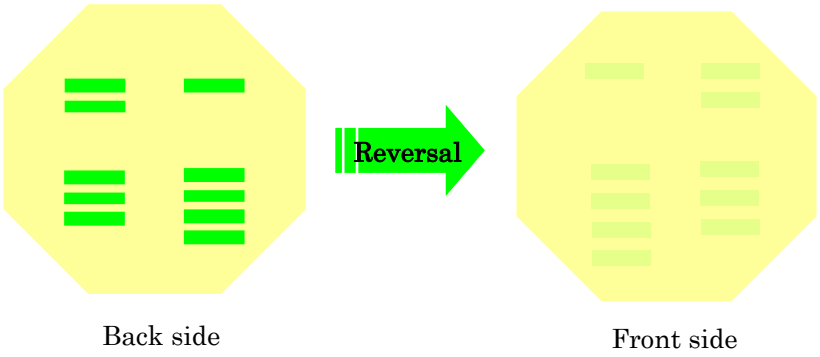

Fig.4.3 Femtosecond laser-irradiated mark on the reverse side of Diamond substrate

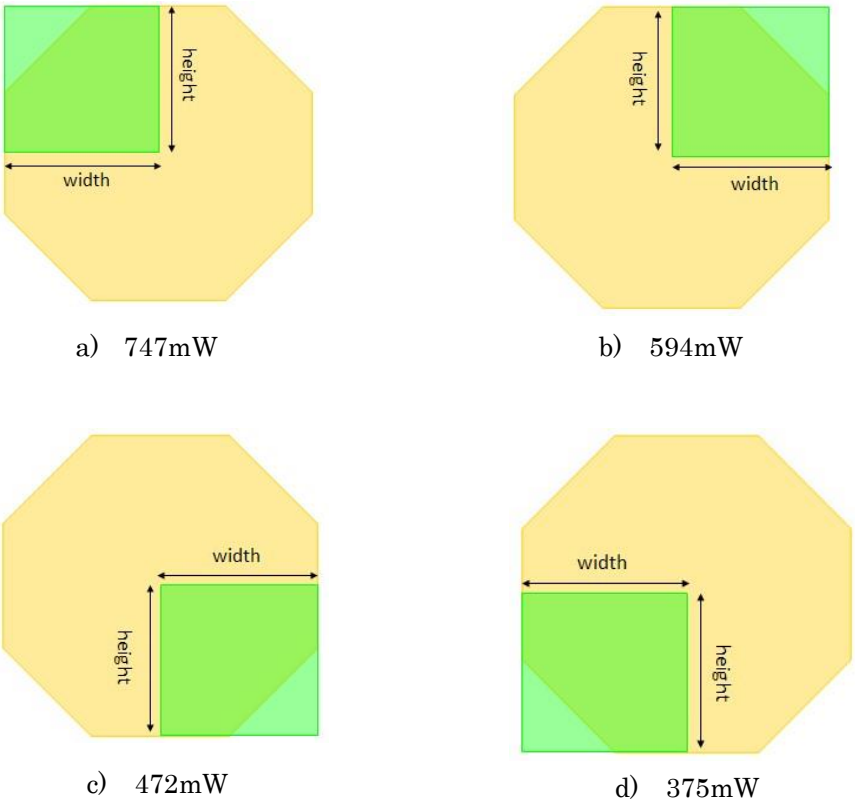

Fig.4.4 Femtosecond laser-irradiated areas of the obverse side on Diamond substrate at different laser power

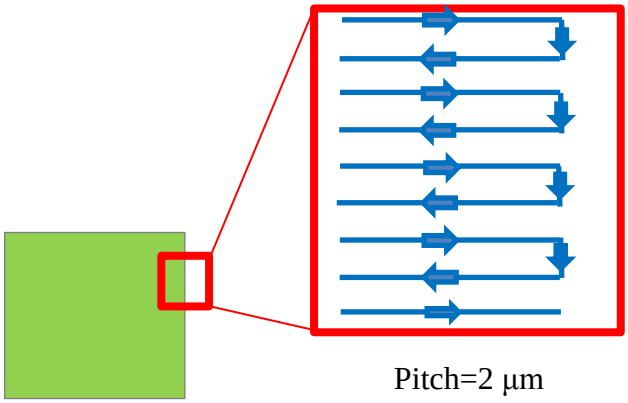

Fig.4.5 Scanning pattern of femtosecond laser process and pitch width

4.4 Experimental results investigation

The irradiated diamond substrate and its amplified images (×5) by confocal laser scanning microscopy are shown in **Fig.4.6**; four parts of its surface were respectively irradiated by fs laser at different output power of 747mW, 594mW, 472mW, 375mW; the scanning speed was 10mm/s; the pulse duration was 10MHz. The surfaces irradiated at the output power 747mW and 594mW became wholly black, while the surfaces irradiated at the output power 472mW and 375mW are still transparent. The lower the output power was, the more tempered the surface was.

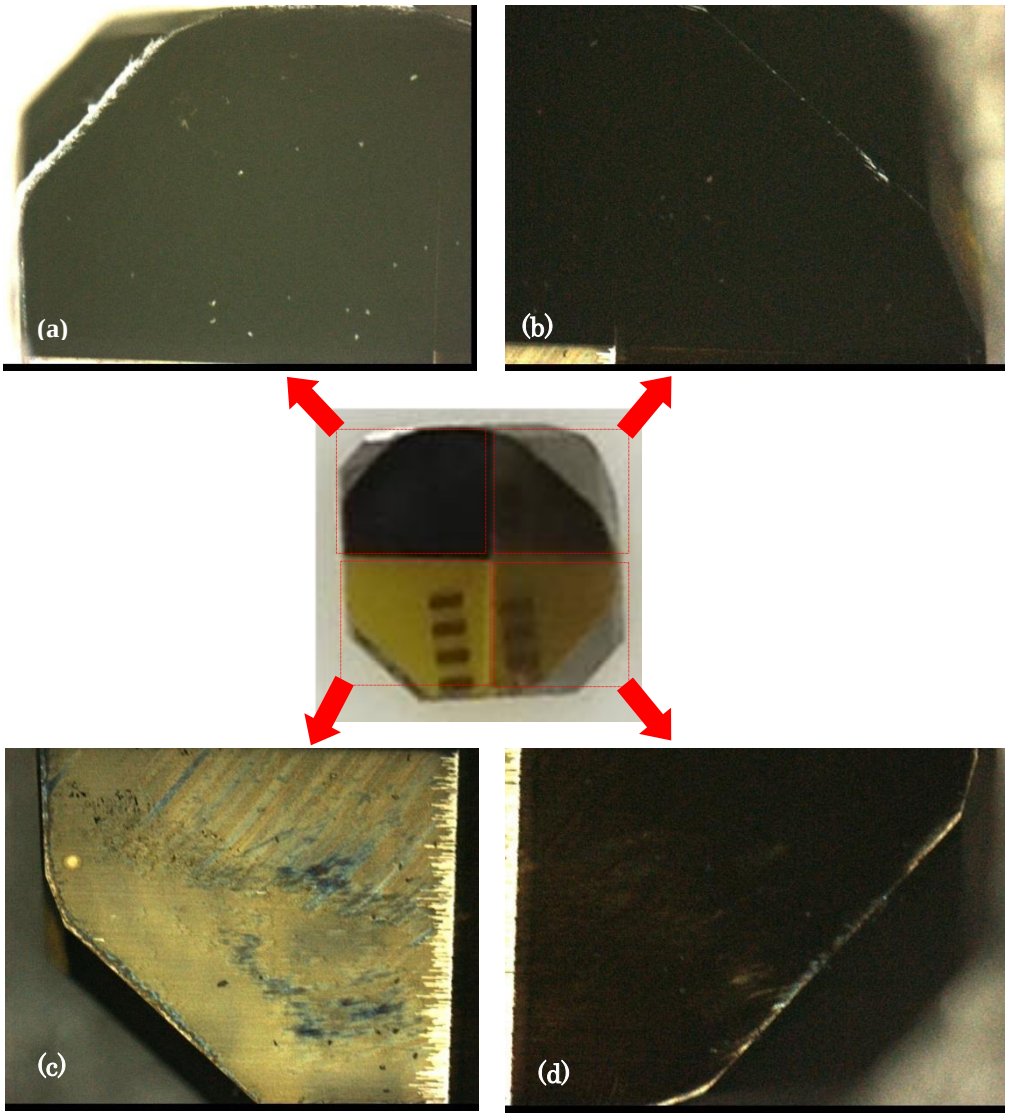

Fig.4.6. Diamond substrate irradiated by fs laser at different output power and the amplified images (× 5)

4.4.1 SEM observation

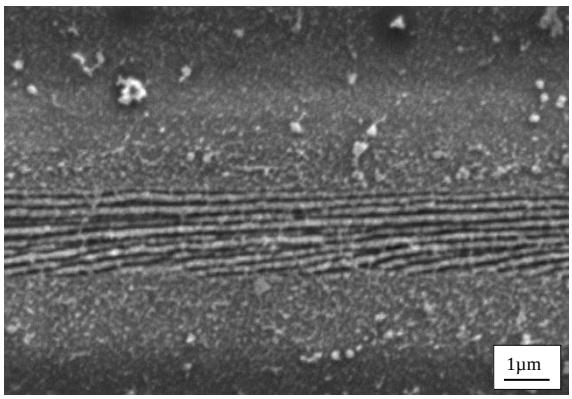

Fig.4.7 Laser-irradiated diamond substrate observed by SEM

Fig.4.7 shows the diamond surface irradiated by femtosecond laser in one-line scanning at a repetition rate of 10MHz, output power of 359mW, and a scanning speed of 100mm/s. Nanoscale ripples as well as debris were found in the diamond surface after laser irradiation. Ripple structures induced by femtosecond laser in the surfaces of semiconductor materials ZnO, AlGaInP, Si, and InP. This kind of structures were attributed to laser fluence [1], pulse duration [2], wavelength, incidence angle, polarization of incident laser beam [3-5] and material thermal properties [2]. The sputtering debris was attributed to the micro-explosion induced by the instantaneous high temperature and high pressure during laser irradiation. From the different color showed in **Fig.4.6**, it is believed that higher output power of femtosecond laser can form more debris.

4.4.2 Raman spectral analysis

Laser Raman Spectral Analysis regarded as non-destructive inspection was

carried out to analyze the substrate irradiated by fs laser. The detection depth of Raman spectrum detector is about 1μm; comparatively detailed information of substrate's surface can be achieved. The analyzed result is shown in **Fig.4.8**. Raman shift 1332cm^{-1} is the inherent shift of diamond; it is usually used to confirm diamond structure. Raman shift 1580cm^{-1} indicates that the structure of amorphous was partly formed on the surface of diamond substrate. The yellow curve (375mW) and the green curve (472mW) indicate that the mixture of diamond and amorphous exits on the surface of diamond substrate. While the blue curve (594mW) and the black curve (747mW) show that the single crystal diamond was totally ablated as amorphous on the surface of diamond substrate. The weaker the output power was, the bigger the peak become.

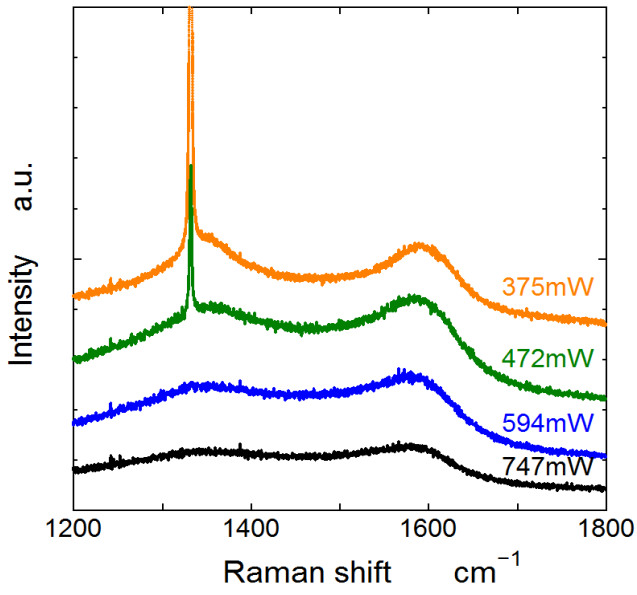

Fig.4.8 Raman spectrum of diamond substrate irradiated by femtosecond laser

4.4.3 TEM cross-section observation

Transmission Electron Microscope (TEM) which can produce high-resolution and two-dimensional images is used in semiconductor analysis at a maximum resolution of 1nm. To evaluate the surface irradiated by fs laser, TEM survey was used to observe the cross-section of diamond substrate. **Fig.4.9** shows the substrate irradiated in preliminary experiment. The blue line was marked by fs laser at 5 times as large as the output power of surrounding irradiated area, while other parts were irradiated at the output power which cannot cause laser abrasion. The cross-section of the marking line was observed by TEM, as shown in **Fig.4.10.**

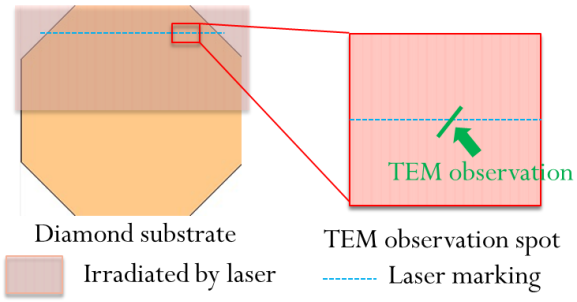

Fig.4.9 Femtosecond laser irradiation condition on diamond substrate

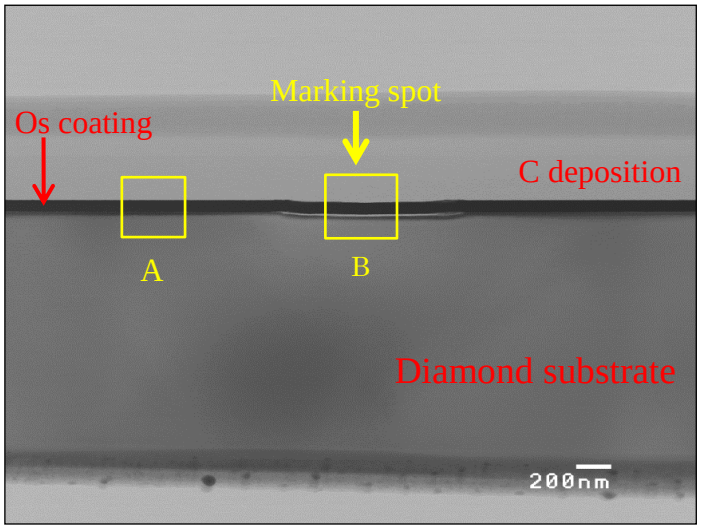

Fig.4.10 TEM cross-section of diamond substrate irradiated by fs laser

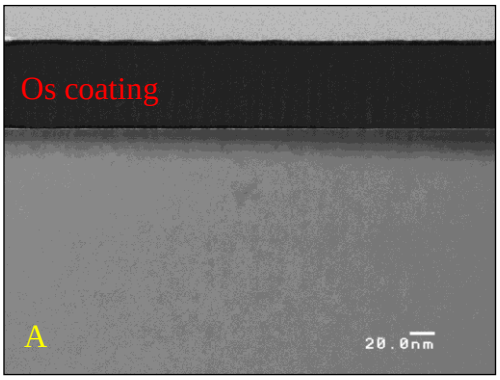

(a) Around marking

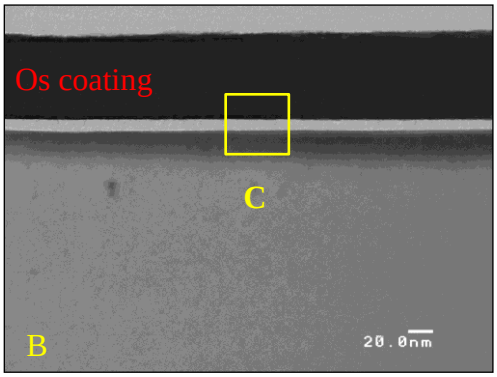

(b) At marking

Fig.4.11 Enlarged part of A and B

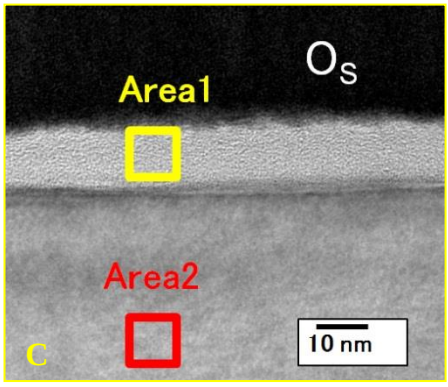

Fig.4.12 Enlarged part of area C

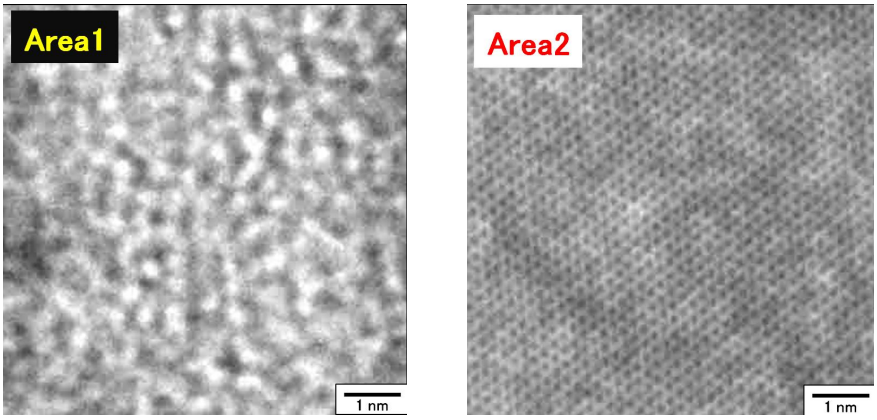

(a) **(b)**

Fig.4.13 High magnification TEM cross-section images of Area 1 and Area 2.

Fig.4.10 shows the TEM cross-section images of diamond substrate. The black contrast layer on the surface is osmium layer, which was used for conductivity and protecting the surface. **Fig.4.11** (a) shows the TEM cross-section of area A irradiated at the output power which couldn't cause laser abrasion. **Fig.4.11** (b) shows the TEM cross-section of marking spot B. The while layer was the quasi-radical site formed by fs laser, while the thickness of which was about 10nm.

Fig.4.12 is the enlarged image of area C. **Fig.4.13 (a)** shows that amorphous state was formed on the surface of diamond (Area1), while **Fig.4.13 (b)** shows the regularly-structured atom array of the diamond substrate subsurface (Area2). That is to say, the layer under the surface was still not be affected by fs laser. From the difference of these two images, it can be concluded that quasi-radical site was formed only on the shallow surface by fs laser. Its thickness is about 10nm.

4.5 Summary

Single crystal diamond substrate was irradiated by femtosecond laser. Ultra-micro defects (quasi-radical site) were formed on the surface of diamond substrate. TEM and Raman spectral analysis were carried out to investigate the formation of quasi-radical site. According to TEM cross-section observation, the thickness of quasi-radical site is about 10nm. As diamond is the hardest material in the earth, it was quite difficult to process by high fluence femtosecond laser. However, since SiC substrate has hardness relatively lower than diamond, it was assumed that the quasi-radical site in SiC substrate was thicker than diamond after femtosecond laser irradiation, which is useful to explain why better surface was obtained on laser-irradiated SiC substrate after CMP process.

Raman spectral analysis indicates that the crystal diamond structure was changed to be structure mixed (as shown in **Fig.4.14**) with amorphous and regularly-structured diamond after laser irradiation. Simultaneously, as the output power of fs laser increased, the peak indicating diamond crystal disappeared, inferring that no crystal component remained in the surface.

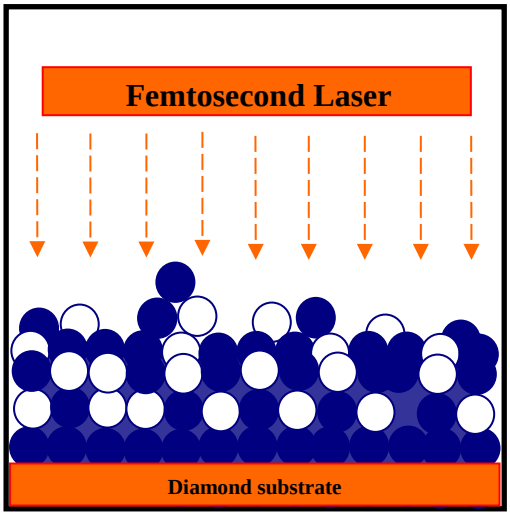

Fig.4.14 Model of femtosecond laser irradiation on diamond substrate surface

Reference

[1] H.X. Qian, W.Zhou, H.Y.Zheng, X.R.Zeng, H.C.Sheng, Evolution of periodic structures on InP(100) surface irradiated with femtosecond laser, Materials Letters 124 (2014) 235–238

[2] P. Simon, J. Ihlemann, Ablation of submicron structures on metals and semiconductors by femtosecond UV-laser pulses, Applied Surface Science 109r110 1997. 25–29

[3] A.Y. Vorobyev, C. Guo, Femtosecond laser structuring of titanium implants, Applied Surface Science 253 (2007) 7272–7280.

[4] R. Serra, V. Oliveira, J.C. Oliveira, T. Kubart, R. Vilar, A. Cavaleiro, Large-area homogeneous periodic surface structures generated on thesurface of sputtered boron carbide thin films by femtosecond laserprocessing, Applied Surface Science 331 (2015) 161–169

[5] M. Huang, F. Zhao, Y. Cheng, N. Xu, Z. Xu, Origin of laser-induced near-subwavelength ripples: interference between surface plasmons and incident laser, ACS Nano 3 (2009) 4062–4070.

[6]Toshiro.K.Doi, et al. Study of a highly efficient precision processing for hard-to-process materials (1st report)-roposal of a polishing process with new concepts—

[7] Fujita, et al. Femtosecond laser process, Journal of Plasma and Fusion Research, Vol.81, Suppl.(2005), pp.195-201

CHATER 5

THE EFFECT OF FEMTOSECOND LASER INTERNAL PROCESSING ON SUBSTRATE MATERIALS

5.1 Introduction

In the previous chapters, we mainly introduced the surface processing of femtosecond laser on hard-to-process materials SiC and diamond as well as the effect of laser irradiation on CMP process. In this chapter, internal processing of femtosecond laser of power device substrate materials Si, sapphire, and SiC were introduced to investigating the defects of their cross sections.

As a laser-based technique, the so-called stealth dicing process plays an important role during the manufacture process of semiconductor devices. In recent years, inner-absorption process was put forward. Comparing to the traditional blade-dicing and laser-ablation dicing, no surface damage as well as no necessity for cleaning are excellent advantages of stealth dicing. Additionally, high precision can be realized without heat affected zone by femtosecond laser. It makes a great significance to develop new dicing technique for hard-to-process materials. In this chapter, we mainly investigated the processing of stealth dicing for substrate materials Si, sapphire, and SiC.

5.2 Experimental

5.2.1 Experimental methods

① Chips cut out from semiconductor wafers were put on the stage of femtosecond laser equipment, as shown in **Fig.5.1 (a).**

② Focus the beam spot on substrate surface, as shown in **Fig.5.1 (a)**.

③ Move the XYZ stage upward; ensure that the beam spot was focused internal the substrate and was moved along the designed focus path shown in **Fig.5.1 (b)** to process the section of **Fig.5.1 (a)**.

④ Cut the substrate along the section and observed the section by CLSM (Confocal Laser Scanning Microscopy).

⑤ Repeat the above steps ①～③ for another section processing.

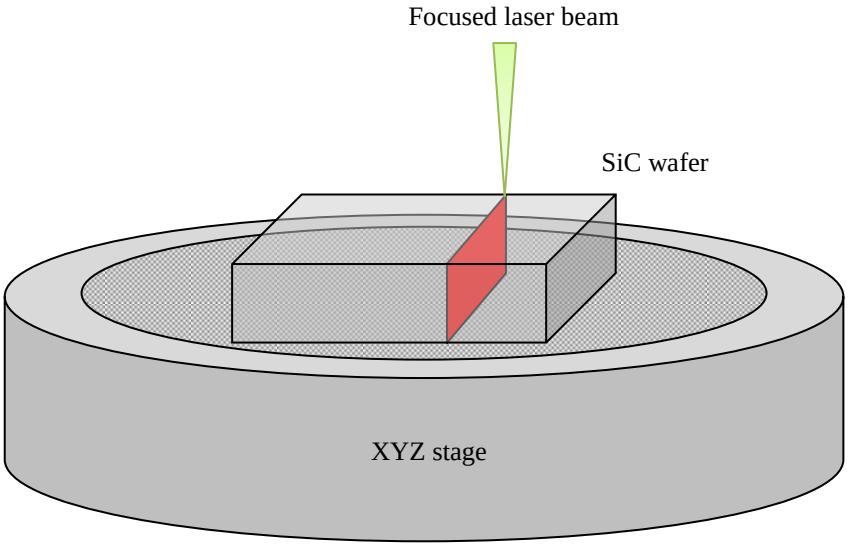

Fig 5.1 (a) Internal processing for SiC substrate

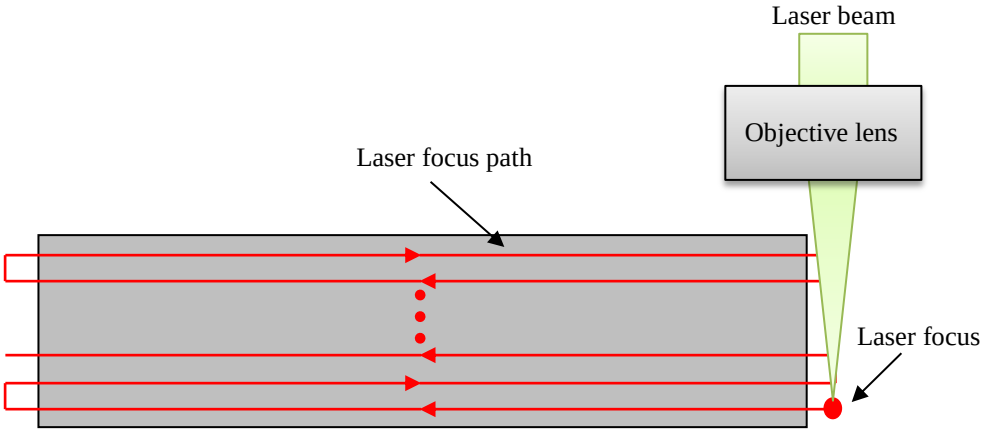

Fig 5.1 (b) Internal processing for SiC substrate

5.2.2 Experimental conditions

In this experiment, hard-to-process semiconductor material SiC was processed according the following conditions shown in **Table 5.1.** The beam spot was focused inner the substrate with a distance of respectively 200 μm, 225 μm, and 250 μm. Other parameters are shown in **Table 5.1**.

Table 5.1 Experimental conditions

	A	B	C
Wafer	SiC		
Focus position before process	200 μm	225 μm	250 μm
Focus displacement for each path	5 μm		
Total displacement	200 μm		
Scanning speed	100 mm/s		
Pulse energy	23 nJ/pulse		
Repetition rate	10 MHz		

5.2.2.1 Experimental results

Fig 5.2 shows the surface and cross section of SiC substrate after laser processing at the same experimental condition A. From **Fig 5.2 (a)**, it can be seen that the inner rather than the surface of transparent SiC substrate was processed by fs laser. However, on the right side, the surface of the substrate was scorched black. It is considered that the inclination of the substrate on XYZ stage led to this phenomenon. Especially, it should be noted that an inner defect layer with a length of about 100μm was induced in the SiC substrate, as shown in **Fig 5.2 (b)**.

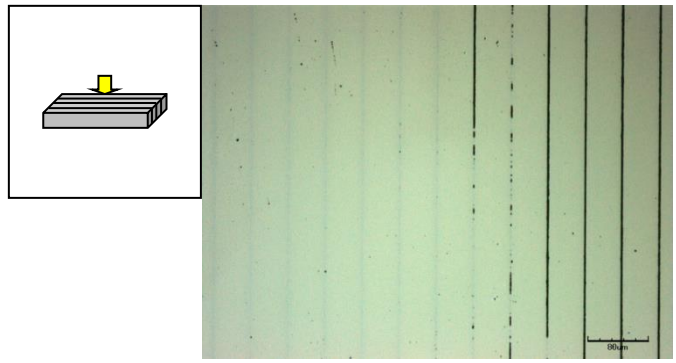

(a) SiC surface (×20)

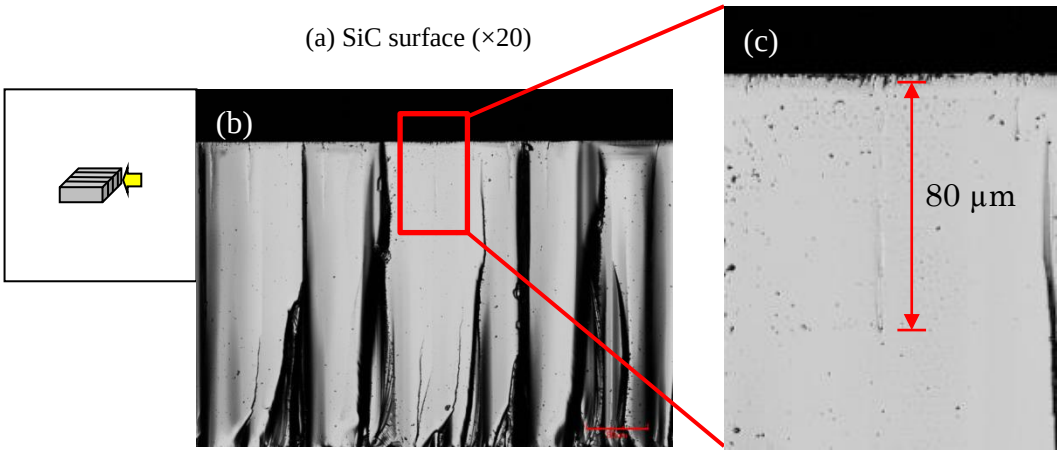

SiC cross section (b) (×20) and (b) (×100)

Fig 5.2 SiC wafer after laser process at condition A (CLSM)

Fig 5.3 shows the surface and cross section of SiC substrate after laser processing at the same experimental condition B. It can be seen that the surface was not scorched, but the inner of SiC substrate was processed. From **Fig 5.3 (b)**, a defect layer with a length of about 30~65μm was fabricated by femtosecond laser.

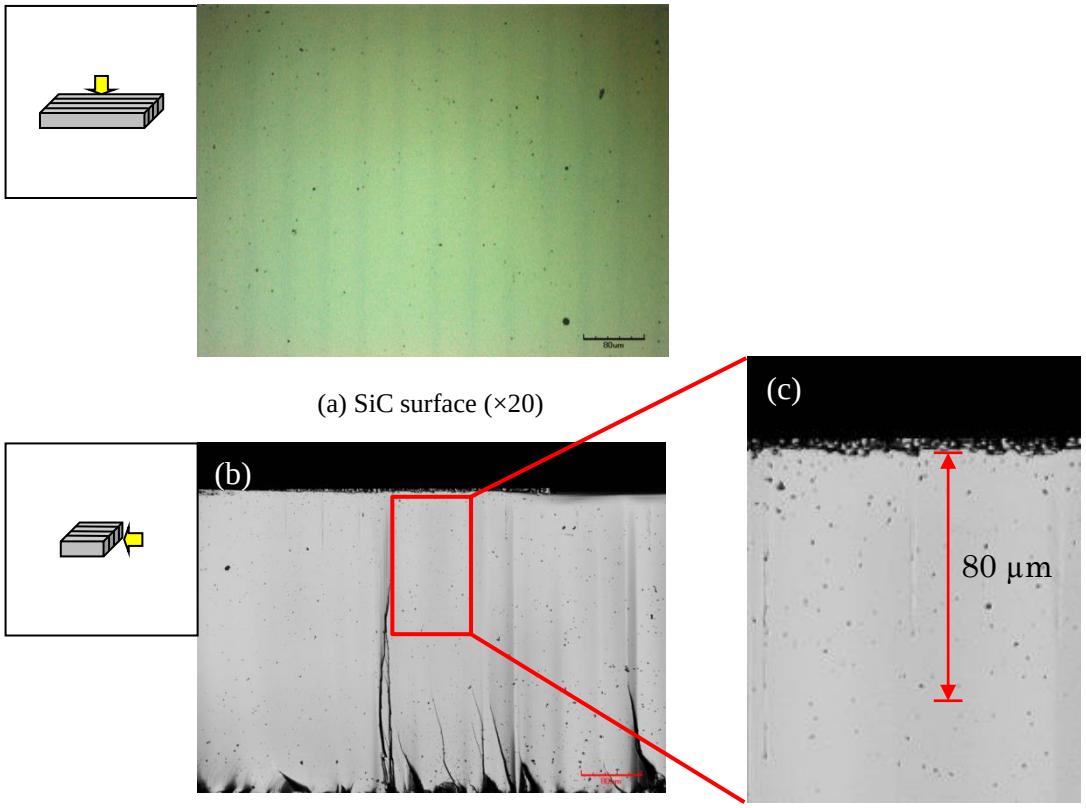

(a) SiC surface (×20)

SiC cross section (b) (×20) and (c) (×100)

Fig 5.3 SiC wafer after laser process at condition B (CLSM)

Fig 5.4 shows the surface and cross section of SiC substrate after laser processing at the same experimental condition C. It can be seen that both the surface and the internal of SiC substrate were not processed by femtosecond laser.

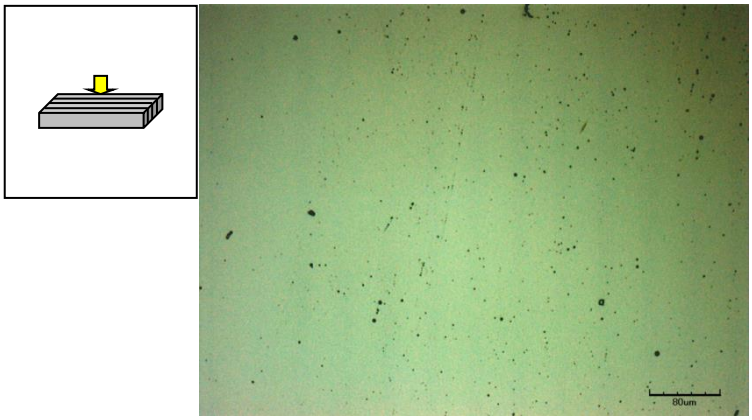

(a) SiC surface (×20)

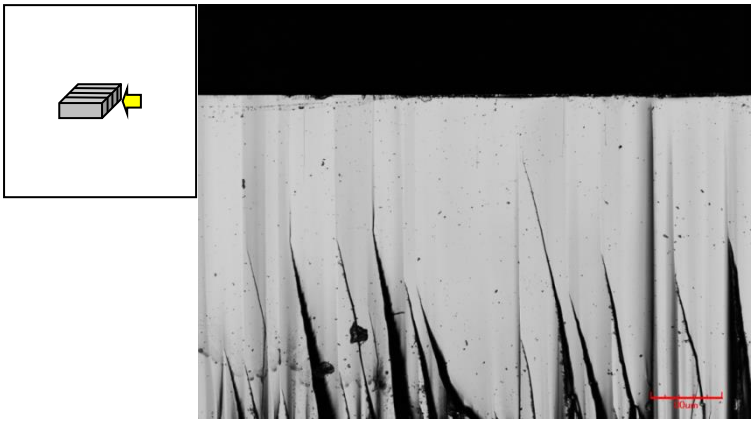

(b) SiC cross section (×20)

Fig 5.4 SiC wafer after laser process at condition C (CLSM)

5.2.2.2 Discussion

Comparing **Fig 5.2 (a)** with **Fig 5.3 (a)**, it is known that the inner defect induced by femtosecond of SiC is independent on the surface process. The defect was attributed to the focused laser beam spot in the substrate. Multiphoton absorption is responsible for this process phenomenon. During multiphoton absorption [1], many photons were absorbed simultaneously around focused beam spot, at which the photon density was extremely high. The laser-induced defect layer was observed with a length shorter than 100μm under the surface at the laser process conditions A, B, and C. As the transmissivity of laser reduced at an exponential relationship with the path length in the longitudinal direction, the attenuated laser energy can no induce more multiphoton absorption in longer path more than 100μm.

5.2.3 Comparison of inner laser process for Si, Sapphire, and SiC

5.2.3.1 Introduction

In this part, the comparison of femtosecond laser internal processing for substrate materials Si, Sapphire, and SiC were implemented. The effect of laser pulse energy on laser-induced defect of SiC substrate was also investigated. The experimental conditions are shown in **Table 5.2.**

Table 5.2 Experimental conditions

	A	B	C	D
Wafer	Si	Sapphire	SiC	
Focus position before laser process	200 μm	200 μm	200 μm	250 μm
Focus displacement for each path	5 μm			
Total displacement	200 μm			
Scanning speed	100 mm/s			
Pulse energy	90 nJ/pulse			
Repetition rate	10 MHz			

5.2.3.2 Experimental results

Fig 5.5 shows the wafer surface and cross section of Si wafer after laser processing at condition A. Grooves in the substrate surface were fabricated, however no inner defect was observed in Si cross section.

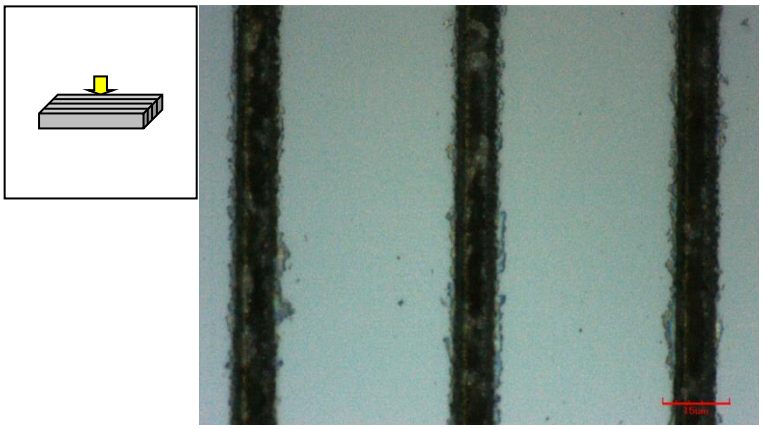

(a) Si wafer surface (×100)

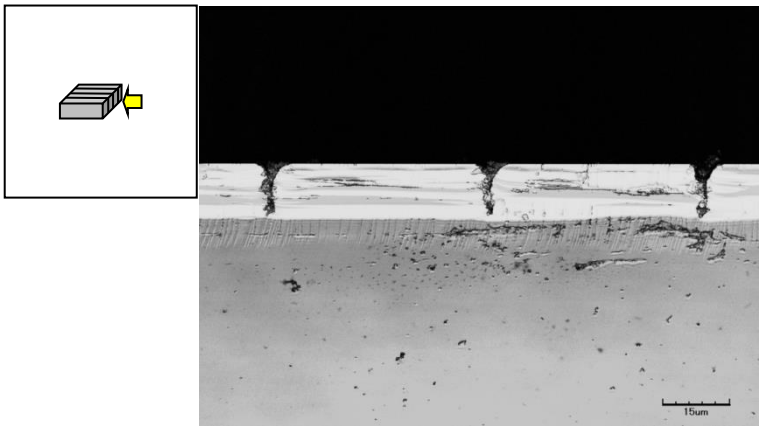

(b) Si cross section (×100)

Fig 5.5 Si wafer processed by laser at condition A (CLSM)

Fig 5.6 shows the surface and cross section of Sapphire substrate after laser processing at condition B. Both surface grooves and inner defects like that shown in **Fig 5.6** were not fabricated.

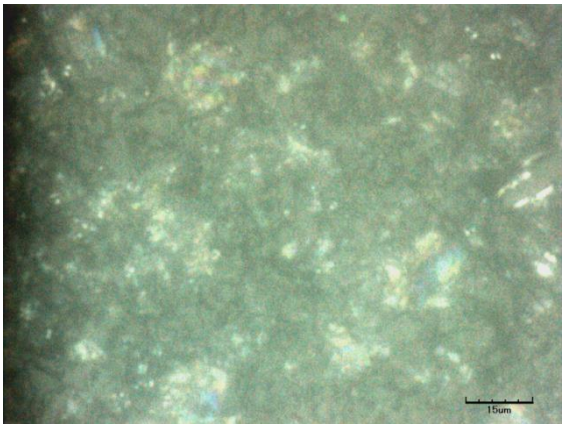

(a) Sapphire surface (×100)

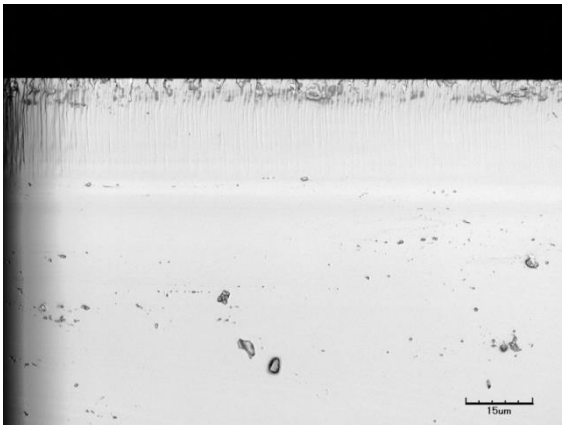

(b) Sapphire cross section (×100)

Fig 5.6 Sapphire substrate processed by laser at condition B (CLSM)

Fig 5.7 shows the wafer surface and cross section of SiC substrate after laser processing at condition C. Grooves as well as inner defect were observed after laser process. Meanwhile, cracks along the depth direction of wafer were also fabricated with a longest depth of about 200μm, which was the same with the focus position below the surface shown in **Table 5.2**.

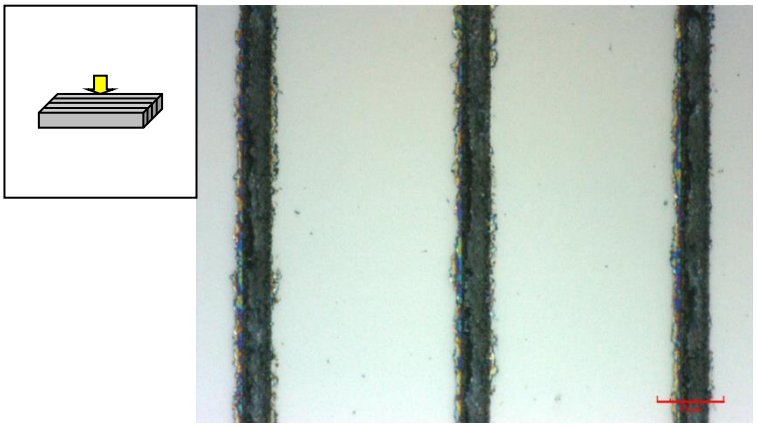

(a) SiC wafer surface (×100)

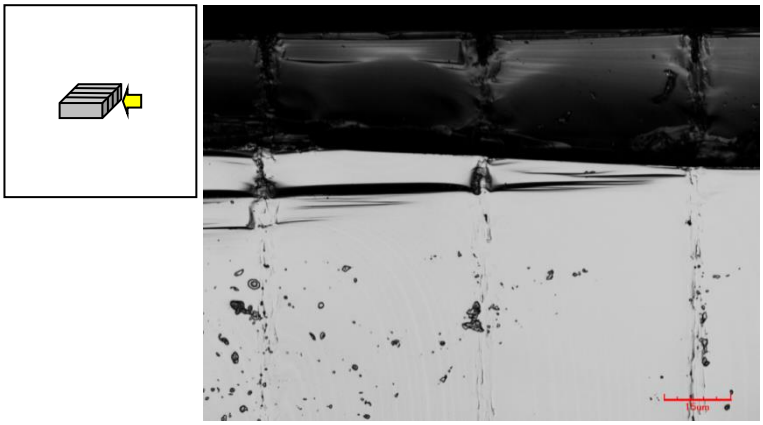

(b) SiC cross section (×100)

(c) SiC cross section (×20)

Fig 5.7 SiC wafer after laser processing at condition C (CLSM)

Fig 5.8 shows the wafer surface and cross section of SiC substrate after laser processing at condition D. Surface grooves were not fabricated by femtosecond laser. In contrast, inner defects were induced with a biggest depth of about 230μm.

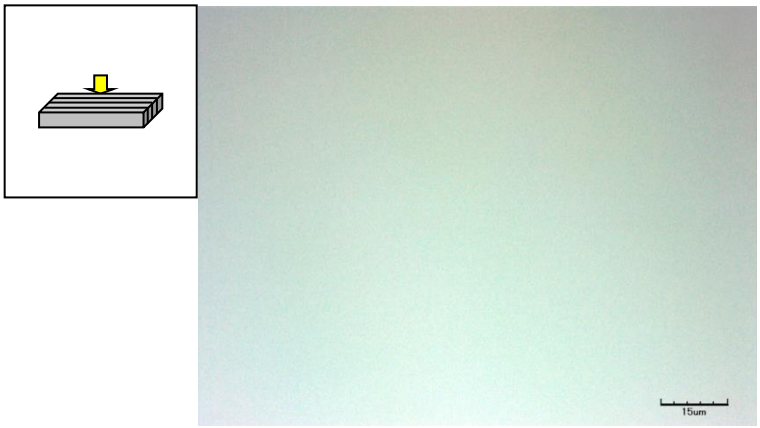

(a) SiC wafer surface (×100)

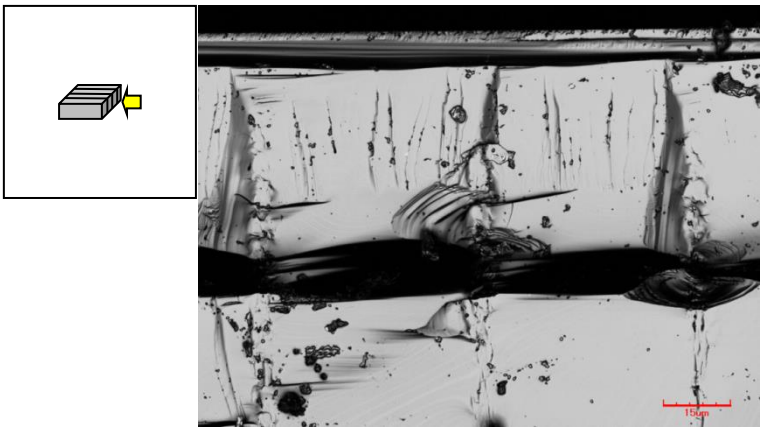

(b) SiC cross section (×100)

Fig 5.8 SiC wafer processed by laser at condition D (CLSM)

5.2.3.3 Discussion

From above results of **Fig 5.5**, it is known that the laser energy was absorbed by Si surface, leading to that no laser propagation inner the Si substrate.

From the results comparison of **Fig 5.7** and **Fig 5.8**, it is known that deeper defects were formed by laser at higher pulse energy. Cracks along depth direction were also observed. Additionally, it should be noted that inner processing was realized without any surface ablation in SiC substrate.

The different processing results of femtosecond laser on Si, SiC, and Sapphire substrates reveal different types of inner absorption. This phenomenon is attributed to the different bandgaps of these materials. Bandgap wavelength (λ_b) corresponding to laser wavelength is widely used in semiconductor science. It plays an important role for laser propagation in semiconductor materials. The laser with a wavelength shorter than the bandgap wavelength is absorbed, leading to rare penetration into the semiconductor material. The following **formula 5.1** [2] shows the relation between bandgap E [eV] and the wavelength λ_b. In the case of Si (E=1.12 eV), the bandgap wavelength (λ_b) is 1110nm, which is longer than the wavelength of this experimental laser beam (λ=1030nm). Consequently, the laser was absorbed by Si surface, resulting in no penetration into the inner.

$$\lambda_b = \frac{1240}{E} \tag{5.1}$$

For SiC and Sapphire, the bandgaps are respectively 3.26 eV and 8 eV. The corresponding λ_b are 380nm and 155nm. Both of them are shorter than the laser

wavelength utilized in this experiment system, leading to the results that the laser was penetrated into the internal of substrates Sapphire and SiC. However, because the threshold of semiconductor sapphire was higher than the output energy of the laser in this experiment, multiphoton absorption was not induced in sapphire substrate.

5.2.4 Investigation of laser process-Slicing

5.2.4.1 Introduction

In this part, laser process for slicing was investigated for Si and SiC. The experimental conditions of laser processing are shown in **Table 5.3**. After laser processing, the substrates of Si and SiC were cut off by the same method for section observation.

Table 5.3 Experimental conditions

	A	B
Wafer	Si	SiC
Focus position before laser process	200 μm	200 μm
Focus displacement for each path	5 μm	
Total displacement	200 μm	
Scanning speed	100 mm/s	
Pulse energy	80 nJ	
Repetition rate	10 MHz	

5.2.4.2 Experimental results

Fig 5.9 shows the surface and cross section of Si substrate after laser processing at experimental condition A. Laser-scorched black area can be clearly seen from the section shown in **Fig 5.9 (b)**.

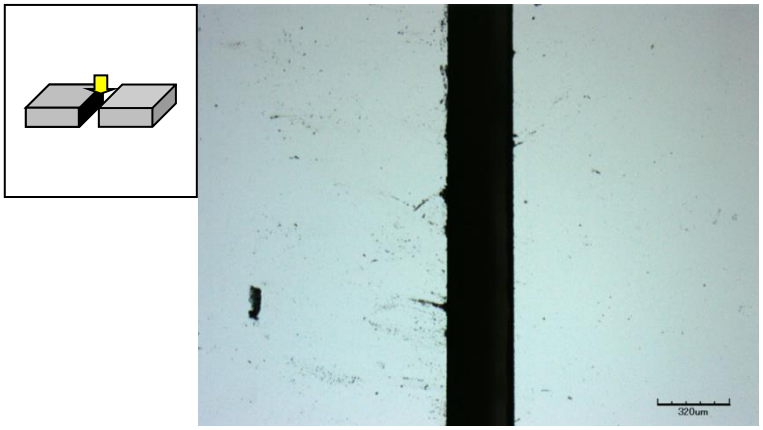

(a) Si surface (×5)

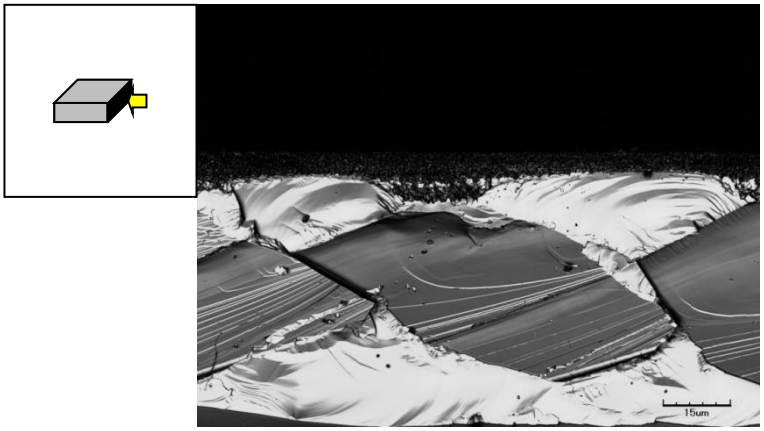

(b) Si cross section (×100)

Fig 5.9 Si wafer after laser slicing process at condition A (CLSM)

Fig 5.10 shows the surface and cross section of SiC substrate after laser processing at experimental condition B. Laser-scorched black area can be clearly seen from the section shown in **Fig 5.10 (b)** and **Fig 5.10 (c)**. Additionally, around the laser- scorched area, lots of defects were observed along the depth direction.

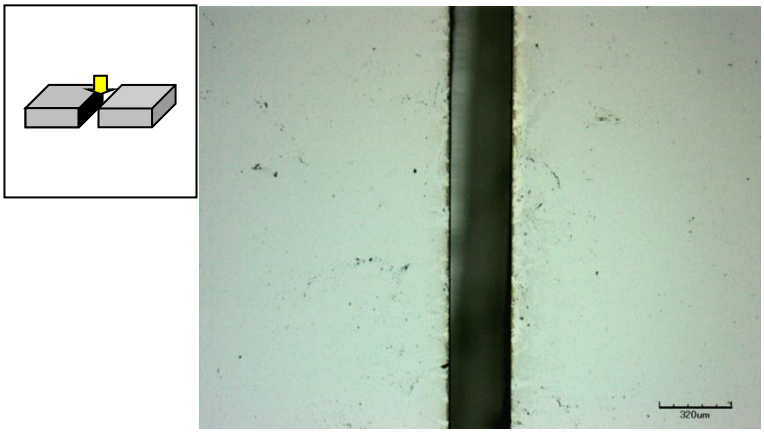

(a) SiC surface (×5)

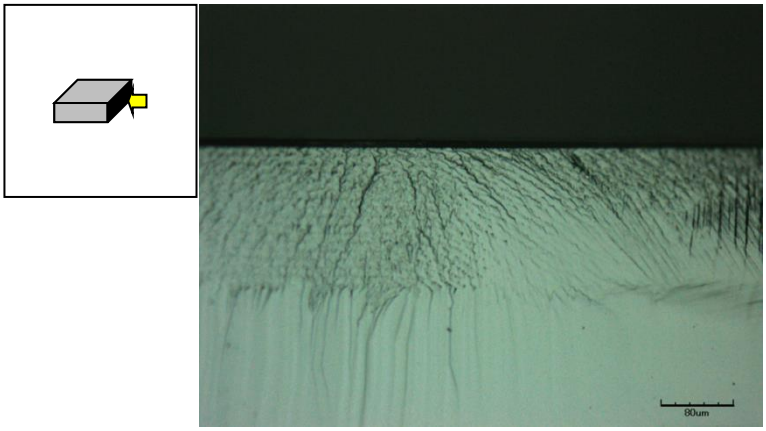

(b) SiC surface (×20)

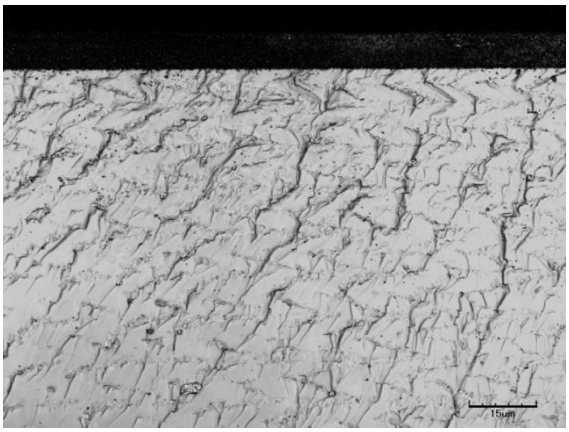

(c) SiC cross section (×100)

Fig 5.10 SiC wafer after laser slicing process at condition A (CLSM)

5.2.4.2 Discussions

The observed black areas in the section were due to laser ablation. During laser ablation, the semiconductor materials SiC reacted with oxygen in the air. The material of the irradiated section was oxidized, leading to occurrence of SiO and C [3]. The wedge-like areas shown in **Fig 5.10 (c)** were attributed to the inner absorption of laser process. Around the focused laser beam spot, the material was evaporated due to multiphoton absorption, leading to extremely strong internal pressure which further destroyed the inner crystal of SiC substrate. Meanwhile, the cracked mentioned in **Fig 5.6** were considered to be related to with the wedge-like areas. Moreover, it should be noted that the color of the wedge-like areas was different from the black oxidized area. This was attributed to that no oxidation occurred during laser ablation of this area.

5.3 Summery

Internal absorption of femtosecond laser processing for different power device substrate materials was carried out. (1) The surface of Si substrate was ablated, with no laser-induced inner defect was observed. This was attributed to that the laser was absorbed by Si wafer which had a relative low bandgap of 1.12eV. (2) For SiC substrate, the surface was ablated at suitable experimental conditions; laser-induced inner defect was observed in the depth direction; wedge-like areas were observed along the diced section. Multiphoton absorption induced by femtosecond laser was responsible for these phenomena. (3) For sapphire substrate, both ablated surfaced and inner defect were not observed. The reason was considered that the present laser intensity was lower that the threshold of sapphire substrate.

Reference

[1] S. Leyder, D. Grojo, P. Delaporte, W. Marine, M. Sentis, O. Utéza, Non-linear absorption of focused femtosecond laser pulses at 1.3 m inside silicon: Independence on doping concentration, Applied Surface Science 278 (2013) 13–18

[2] Bahaa E. A. Saleh, Malvin Carl Teich, Semiconductor photon detectors, Fundamentals of Photonics, 1991

[3] Pascale Rudolph, Klaus-Wemer, Rolf Wäshe, Wolfgan Kautek, "Physical chemistry of the femtosecond and nanosecond laser-material interaction with SiC and a SiC-TiC-TiB2 composite ceramic compound" Applied Surface Science, Volumes 208–209, 15 March 2003

[4] Gabriel Vankoa, Peter Hudekb, Johann Zehetnerb, Jaroslav Dzubaa, Pavlina Cholevab, Vladimír Kutišc, Martin Valloa, Ivan Rýgera, Tibor Lalinskýa, "Bulk micromachining of SiC substrate for MEMS sensor applications" Microelectronic Engineering Volume 110, October 2013, p260 - 264

[5] E. Ohmura, Fumitsugu Fukuyo, Kenshi Fukumitsu, Hideki Morita, "Internal modified-layer formation mechanism into silicon with nanosecond laser", Int. J. of Computational Materials Science and Surface Engineering, 2007 Vol.1, No.6, pp.677 - 691

[6] M. Kumagai, N. Uchiyama, E. Ohmura, R. Sugiura, K. Atsumi, K. Fukumitsu, "Advanced Dicing Technology for Semiconductor Wafer - Stealth Dicing", IEEE Transactions on Semiconductor Manufacturing 20, 2007

[7] Ohmura Etsuji, Kumagai Masayoshi, Nakano Makoto, Kuno Koji, Fukumitsu Kenshi, Morita Hideki, "Analysis of Processing Mechanism in Stealth Dicing for Ultra-thin Silicon Wafer", Journal of Advanced Mechanical System Design, Systems, and Manufacturing 2008 Vol.2, NO.4, p540 - 549

[8] Ahmed H. Zewail, "Femtochemistry: Atomic-Scale Dynamics of the Chemical Bond", J. Phys. Chem. A, 2000, 104 (24), p 5660 - 5694

[9] CHENGDE LI, SEONGKUK LEE, SUWAS NIKUMB," Femtosecond Laser Drilling of Alumina Wafers", Journal of Electronic Materials September 2009, Vol. 38, Issue 9, pp 2006-2012

CHAPTER 6

CONCLUSION AND FUTURE WORKS

6.1 Introduction

This chapter summarizes the main highlights of this study focusing on femtosecond laser irradiation on hard-to-process materials diamond and SiC, and discussing the effect of laser irradiation on CMP process.

6.2 Conclusion

The evolution of surface morphology changes induced on SiC substrates by femtosecond laser according to different process parameters was elaborated. We discussed the formation mechanism of Laser induced periodic surface structures (LIPSS). The energy accumulation of different overlapped areas led to different surface morphologies. The polishing behaviors of laser-irradiated SiC (Si-face) surfaces were investigated. The oxidized areas were removed much faster in CMP process than non-irradiated areas and the areas irradiated but without oxidized parts. At near-threshold laser fluence, discontinuous laser-irradiated areas of SiC substrate were formed by inhomogeneous energy absorption due to incubation effect.

By utilizing the results above, we carried out CMP process to investigate the effect of high fluence laser irradiation on SiC C-face. After polishing the substrates of Transverse model irradiation and Cross-scan model irradiation, we found that

the material remove rate (MRR) of transverse irradiation model was 27nm/min which was about 3 times higher than that of non-irradiated substrate. The MRR of cross-scan irradiation model is 16nm/min, smaller than that of transverse irradiation model but have much better surface roughness.

Quasi-radical site with a thickness of approximately 10nm as well as laser-induced ripples were observed on diamond substrate after femtosecond laser irradiation. A structure mixed with amorphous and regularly-structured diamond was demonstrated by Raman spectral analysis.

Finally, the author introduced the internal process of femtosecond laser for materials Si, sapphire substrate, and SiC. Different phenomena of internal absorption type process as well as the reasons were discussed.

6.3 Future works

◆ In future, the evolution of surface morphology changes induced by femtosecond laser on Diamond substrate will be investigated.

◆ In chapter 2, the author elaborated the evolution of surface morphology changes induced by femtosecond laser on SiC substrates at series of laser processing parameters such as different scanning pitches, different scanning velocities and repetition rates as well as different fluences. In future, CMP process for the irradiated SiC substrates mentioned above will be carried out to investigate their polishing behaviors.

◆ Transmission Electron Microscope (TEM) observation will be implemented to investigate the cross section of the areas A', B' and C' shown in chapter 2 **Fig.2.17** in which no laser-ablated areas were observed.

◆ As shown in **Fig.6.1** of chapter 3 **[Fig.3.10** (c)**]**, oxidized areas of dendritic pattern were induced after femtosecond laser irradiation. The formation mechanism will be further studied in our future study.

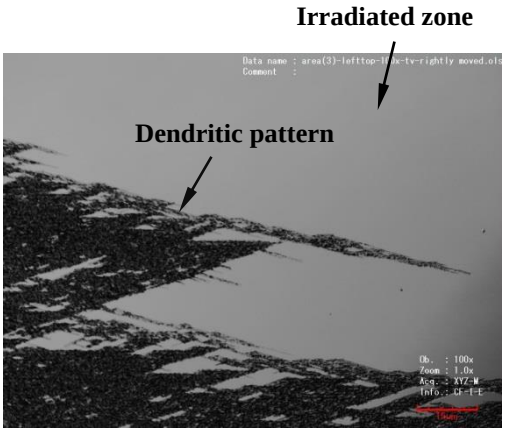

Fig.6.1 Area B of laser-irradiated area A3', Amplified image (×100), Before CMP process

◆ The surface hardness of laser-irradiated hard-to-process materials Diamond, SiC, and sapphire will be investigated. The chemical reaction between laser-induced ripples in colloidal SiO_2 slurry will be further studied.

◆ The effect of laser processing parameters, such as pulse energy, repetition rate, scanning speed of focused beam spot as well the focus position, will be investigated for internal processing of hard-to-process materials Diamond, SiC, and Sapphire.

Acknowledgment

The author also deeply thanks his Professor Syuhei Kurokawa, Precision Machining Laboratory, Dept. of mechanical engineering, faculty of engineering graduate school, Kyushu University for his insightful academic guidance, patient revising, and his necessary assistance.

The heartfelt acknowledgements of the author should go to Professor Toshiro Doi of Art, Science and Technology Center for Cooperative Research, Kyushu University, who has ever offered careful guidance and precious advice on admission guidance as well as academic guidance.

The heart-felt gratitude of the author also goes to Professor Renshi Sawada of Nano Micro Biomedical Engineering Laboratory, Graduate School of Life Science, Kyushu University for his careful and responsible inspection and useful academic advice on the dissertation.

The author would like to deeply express his appreciations to Professor Julong Yuan of Zhe Jiang University of Technology for his academic guidance and assistance on overseas study.

The author also expresses his heartfelt gratitude to associated professor Terutake Hayashi, assistant professor Yoji Umezaki, and Technical staff Yoji Matsukawa of Precision Machining Laboratory, Dept. of mechanical engineering, faculty of engineering graduate school, Kyushu University for their academic guidance or technical assistance.

The author would like to express his appreciations to laboratory secretary Azusa Suematsu as well as Yoko Yamada and other staffs of Precision Machining Laboratory, Dept. of mechanical engineering, faculty of engineering graduate school, Kyushu University for their advices and necessary assistance.

The author also thanks Shin-ichi Komai and Ji Zhang as well as other students

of Precision Machining Laboratory, Dept. of mechanical engineering, faculty of engineering graduate school, Kyushu University for their necessary assistance.

Finally, the author is pleased to express great acknowledgements to China Scholarship Council and Grant-in-Aid for Scientific Research for financial supports.

The deepest respects and thanks of the author are given to his both parents and brothers and sisters for their supports, understanding and encouragements.